İSTANBUL TECHNICAL UNIVERSITY ★ INSTITUTE OF SCIENCE AND TECHNOLOGY

MODELING AND CONTROL OF VARIABLE-SPEED DIRECT-DRIVE WIND POWER PLANT

M.S. Thesis by
Yusuf GÜRKAYNAK

Department : **Electrical Engineering**

Programme: **Control and Automation Engineering**

AUGUST 2006

İSTANBUL TECHNICAL UNIVERSITY ★ INSTITUTE OF SCIENCE AND TECHNOLOGY

MODELING AND CONTROL OF VARIABLE-SPEED DIRECT-DRIVE WIND POWER PLANT

M.S. Thesis by
Yusuf GÜRKAYNAK

(504041119)

Date of submission : **14 August 2006**

Date of defence examination: **16 August 2006**

Supervisor (Chairman): **Asst. Prof. Dr. Deniz YILDIRIM**

Members of the Examining Committee **Asst. Prof. Dr. Levent OVACIK**

Asst. Prof. Dr. Tarık DURU (KÜ.)

AUGUST 2006

PREFACE

"The power without control is not a power". These words which come from an advertisement for a tire trademark are my study philosophy on my academic studies. Power is all around us in different forms and they are meaningless without consider. Taking power under control will make power useful for humans. By working on this thesis my aim was to make one more step to control the wind power or energy, and make this energy more reliable for the humans.

I would like to say thank you to my family and to my friends who always supported me, to my professors who educated me in my 6 years of university life. Special thanks to my supervisor Assistant Prof. Dr. Deniz YILDIRIM, who helped me to achieve this thesis in a limited time. Lastly I would like to say thanks to TUBİTAK-BAYG for their scholarship during my graduate study.

August-9

Yusuf GÜRKAYNAK

CONTENTS

ABBREVIATIONS

AEP	: Annual Energy Production
ARMA	: Auto Regressive Mean Average
CC	: Current Controller
DFIG	: Doubly Fed Induction Generator
EMI	: Electromagnetic Interference
FOC	: Field Orientation Control
MPPT	: Maximum Power Point Tracker
PCC	: Point of Common Coupling
PMSG	: Permanent Magnet Synchronous Generator
PRBS	: Pseudo Binary Sequence Signal
PWM-VSI	: Pulse Width Modulation Voltage Source Inverter
SCIG	: Squirrel Cage Induction Generator
SG	: Synchronous Generator
WECS	: Wind Energy Conversion Scheme
WFSG	: Wound Field Synchronous Generator
WTS	: Wind Turbine System

FIGURE LIST

LIST OF SYMBOLS

α	: Learning coefficient
B_s	: Damping factor of shaft
β	: Blade angle
C_p,C_Γ	: Power and torque coefficient
g	: Air gap length
i_i	: i^{th} phase current
I_{ref}	: Reference current
K_s	: Stiffness of the shaft
l	: Rotor length
L_{ii}	: Self inductance of the i^{th} phase winding
L_{ij}	: Mutual inductance between i^{th} and j^{th} phase windings
L_{ls}	: Linkage inductance
L_s	: Source inductance
λ	: Tip speed ratio
λ_f	: Maximum value of the permanent magnet flux linkage
λ_{is}	: Stator i^{th} phase total flux linkage
N_s	: Number of turns in a stator phase winding
p	: Number of pair of poles
P_t	: Turbine mechanical power
r	: Rotor radius
R	: Blade length
R_{dc}	: Rectifier equivalent circuit resistance
R_s	: Stator phase resistance
S_i	: i^{th} switch logic position
T_e	: Induced torque
θ_g	: Generator angular position
θ_r	: Rotor angular position
θ_t	: Turbine angular position
ω_g	: Generator angular velocity
ω_r	: Rotor angular velocity
ω_t	: Turbine angular velocity
v_1,v_2	: Wind speed before and after wind turbine
V_d	: Rectifier equivalent circuit output voltage
V_{d0}	: Rectifier equivalent circuit average voltage
V_{LL}	: Line to line phase voltage

DOĞRUDAN SÜRÜŞLÜ, DEĞİŞKEN HIZLI RÜZGAR ENERJİ SANTRALİNİN MODELLENMESİ VE KONTROLLÜ

ÖZET

Günümüzde en önemli problem ve tabii ki en büyüğü enerjiye olan ihtiyaçtır. Bu ihtiyacı karşılayacak bir çok yöntem varken, araştırmacılar günümüzde yenilebilir enerji kaynaklarını içeren çözümlere ağırlık vermiştir. Bunun sebebi bu kaynakları sınırsız olması ve doğaya herhangi bir zararının olmamasıdır. Bu tezin amacı bu kaynaklardan biri olan rüzgardan maksimum enerjiyi alma yöntemlerinden birini incelemek ve gerçeklenebilirliğini irdelemektir. Bu bağlamda ilk kısımda geleneksel rüzgar türbinlerine ve günümüzde kullanılan değişken hızlı rüzgar türbinlerine genel bakış yapılmış ve literatürde geçen bazı MPPT yapıları anlatılmıştır. İncelenmek üzere basit yapılı, değişken hızlarda çalışabilme özelliğine sahip ve dişli kutusuna ihtiyaç duymayan bir topoloji seçilmiştir. Bu topolojide generatör olarak oluk genişliği, kutup sayısını artırabilmek için uygun olan, fırçasız olmasından dolayı bakımı az olan sabit mıknatıslı senkron makine seçildi. İkinci kısımda ise seçilen bu topolojideki kontrolsüz tam dalga doğrultucu, türbin, senkron makine ve eviriciye ait modeller beyaz kutu modellemesi yöntemiyle modellenmiştir. Üçüncü kısımda bu sistemin optimum şekilde çalışması için bir MPPT algoritması önerilmiştir. Bu algoritma bir en iyileme yöntemi olan basamaksal artım (stepeest decent) yöntemini ve ani hız değişimlerine göre karar verecek dalları barındırmaktadır. Eviriciyi denetlemek için, bir akım denetleyicisi olan histerezis denetleyicisi seçilmiştir. Bu denetleyici gerekli emirleri MPPT den alacak ve bu emri eviriciyi kullanarak sisteme uygulayacak şekilde çalışır. Bu denetleyicinin özellikleri dayanıklı olması, davranışının sistem katsayılarından bağımsız olması, geçici hal davranışı göstermemesi ve güç faktörünü bağımsız olarak değiştirebilmesidir. Son kısımda ise seçilen topoloji, önerilen denetleyici sistemiyle beraber bir benzeteç programında (Matlab-Simulink) kuruldu. Farklı rüzgar değişim senaryoları için benzeteç programı koşturuldu. Çıkan sonuçlardan denetleme sistemin istenilen biçimde çalıştığı, sistemi her halükarda kararlı tuttuğu, en yüksek güç noktasını küçük bir hatayla yakaladığı gözlendi. Bu hatanın en büyük değeri 11 KW turbin gücü için 40 W olduğu görüldü. Son kısımda, önerilen bu denetleme sistemini iyileştirmek ve geliştirmek için gereken yöntemler anlatıldı.

MODELLING AND CONTROL OF VARIABLE-SPEED DIRECT-DRIVE WIND POWER PLANTS

SUMMARY

Nowadays the most important problem and also the biggest one is the need of energy. Although there are several solutions to this problem, researchers headed toward working on the solutions with renewable sources, because these kinds of sources are harmless to the environment and they are limitless. The aim of this thesis is to investigate the wind energy which is a renewable source, and to examine one of the ways or methods to harvest the maximum energy from the wind. On this way, in the first part an overview is given for conventional wind turbines and for several variable speed wind power plants which are currently in use, then some MPPT techniques are introduced. After that, a topology which has basic structure, has the ability of working under variable rotor speeds and does not employ gearbox, is selected. For this topology PMSG is selected as the generator whose maintenance costs are low, because of its brushless structure. At the second part, the components of this topology mainly uncontrolled rectifier, wind turbine, PMSG and inverter are modeled by white box approach. At the third part an algorithm (MPPT) which directs the system to work at the optimum point, is suggested. This algorithm consists of steepest decent optimization algorithm and some parts which will keep the system stable under sudden changes in wind speed. Hysteresis controller is selected as the current controller for the control of the inverter. The benefit of this controller is that, it is robust, it's behavior is independent from system parameters and it can control the power factor independently. At last part the selected topology with the proposed control system is built on the simulator (Matlab-Simulink) and some scenarios of sudden wind changes are investigated. It observed that for each scenario, control system worked properly, kept the system stable and MPPT found the optimum point each time. The maximum error of the MPPT is 40 W for 11KW turbine power. At last section, to improve the control system, new methods and new approaches are introduced.

1. INTRODUCTION

Global warming has been attributed to the increase of the greenhouse gas concentration produced by the burning of fossil fuels. Wind power generation is an important alternative to mitigate this problem mainly due to its smaller environmental impact and its renewable characteristic that contribute for a sustainable development. Three factors have made wind power generation cost-competitive, these are:

(i) The state incentives

(ii) The wind industry that have improved the aerodynamic efficiency of wind turbine

(iii) The evolution of power semiconductors and new control methodology for the variable-speed wind turbine that allow the optimization of turbine performance.

Nowadays, various wind turbine systems (WTS) compete in the market. They can be gathered in two main groups.

(i)Danish concept wind power plants

(ii)Variable-speed wind power plants

The first group operates with almost constant speed “Danish concept” [2]. In this Danish concept case, the output of generator is directly connected to utility. The main components can be summarized as follows [1].

Anemometer: Measures the wind speed and transmits wind speed data to the controller.

Blades: Most turbines have either two or three blades. Wind blowing over the blades causes the blades to "lift" and rotate.

Brake: A disc brake which can be applied mechanically, electrically, or hydraulically to stop the rotor in emergency situations.

Controller: The controller starts up the machine at wind speeds of about 3.3 to 6.6 meter per second [m/s] and shuts off the machine at about 30 m/s. Turbines cannot operate at wind speeds above about 30 m/s because their generators could overheat.

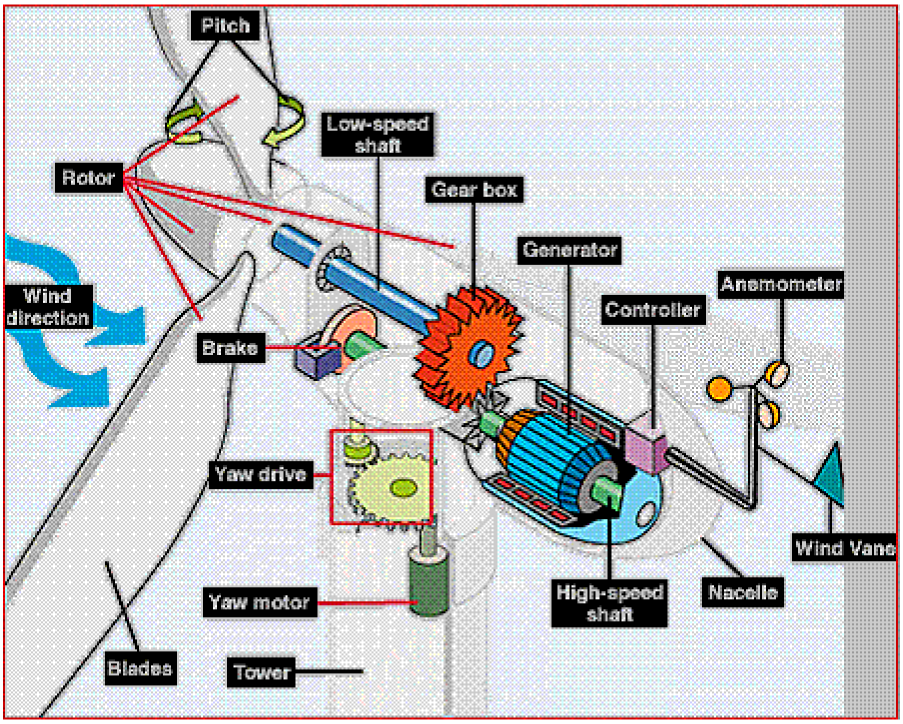

Figure 1.1: Conventional danish concept wind power plant [1]

Gear box: Gears connect the low-speed shaft to the high-speed shaft and increase the rotational speeds from about 30 to 60 revolutions per minute (rpm) to about 1200 to 1500 rpm which is the rotational speed required by most induction generators to produce electricity. The gear box is a costly (and heavy) part of the wind turbine and engineers are exploring "direct-drive" generators that operate at lower operational speeds that do not require gear boxes.

Generator: An off-the-shelf induction generator that produces 50-cycle AC electricity is usually employed. The speed-torque curve is given in Figure 1.2. The intermittent dashed line which separates the generator and motor regions, shows the operating point of the generator.

High-speed shaft: The part of the drive train connected to the generator.

Low-speed shaft: The rotor turns the low-speed shaft at about 30 to 60 rpm.

Nacelle: The rotor attaches to the nacelle, which sits atop the tower and includes the gear box, low- and high-speed shafts, generator, controller, and mechanical (disk) brake. A cover protects the components inside the nacelle. Some nacelles are large enough for a technician to stand inside while working.

Pitch: Blades are turned, or pitched, out of the wind to keep the rotor from turning in wind speeds that are too high or too low to produce electricity.

Rotor: The blades and the hub together are called the rotor.

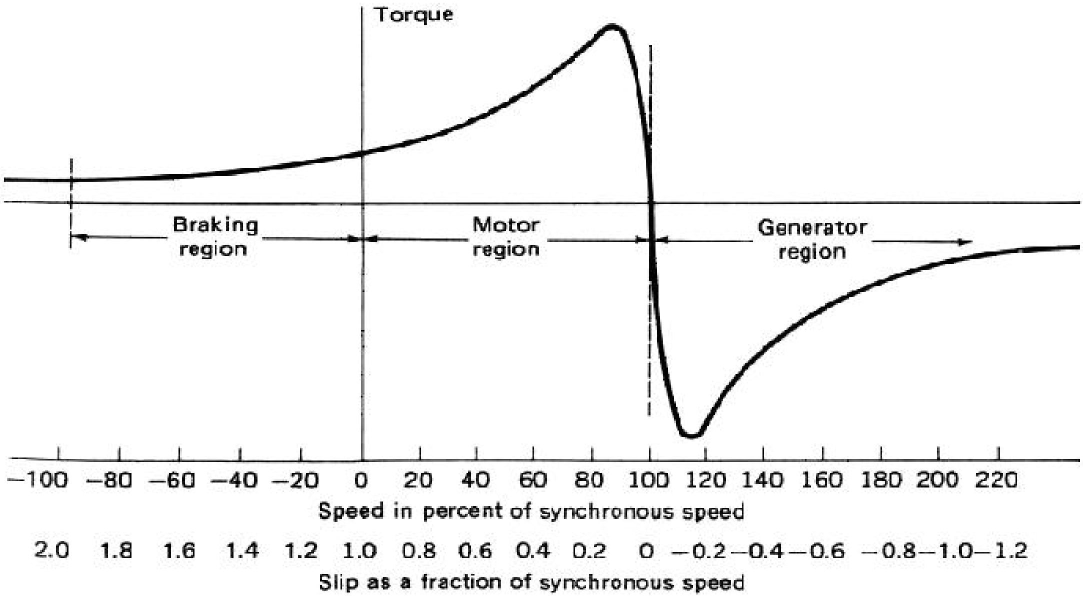

Figure 1.2: The torque-speed curve of induction machine [3]

Tower: Towers are made from tubular steel or steel lattice. Because wind speed increases with height, taller towers enable turbines to capture more energy and generate more electricity.

Wind direction: This is an "upwind" turbine, so-called because it operates facing into the wind. Other turbines are designed to run "downwind", facing away from the wind.

Wind vane: Measures wind direction and communicates with the yaw drive to orient the turbine properly with respect to the wind.

Yaw drive: Upwind turbines face into the wind; the yaw drive is used to keep the rotor facing into the wind as the wind direction changes. Downwind turbines do not require a yaw drive, the wind blows the rotor downwind.

Yaw motor: Powers the yaw drive.

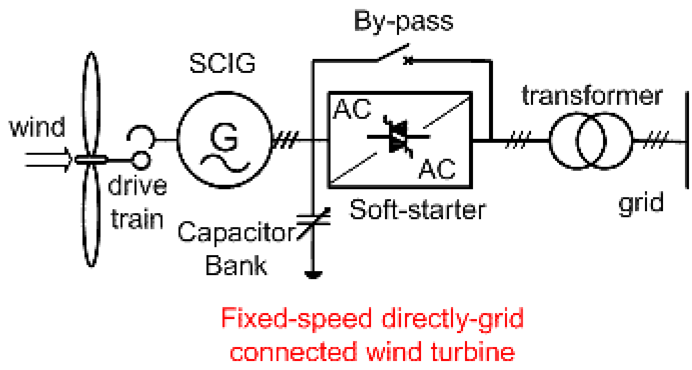

Figure 1.3: The Grid Connection of a Squirrel Cage Induction Generator [3]

The second one operates with variable speed; In this case, the generator does not directly couple the drive train to grid. Thereby, the rotor is permitted to rotate at any speed by introducing power electronic converters between the generator and the grid. The constant speed configuration is characterized by stiff power train dynamics due to the fact that electrical generator is locked to the grid; as a result, just a small variation of the rotor shaft speed is allowed. The construction and performance of this system are very much dependent on the mechanical characteristic of the mechanical subsystems, pitch control time constant, etc. In addition, the turbulence and tower shadow induces rapidly fluctuating loads that appear as variations in the power. These variations are undesired for grid-connected wind turbine, since they result in mechanical stresses that decrease the lifetime of wind turbine and decrease the power quality. Furthermore, with constant speed there is only one wind velocity that results in an optimum tip-speed ratio. Therefore, the wind turbine is often operated off its optimum performance, and it generally does not extract the maximum power from the wind.

Alternatively, variable speed configurations provide the ability to control the rotor speed [2]. This allows the wind turbine system to operate constantly near to its optimum tip-speed ratio. The following advantages of variable-speed over constant-speed can be highlighted:

(i) The Annual Energy Production (AEP) increases because the turbine speed can be adjusted as a function of wind speed to maximize output power. Depending on the turbine aerodynamics and wind regime, the turbine will on average collect up to 10% more annual energy [2]

(ii) The mechanical stresses are reduced due to the compliance to the power train. The turbulence and wind shear can be absorbed, i.e., the energy is stored in the mechanical inertia of the turbine, creating a compliance that reduces the torque pulsations

(iii) The output power variation is somewhat decoupled from the instantaneous condition present in the wind and mechanical systems. When a gust of the wind arrives at the turbine, the electrical system can continue delivering constant power to the network while the inertia of mechanical system absorbs the surplus energy by increasing rotor speed.

(iv) Power quality can be improved by reducing the power pulsations. The reduction of the power pulsation results in lower voltage deviations from its rated value in the point of common coupling (PCC).

(v) The pitch control complexity can be reduced. This is because the pitch control time constant can be longer with variable speed

(vi) Acoustic noises are reduced. The acoustic noise may be an important factor when installing new wind farms near populated areas.

Although the main disadvantage of the variable-speed configuration are the additional cost and the complexity of power converters required to interface the generator and the grid, its use has been increasing steadily due to the above mentioned advantages.

1.1 Generators and Topologies

1.1.1 Synchronous Generators

A synchronous generator usually consist of a stator holding a set of three-phase windings, which supplies the external load, and a rotor that provides a source of magnetic field. The rotor magnetic field may be supplied either from permanent magnets or from a direct current flowing in a coil [2].

1.1.1.1 Wound Field Synchronous Generator (WFSG)

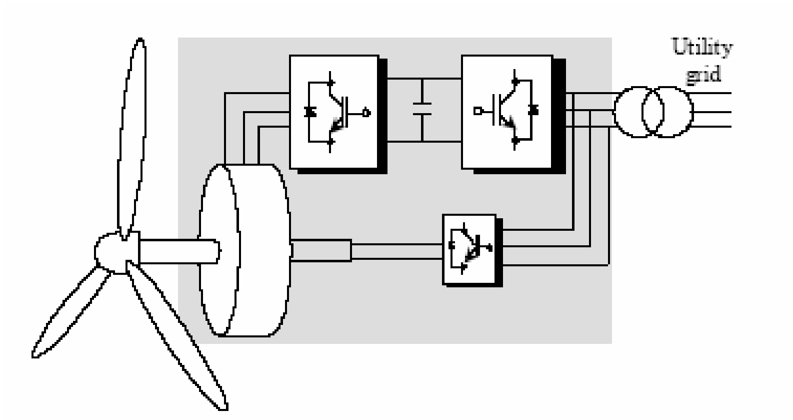

Figure 1.4: Wound field synchronous generator [2]

The WPS with wound field synchronous generator is shown in Figure 1.4. The stator winding is connected to utility through a four-quadrant power converter comprised of two back-to-back PWM-VSI. The stator side converter regulates the electromagnetic torque, while the supply side converter regulates the real and reactive power delivered by the WPS to the utility. The Wound Field Synchronous Generator has the following advantages [2]:

• The efficiency of this machine is usually high, because it employs the whole stator current for the electromagnetic torque production

• The main benefit of the employment of wound field synchronous generator with salient pole is that it allows the direct control of the power factor of the machine, consequently the stator current may be minimized out any operation instances.

• The pole pitch of this generator can be smaller than that of induction machine. This could be a very important characteristic in order to obtain low speed multipole machines, eliminating the gearbox.

The existence of a field winding in the rotor may be a drawback as compared with permanent magnet excitation. In addition, to regulate the active and reactive power generated, the converter must be sized typically 1.2 times the WPS rated power.

1.1.1.2 Permanent-Magnet Synchronous Generator

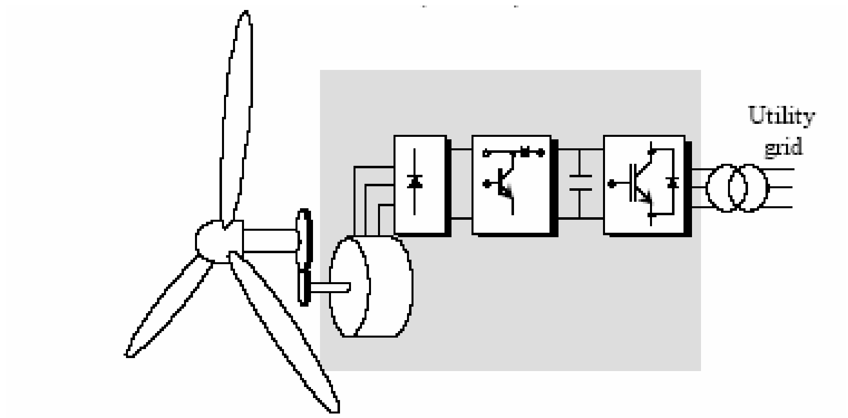

Figure 1.5: Permanent-magnet synchronous generator with boost converter [2].

Figure 1.5 shows a WPS where a permanent magnet synchronous generator is connected to a three-phase rectifier followed by a boost converter. In this case, the boost converter controls the electromagnetic torque. The supply side converter regulates the DC link voltage as well as control the input power factor. One drawback of this configuration is the use of diode rectifier that increases the current amplitude. As a result this configuration has been considered for small size WPS (smaller than 50 kW) [2].

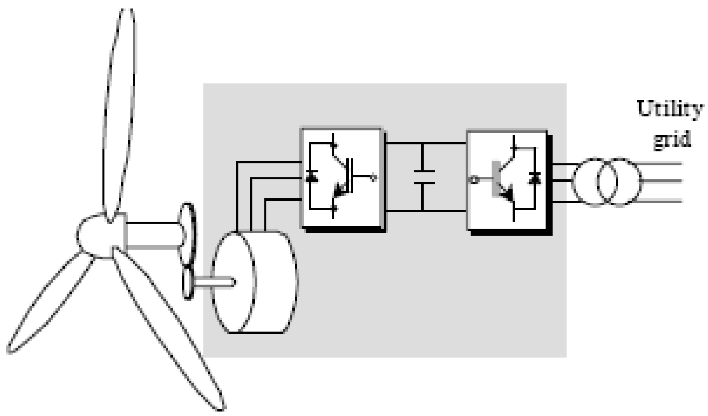

Figure 1.6: Permanent-magnet synchronous generator with four quadrant converter [2].

Other scheme using PMSG is shown in Figure 1.6, where, the PWM rectifier is placed between the generator and the DC link, and PWM inverter is connected to the utility. The advantage of this system regarding the system shown previously is the use of field orientation control (FOC) that will allow the generator to operate near its optimal working point in order to minimize the losses in the generator and power electronic circuit. However, the performance is dependent on the good knowledge of the generator parameter that varies with temperature and frequency. The main drawbacks, in the use of PMSG, are the cost of permanent magnet that increase the price of the machine, demagnetization of the permanent magnets and it is not possible to control the power factor of the machine [2].

1.1.2 Induction Generators

The AC generator type that has most often been used in wind turbines is the induction generator. There are two kinds of induction generator used in wind turbines that are: squirrel cage and wound rotor [2].

1.1.2.1 Doubly Fed Induction Generator (DFIG)

The wind power system shown in Figure 1.7 consists of a doubly fed wound-rotor induction generator (DFIG), where the stator winding is directly connected to the utility and the rotor winding is connected to the grid through a four quadrant power converter comprised of two back-to-back PWM-VSI. The SCR based converter can also be used but they have limited performance.

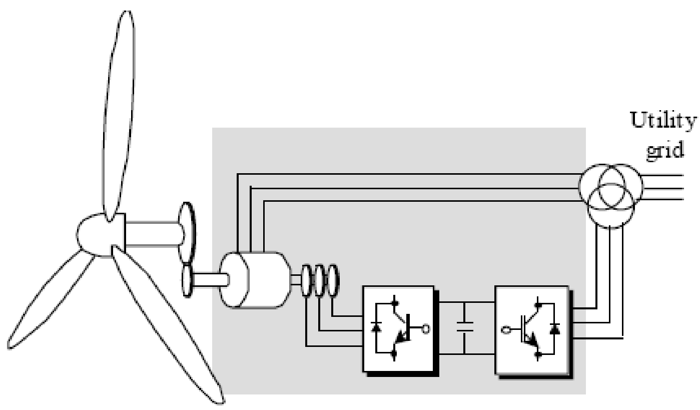

Figure 1.7: Doubly fed induction generator (DFIG) [2].

Usually, the controller of the rotor side converter regulates the electromagnetic torque and supplies part of the reactive power to maintain the magnetization of the machine. On the other hand, the controller of the supply side converter regulates the DC link. Compared to synchronous generator, this DFIG offers the following advantages [2]:

• Reduced inverter cost, because inverter rating is typically 25% of the total system power. This is because the converters only need to control the slip power of the rotor

• Reduced cost of the inverter filter and EMI filters, because filters rated for 0.25 p.u. total system power, and inverter harmonics represent a smaller fraction of total system harmonics

• Robustness and stable response of this machine facing against external disturbances.

One drawback of DFIG is the use of slip rings that require periodic maintenance, especially at sea shore sites.

The WPS of Figure 1.8 shows a doubly fed fully-controlled induction generator, with a dc-transmission link. This type of WPS allows controlling the voltages and frequencies of the rotor and stator, consequently this system provide a higher flexibility on the control system than the conventional doubly-fed induction generator shown in previous Figure 1.7. In addition, this WPS has been considered for offshore sites, which are connecting to land by submarine cables. There are other methods of interface the DFIG to the grid. Among them, are:

(i) Cycloconverter

(ii) Matrix converter

However they have some disadvantages over the one presented in Figure 1.7, those are: poor line power factor, high harmonic distortion in line and machine current for a cycloconverter and for a matrix converter, despite elimination of the dc capacitor, this converter is more complex and its technology is less mature.

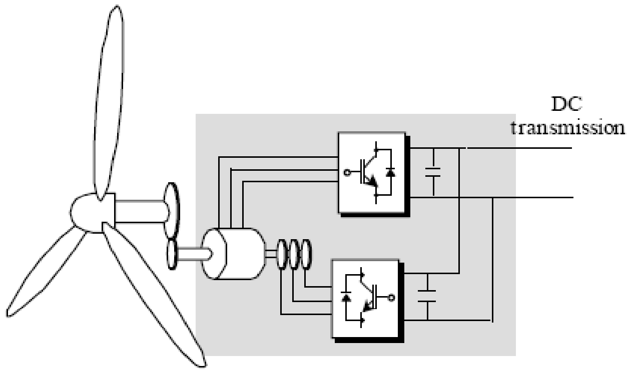

Figure 1.8: Doubly fed full-controlled induction generator [2].

1.1.2.2 Squirrel Cage Induction Generator (SCIG)

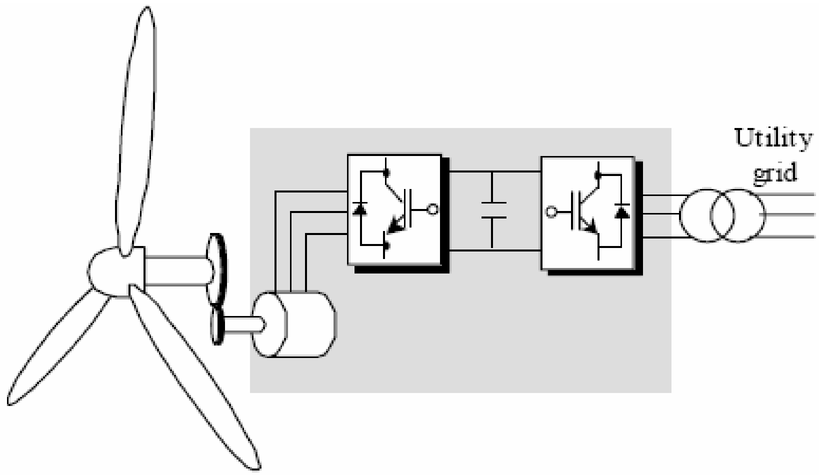

Figure 1.9: Squirrel cage induction generator (SCIG) [2].

A WPS with squirrel cage induction generator is shown in Figure 1.9. The stator winding is connected to utility through a four-quadrant power converter comprised of two PWM VSI connects back-to-back trough a DC link. The control system of the stator side converter regulates the electromagnetic torque and supplies the reactive power to maintain the machine magnetized. The supply side converter regulates the real and reactive power delivered from the system to the utility and regulates the DC link. The uses of squirrel cage induction generator have some advantages [2]:

• The squirrel cage induction machine is extremely rugged; brushless, reliable, economical and universally popular,

• Fast transient response for speed is possible,

• The inverter can be operated as a VAR/harmonic compensator when spare capacity is available,

Among the drawbacks are:

Complex system control (FOC) whose performance is dependent on the good knowledge of the generator parameter that varies with temperature and frequency.

The stator side converter must be oversized 30-50% with respect to rated power, in order to supply the magnetizing requirement of the machine [2].

1.2 Various Type of MPPT's for Different Topologies

MPPT (maximum power point tracker) is an algorithm that is designed to control the power flow in the wind power plant such a way that, the generated power should be as high as possible at every wind speeds. In basic, MPPT is a block that has inputs from the system measurements (rotor speed, frequency, dc voltage, dc current …) and has an output of new reference of the system (system working point). By using the measurements, it calculates or finds out the new operating point for the system. The algorithm inside the MPPT depends on the topology of the plant. In the following, some examples of proposed MPPT structure for different wind power plants will be introduced.

1.2.1 Mapping Power Technique

This is based on the look up tables, that MPPT determines the working point of the system by using the previously prepared tables instead of making calculations, just like an explorer who finds his way by using a map. An example for this technique is given below in Figure 1.10.

This topology consists of wind turbine, PMSG, uncontrolled rectifier and inverter. Inverter is controlled to keep the dc voltage value equal to the operating voltage. The block diagram shown in Figure 1.10, is the preliminary design of the sensorless WECS controlled system. In the preliminary design stage, the system does not include the minimum dc link voltage limitation, cut-in and cutout wind speed control features. The control system consists of two signal-tracking loops, namely the "power-mapping" loop and generator frequency derivative loop. The tracking signals required for both loops are the output power from the WECS that is transferred to the dc link and PMSG stator frequency [14].

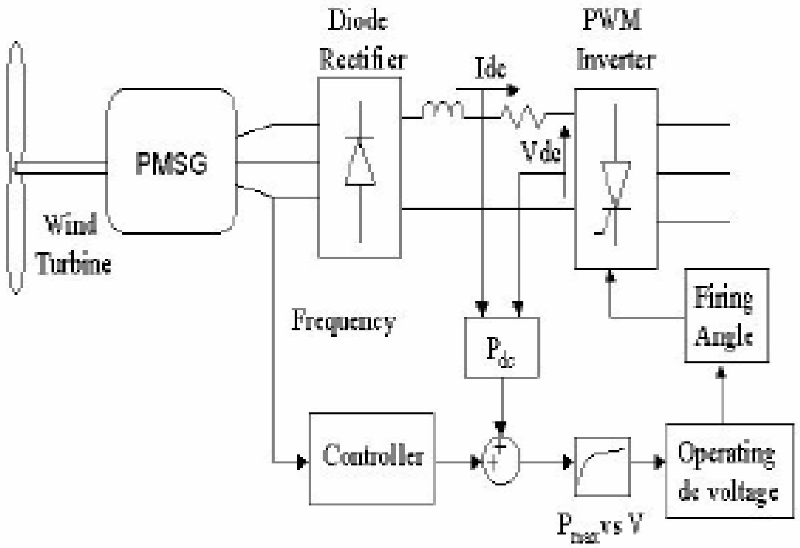

Figure 1.10: Block diagram of the sensorless WECS controlled system [14]

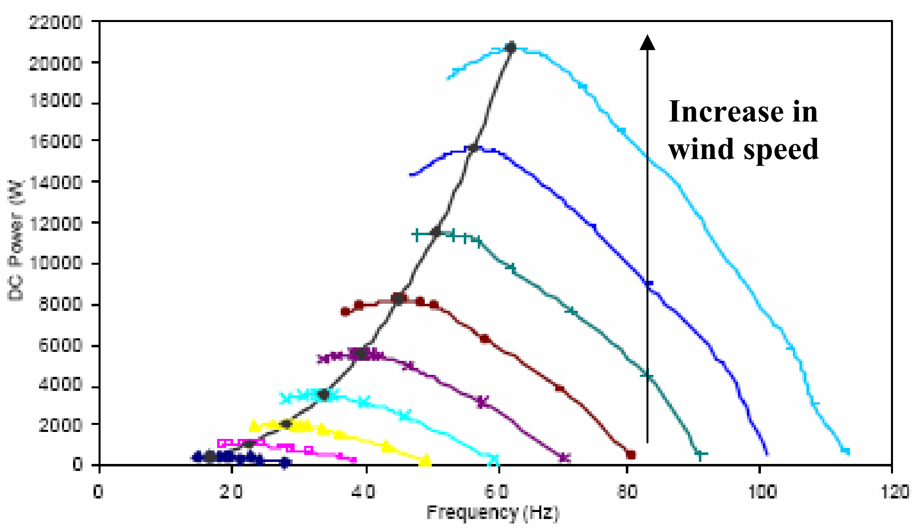

Figure 1.11: Predicted characteristic (dc power-stator frequency) of the WECS [14].

It is recognized that the inverter has the flexibility to operate over a wide range of DC input voltages. At a given wind speed, the output DC link power is used to estimate the optimal DC operating voltage from the "power-mapping" maximum power vs. DC voltage curve shown in Figure 1.12. Due to the sensitivity of P_{dc} to the changes in V_{dc} for the PMSG, the P_{dc} and the V_{dc} will continue to increase or decrease till the intersection of P_{dc} and V_{dc} at the maximum power for the given wind speed [14].

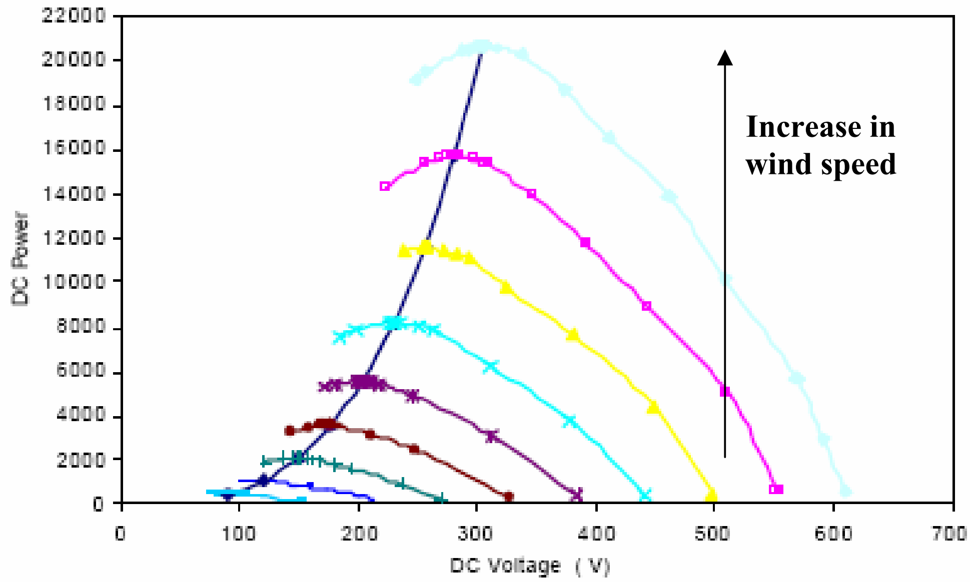

Figure 1.12: Predicted characteristic (dc power-dc voltage) of the WECS [14]

The stator frequency will also be changing (increasing or decreasing) during the change of the operating dc voltage. In the alternator frequency derivative loop, the derivative control action provides a means of obtaining the controller with higher sensitivity. This derivative control responds to the rate of changes of the stator frequency (Figure 1.11) and can produce a significant correction to the operating DC voltage. The gain value from frequency derivative loop will become zero when the operating dc voltage is optimal one which leads to the maximum power point. Using the results determined by both loops, the controller allows the DC bus voltage to vary to value corresponding to the maximum power operating point [14].

1.2.2 The Hill Climbing Method

This method is based on changing the operating point of the system step by step. MPPT observes the changes on generated power and rotor speed. According to these changes, it determines whether to increase or decrease the value of the set operating point of the plant at each sampling period. The changing value of the reference can be a constant value or calculated value. An example for this kind of MPPT which is based on the Figure 1.13, is given below [15]:

The set point input of the speed control must increase if,

The rotor power P increases and the rotor speed ω_{act} is constant or increases,

Both P and ω_{act} decrease.

On the other hand, the set point input must decrease if

The rotor power P decreases and the rotor speed ω_{act} is constant or increases,

P increases and ω_{act} decreases.

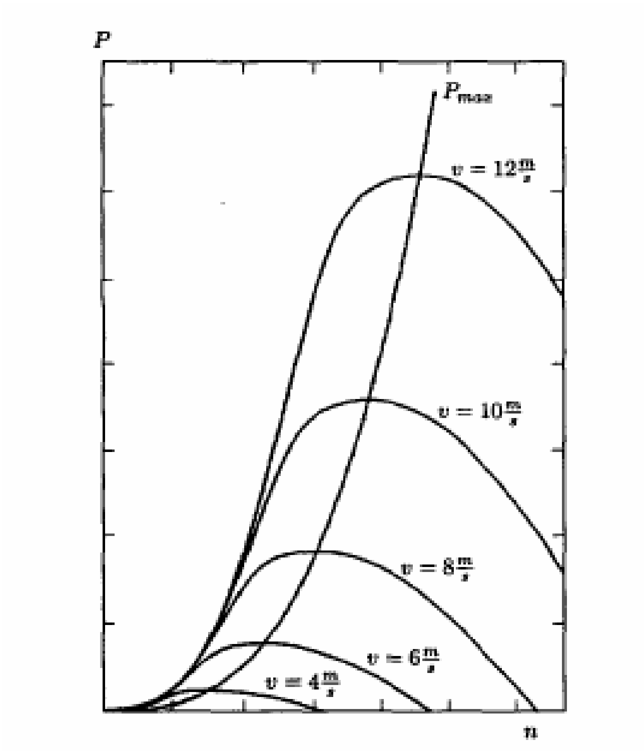

Figure 1.13: Rotor power P versus rotor speed n [15].

The flow chart of this kind of MPPT technique is given in Figure 1.14. As seen from the chart, slope (change in reference) has a constant value of "1" [15].

This technique does not need any previous knowledge about the system. So that, the preparation of a look up table or map is not required. On the other hand, it requires measurement of the rotor speed and continuously searches for the optimum point with a constant step. If the system is far away from the optimum operating point, it will take so many times to reach the optimum point. Process can be shortened by using variable slope instead of a constant one.

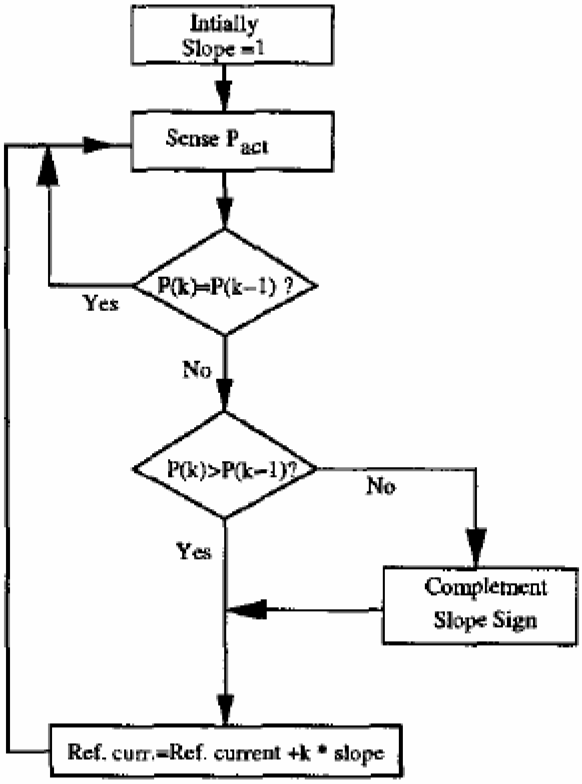

Figure 1.14: The flow chart of MPPT which uses hill climbing technique [16].

1.2.3 Varying Duty Ratio Method

This is a special method that it can only be used for the topologies which use DC chopper behind the uncontrolled rectifier. It bases on applying variable duty ratio to the DC chopper which controls the speed of the generator by changing the effective value of input voltage of the uncontrolled rectifier. MPPT searches the optimum operating point by observing system response to the varying duty ratio. An example of this system is given in Figure 1.15 [16].

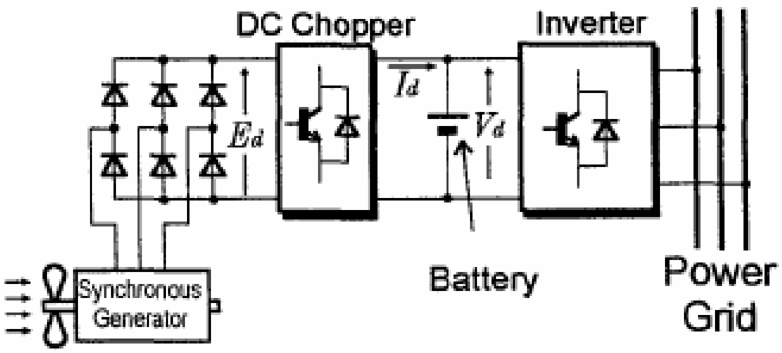

Figure 1.15: The Proposed System for Varying Duty Ratio Technique [16]

The output power characteristic of wind turbine is shown in Figure 1.16. These characteristic curves are divided into directions A and B by dotted line (maximum power line)

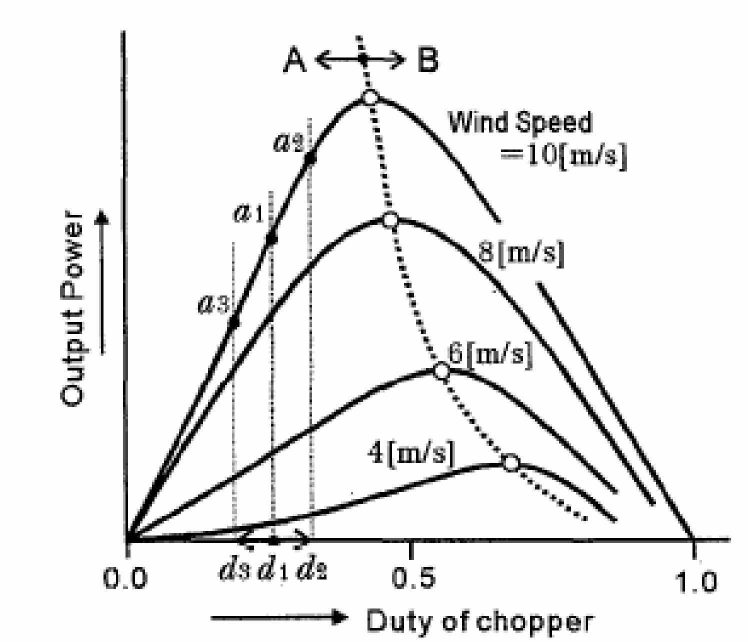

Figure 1.16: General Wind Turbine Characteristic [16]

For example, when the operating point is at a_1 (when the duty is d_1 at this point) the duty ratio is changed in the range between d_2 and d_3 continuously and slowly for searching the maximum power point. In practical, the duty of this chopper is changed like in the Figure 1.16 [16].

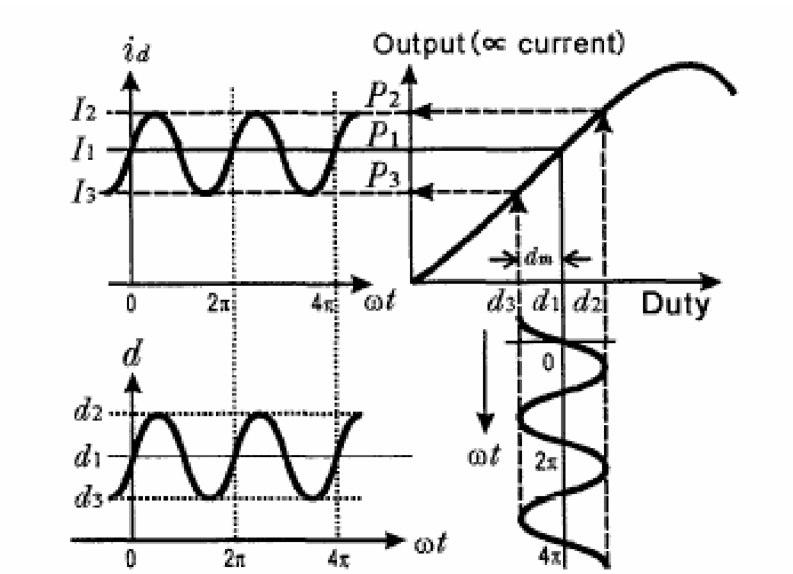

Figure1.17: Maximum power tracking control method [16].

$$d = d_1 + d_m \sin \omega t \qquad \textbf{(1.1)}$$

$$d_m = d_2 - d_1 = d_1 - d_3 \qquad \textbf{(1.2)}$$

If operating point exists in the area A as shown in Figure 1.16, the relationship of $P_2 > P_3$ is satisfied. If this point is in direction B $P_3 > P_2$ is satisfied. Then we detect the points P_2 and P_3, and determine d_1 by the following equation [16]:

$$d_1 = K_p \int (P_2 - P_3) dt \qquad \textbf{(1.3)}$$

In practice, the values of i_d (the DC bus current) is detected and sampled – hold corresponding to a_2 and a_3 from current transformer. Finally, the duty of the chopper is obtained as follows:

$$d_1 = K \int (I_2 - I_3) dt \qquad \textbf{(1.4)}$$

In order to realize an appropriate experiment, $d_m = 0.05$ and $\omega = 4\pi$ [rad/s] are selected [16].

This method is better than the other techniques, because it does not require many measurements, especially there are no mechanical measurements and it does need any information or any knowledge about the system. On the other hand, the control system is too sensitive to measurements errors, so that a proper filter and highly accurate current transformers should be chosen.

1.3 The Selected Topology

The selected topology for the wind power system is given in Figure 1.17. The system is connected to the grid with a series of converters which means that system can work at different wind speeds and also means that a MPPT algorithm which commands the system to run at the optimum angular speed can be implemented. The shaft of the PMSG is connected directly to wind turbine without a gearbox. This will eliminate the noise and the losses caused by the gearbox. The generator is chosen as a permanent magnet synchronous generator, which means that the maintenance costs will be low. The reactive power in the machine can not be controlled. Electronic side consists of an uncontrolled rectifier, LC filter which will filter the harmonics on the dc bus and IGBT inverter which can control the amplitude and the phase shift of the line current meaning that inverter directly control the active and reactive power transferred to the grid at constant line voltage.

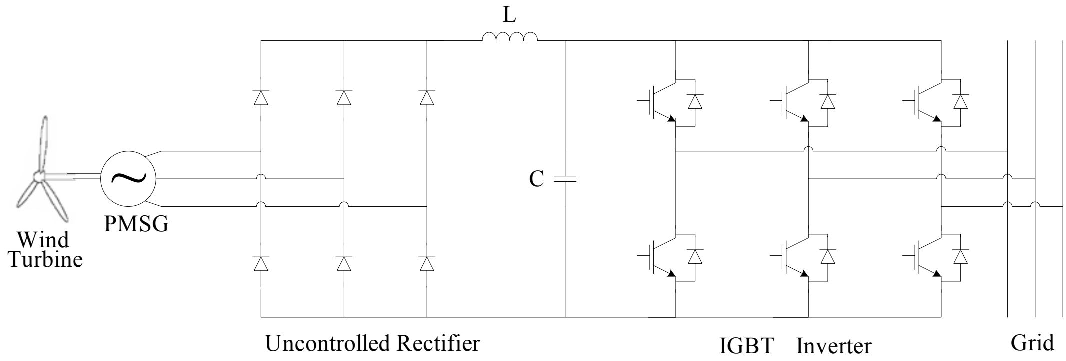

Figure 1.18: The selected topology for variable-speed wind turbine

2. Modeling of the Selected Topology

2.1 Introduction

The mathematical modeling of the real physical system is an important concept in many engineering and science disciplines. The derived models can be used in simulation, controller design, and design of a new process without any physical work. There three main groups in modeling [4]:

1) White box approach

2) Black box approach

3) Grey box approach

2.1.1 White Box Modeling

Conventionally modeling is to understand the nature and the behavior of the system and to state them mathematically. This approach is called white box modeling. For white box modeling, physical and chemical laws are used. As an example in modeling of a electromechanical system, electrical laws (Kirchoff voltage and current law, Faraday's law, Ampere's law,…), mechanical laws (the continuity of space, Dalembert's law, Newton's law,…) and the conservation of energy law are used. For nonlinear and complex systems, this type of modeling is hard and sometimes impossible. In general for complex systems, some assumptions can be done to reduce of the complexity [4].

2.1.2 Black Box Modeling

It is used for physically unknown systems. The only similarity between the model and the physical system is the behavior of them for the same inputs, but interior behavior is almost different. Fuzzy and artificial neural network modeling are an example for the black box [4].

2.1.3 Grey Box Modeling

This is the combination of both white box and the black box modeling. The physically well known or semi-known parts are modeled like white box and unknown parts are modeled by black box. The common methods for grey box modeling are system identification methods [4].

For modeling the selected topology, white box approach will be used, but for determining the parameters or the coefficients of the model, system identification experiments can be done. It is required to make some assumptions to reduce the complexity of the system. For electrical converter side (inverter and rectifier) it is assumed that the semiconductor switches are lossless and switchings are instantaneous. For turbine side, it is assumed that the mass of inertia is focused on a single point (lumped parameter model). For generator side it is assumed that, the windings in stator are distributed in a way that the flux in the air gap is in a sinusoidal form; there are no any saturation, slot effects, hysteresis and skin effect; magnetic permeability of the generator core is infinite and winding resistance and inductance values are independent from temperature. The saliency effects of the permanent magnets are neglected and it is assumed that a single large magnet is located in rotor of the generator.

2.2 Wind Turbine Modeling

2.2.1 Wind Stream Power

The Kinetic energy of air as an object of mass m [kg] moving with speed v [m/s] is equal to[5]:

$$E = \frac{1}{2} m v^2 \tag{2.1}$$

The power of the moving air (assuming constant wind velocity) is equal to:

$$P_{wind} = \frac{dE}{dt} = \frac{1}{2} \dot{m} v^2 \tag{2.2}$$

where $\dot{m}$ [kg/s] is the mass flow rate per second. When the air passes across an area A [m^2] (for example: the area swept by the rotor blades), the power of the wind can be computed as [5]:

$$P_{wind} = \frac{1}{2}\rho A v^3 \qquad \textbf{(2.3)}$$

where ρ (kg/m^3) is the air density which depends on the air temperature and air pressure. According to gas law:

$$\rho = m_m \frac{p}{RT} \qquad \textbf{(2.4)}$$

Where p [atm] is the pressure, R $(8.2057x10^{-5}\ \frac{m^3 atm}{mol\,K})$ is the gas constant, T [K] is the temperature of air and m_m [kg/mol] molar mass of the air [5]. The air density is 1.255 kg/m^3 under the conditions of 1 atm air pressure and 15 ^{o}C ambient temperature.

2.2.2 Mechanical Power Extracted From the Wind

The wind energy as described can not be transferred into another type of energy with %100 conversion efficiency by any energy converter. In fact, the power extracted from the air stream by any energy converter will be also less than the wind power P_{wind} because the power achieved by the energy converter P_{ww} can be computed as the difference between the power in the moving air before and after the converter [5] The air stream cross-section area of moving air before turbine A_1 is smaller than the one after turbine A_2.

$$P_{ww} = P_{wind1} - P_{wind2} = \frac{1}{2}\rho(A_1 v_1{}^3 - A_2 v_2{}^3) \qquad \textbf{(2.5)}$$

From the Figure 2.1 v_1 is the speed of the wind before the wind turbine, and v_2 is the speed of the wind after the wind turbine. Full conversion of wind power requires that air velocity after converter v_2 becomes zero, which is physically, makes no sense, because it constrains the air to be still and further it requires the air velocity before the converter v_1 to be equal to zero also.

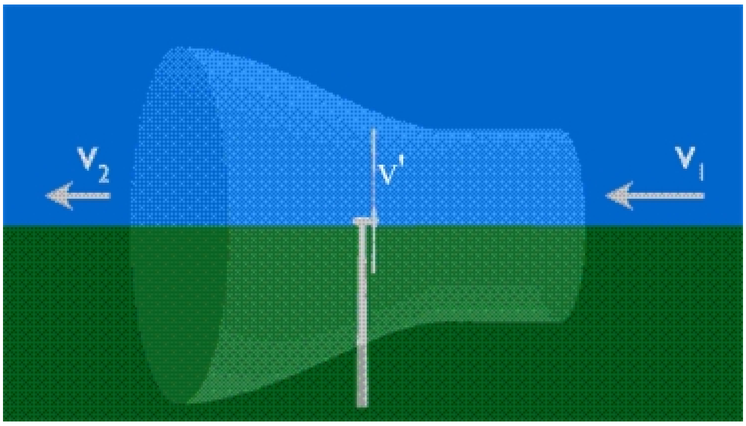

Figure 2.1: Wind speeds before and after wind turbine [3]

The real energy converter must be considered as a type of bulkhead. Then the flowing air exerts a force on the converter. The result of being that, the pressure before the converter increases and simultaneously the air velocity in front of the wind converter *($v^{'}$)* decreases [5].

The force [N] exerted on the converter can be found from the change of momentum.

$$F = \dot{m}(v_1 - v_2) \tag{2.6}$$

The extracted mechanical power by this force is equal to:

$$P_{WW} = Fv^{'} = \dot{m}(v_1 - v_2)v^{'} \tag{2.7}$$

Assuming that the mass flow rate is constant, it can be seen that the air velocity through the converter is equal to average of v_1 and v_2.

$$v^{'} = \frac{1}{2}(v_1 + v_2) \tag{2.8}$$

Then the mechanical power *(P_{WW})* extracted from the air stream by the energy converter is equal to

$$P_{WW} = \frac{1}{4}\rho A(v_1^2 - v_2^2)(v_1 + v_2) \tag{2.9}$$

and it is less than the power in the air stream before the converter P_{wind}. The equation (2.9) can also be written as follows:

$$P_{WW} = C_p P_{wind} = C_p \frac{1}{2} \rho A v_1^{\,3} \tag{2.10}$$

where the coefficient $C_p < 1$ (defining the ratio of the mechanical power extracted by the converter to the power in the air stream) is called the power coefficient (Betz's factor). This coefficient is equal to [5]:

$$C_p = \frac{1}{2}\left(1 - \left(\frac{v_2}{v_1}\right)^2\right)\left(1 + \frac{v_2}{v_1}\right) \tag{2.11}$$

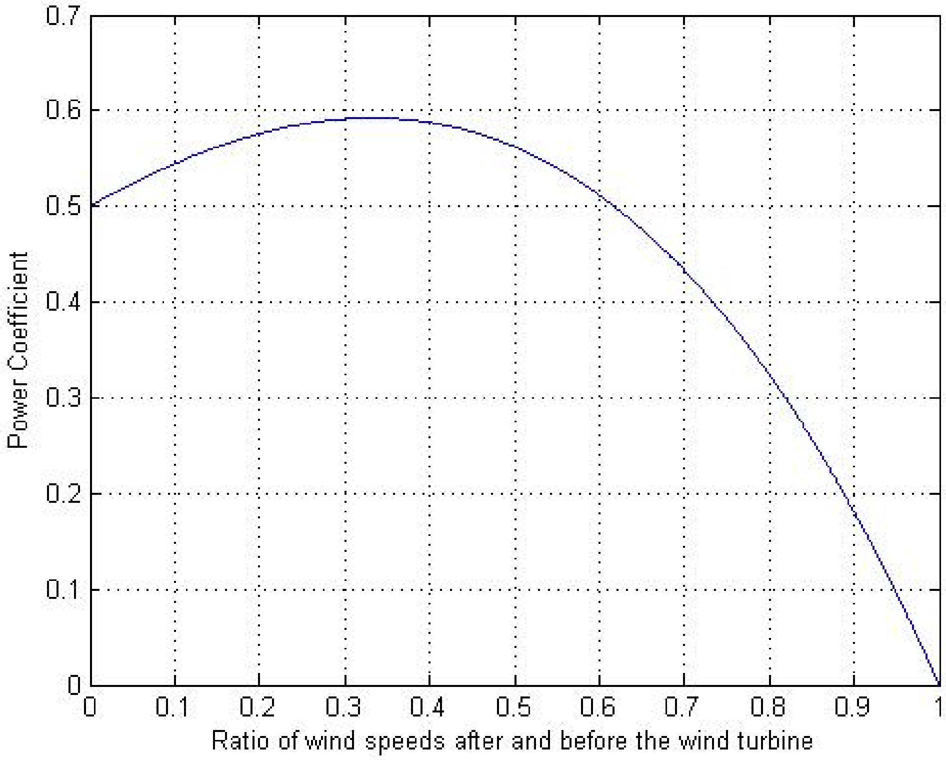

Figure 2.2: Power Coefficient-Speed Ratio

From the Figure 2.2, or by simply taking derivative of C_p with respect to v_2/v_1 and equating it to zero, will indicate a maximum value of C_p is nearly 0.593. At this maximum value, speed ratio is equal to $v_2/v_1=1/3$. Then in front of and behind the energy converter the wind speed is equal to $v' = 2v_1/3$, $v_2 = v_1/3$ respectively.

The power coefficient of real converters C_p achieves lower values than that of computed above, because of various aerodynamic losses that depend on the rotor construction (number and shape of blades, weight, stiffness, etc.). The rotor power coefficient is usually given as a function of two parameters: tip speed ratio (λ) and the blade pitch angle (β). The blade pitch angle is defined as the angle between the plane of rotation and the blade cross-section chord (Figure 2.3).

The tip speed ratio λ is defined as.

$$\lambda = \frac{u}{v_1} = \frac{\omega R}{v_1} \tag{2.12}$$

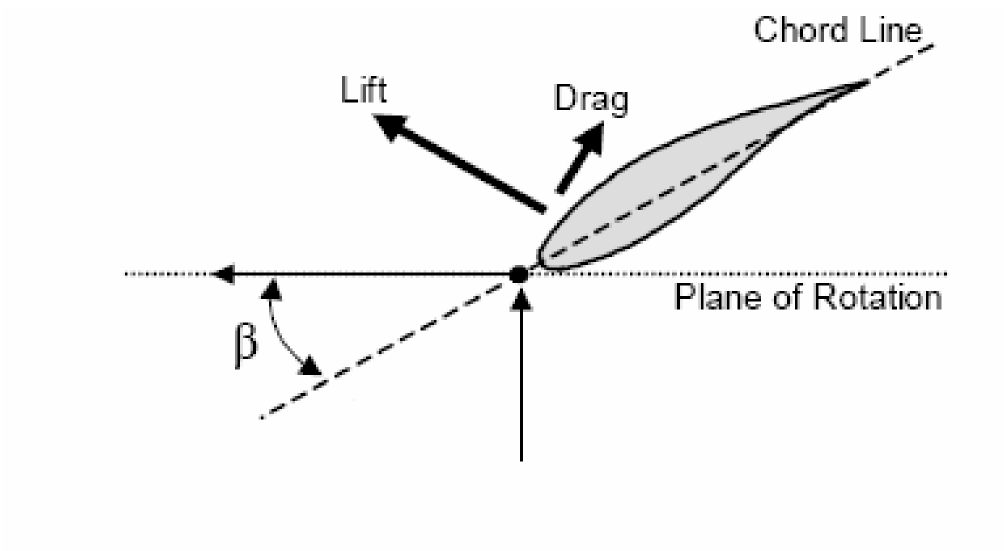

Figure 2.3: Wind turbine blade [2]

where u [m/s] is the tangential velocity of the blade tip, ω [rad/s] is the angular velocity of blade tip, R is rotor radius or blade length.

Figure 2.4 can only be obtained by experiments. A generic equation is used to model $C_p(\lambda, \beta)$. This equation is based on the modeled turbine characteristic and is given as [6]

$$C_p(\lambda, \beta) = c_1\left(\frac{c_1}{\lambda_i} - c_3\beta - c_4\right)e^{-\frac{c_5}{\lambda_i}} + c_6\lambda$$
$$\frac{1}{\lambda_i} = \frac{1}{\lambda + 0.008\beta} - \frac{0.035}{\beta^3 + 1} \tag{2.13}$$

where c_i are the coefficients which depend on turbine type. For a three blade turbine the coefficients c_1 = 0.5176, c_2 = 116, c_3 = 0.4, c_4 = 5, c_5 = 21 and c_6 = 0.0068 the C_p-λ curve for different blade angles can be drawn like in Figure 2.5 [6]. In some cases pitch control is not used, instead the blade angle is fixed to value zero (stall control). An example for a stall controlled wind turbine power diagram is given in Figure 2.6 [6].

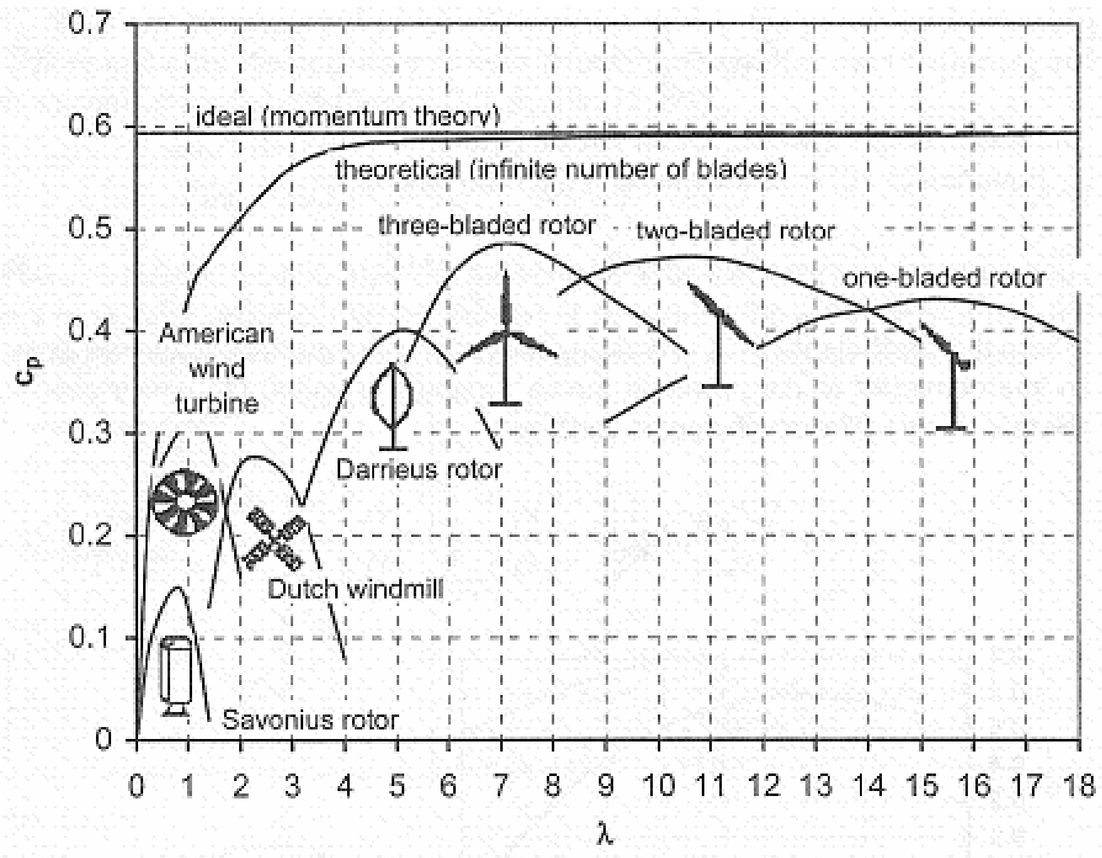

Figure 2.4: Turbine curves for different types of wind turbines [5]

The model of blade pitch control will not be discussed in this thesis.

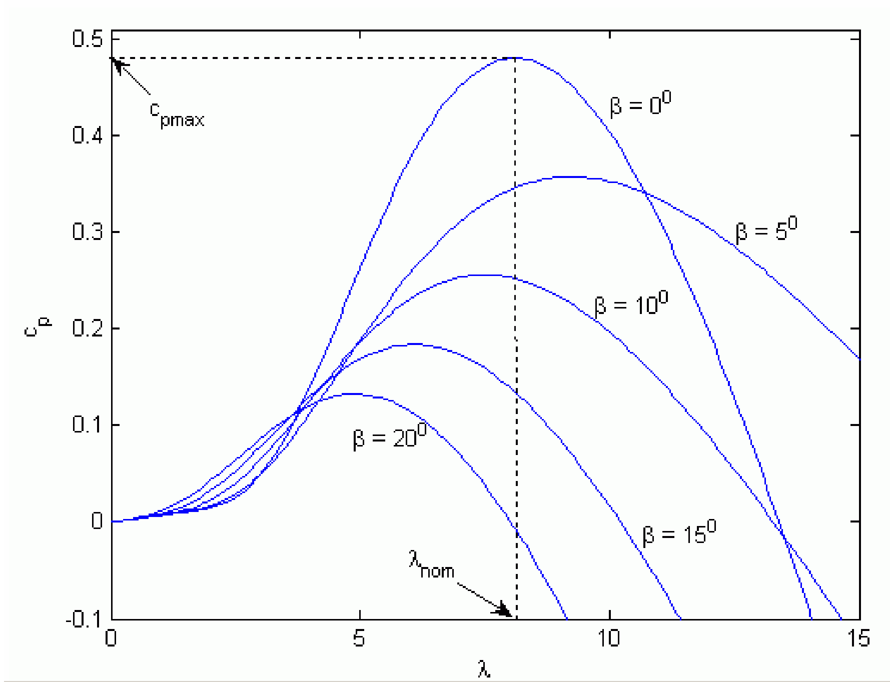

Figure 2.5: C_p- λ curve for different blade angles [6]

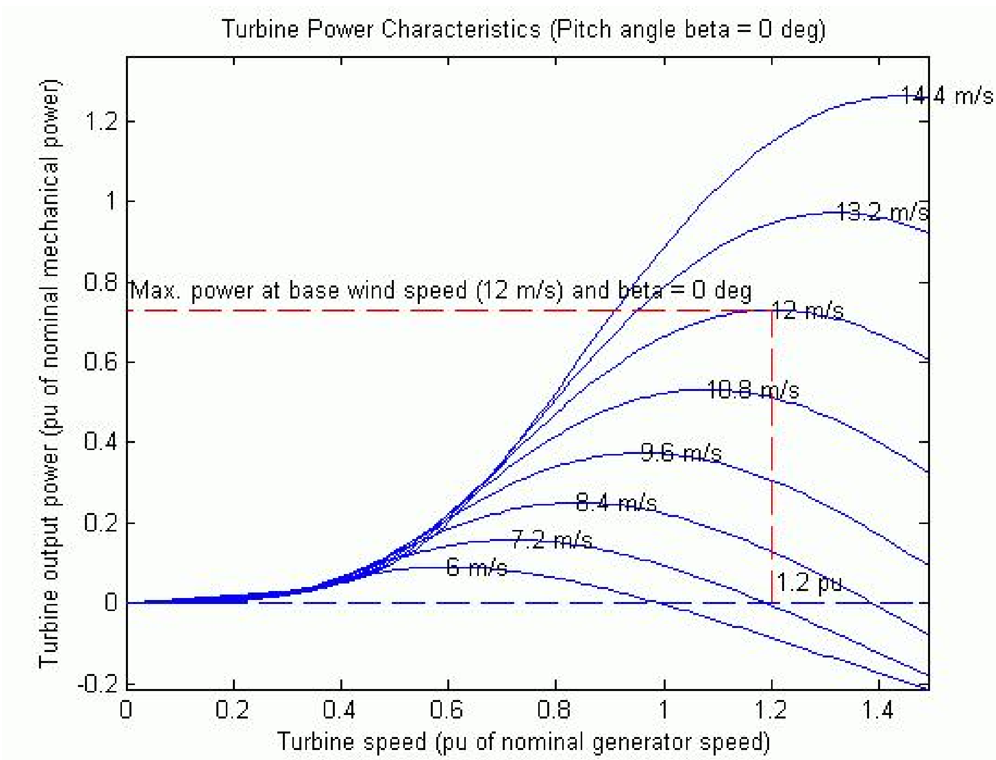

Figure 2.6: An example of a turbine characteristic with different wind speeds with stall control [6].

2.2.3 Drive Train (Shaft) Model (Dynamic Model)

Wind turbine consists of many mechanical components. Each component has its own dynamic behavior but the dynamic of the drive train is dominant to other parts. Thus the dynamic model of the drive train can be said to be the dynamic model of the whole turbine [5].

The drive train of a wind turbine generator system in general consists of blade pitching mechanism with a spinner, a hub with blades, a rotor shaft and generator. The moment of inertia of the wind wheel (hub with blades) is about %90 of the drive train total moment of inertia, while the generator rotor moment of inertia is equal to about 6-8%. The remaining parts of the drive train comprise the rest (2-4%) of the total moment of inertia [5].

The acceptable (and common) way to model the WTGS rotor is to treat the rotor as a number of discrete masses connected together by springs defined by damping and stiffness coefficients. Therefore the equation of the i^{th} mass motion can be described as follows [5]:

$$J_i \frac{d^2\delta_i}{dt^2} = T_i + T_{i,i+1} - T_{i,i-1} - B_i \frac{d\delta_i}{dt} \quad \textbf{(2.14)}$$

where J_i is the moment of inertia of i^{th} mass, δ_i (rad) torsional angle of i^{th} mass , T_i is the external torque applied to i^{th} mass, $T_{i,i-1}$ and $T_{i,i+1}$ are the torques applied to i^{th} mass (from $i,(i-1)^{th}$ and $i,(i+1)^{th}$ shafts respectively), B_i is the damping coefficient representing various damping effects. The torques $T_{i,i+1}$, T_{i-1} can be written as follows:

$$T_{i,i+1} = K_{i,i+1}(\delta_{i+1} - \delta_i) + B_{i,i+1}\left(\frac{d\delta_{i+1}}{dt} - \frac{d\delta_i}{dt}\right) \quad \textbf{(2.15)}$$

$$T_{i,i-1} = K_{i,i-1}(\delta_i - \delta_{i-1}) + B_{i,i-1}\left(\frac{d\delta_i}{dt} - \frac{d\delta_{i-1}}{dt}\right) \quad \textbf{(2.16)}$$

where $K_{i,i+1}, K_{i,i-1}$ are the stiffness coefficients of the shaft sections between mass $i,(i+1)^{th}$ and $i,(i-1)^{th}$ respectively and $B_{i,i+1}, B_{i,i-1}$ are the damping coefficients of the shaft sections. By combining these equations, equation of motion of the i^{th} mass can be obtained [5].

$$J_i \frac{d^2\delta_i}{dt^2} = T_i + K_{i,i+1}(\delta_{i+1} - \delta_i) + B_{i,i+1}\left(\frac{d\delta_{i+1}}{dt} - \frac{d\delta_i}{dt}\right) - B_i \frac{d\delta_i}{dt}$$

$$- K_{i,i-1}(\delta_i - \delta_{i-1}) - B_{i,i-1}\left(\frac{d\delta_i}{dt} - \frac{d\delta_{i-1}}{dt}\right) \quad \textbf{(2.17)}$$

For many types of analysis, a set of first-order differential equations is a useful form of equation because they can be written in matrix form and can be solve easily. Thus the equation above takes the form of these two equations:

$$\frac{d\delta_i}{dt} = \Delta\omega_i \quad \textbf{(2.18)}$$

$$J_i \frac{d\Delta\omega_i}{dt} = T_i + K_{i,i+1}(\delta_{i+1} - \delta_i) + B_{i,i+1}(\Delta\omega_{i+1} - \Delta\omega_i) - B_i\Delta\omega_i \quad \textbf{(2.19)}$$

$$- K_{i,i-1}(\delta_i - \delta_{i-1}) - B_{i,i-1}(\Delta\omega_i - \Delta\omega_{i-1})$$

Considering the drive train as consisting of *N* discrete masses, we obtain a set of *2N* differential equations. It is difficult to solve these equations and also to suggest a controller for the system. Therefore, lumped parameter approach will be used to simplify and to reduce the number of equations. The minimal realization of the drive train model utilized in the power system operation analysis is based on the assumption of the two lumped – masses only. The structure of the model is presented in Figure 2.7.

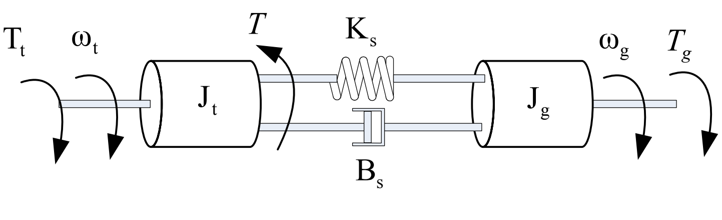

Figure 2.7: The dynamic model of the drive train

$$\frac{d\theta_t}{dt} = \omega_t \quad \textbf{(2.20)}$$

$$\frac{d\theta_g}{dt} = \omega_g \tag{2.21}$$

$$T - T_t = J_t \frac{d\omega_t}{dt} \tag{2.22}$$

$$T - T_g = J_g \frac{d\omega_g}{dt} \tag{2.23}$$

$$T = K_s(\theta_t - \theta_g) + B_s(\omega_t - \omega_g) \tag{2.24}$$

where θ_t, θ_g are the angular positions of turbine and generator shafts, respectively ω_t, ω_g are the angular speeds of turbine and generator shaft, respectively, T_t, T_g are the torques that applied to shaft by the turbine and generator, respectively, T is the net torque on the shaft, B_s is the damping coefficient of shaft and K_s is the stiffness of the shaft. By combining these equations and writing them in state space, the following matrix is achieved:

$$\frac{d}{dt}\begin{bmatrix} \omega_t \\ \omega_g \\ \theta_t \\ \theta_g \end{bmatrix} = \begin{bmatrix} \frac{B_s}{J_t} & \frac{-B_s}{J_t} & \frac{K_s}{J_t} & \frac{-K_s}{J_t} \\ \frac{B_s}{J_g} & \frac{-B_s}{J_g} & \frac{K_s}{J_g} & \frac{-K_s}{J_g} \\ 1 & 0 & 0 & 0 \\ 0 & 1 & 0 & 0 \end{bmatrix} \begin{bmatrix} \omega_t \\ \omega_g \\ \theta_t \\ \theta_g \end{bmatrix} + \begin{bmatrix} -1 & 0 \\ 0 & -1 \\ 0 & 0 \\ 0 & 0 \end{bmatrix} \begin{bmatrix} T_t \\ T_g \end{bmatrix} \tag{2.25}$$

If we assume that the angular speed of generator and turbine is equal, in general this equation can be solved like this:

$$T_t = (J_g + J_t)\frac{d\omega_g}{dt} - T_g \tag{2.26}$$

2.2.4 Relation between Static and Dynamic Model of Wind Turbine

In static model of the turbine the relationship between the power of the turbine and speed of the turbine is expressed for a given wind speed. As for dynamic model, the relationship between the speed of the shaft, the torque of the generator and the torque of the wind turbine is derived. The relation between torque and power of the turbine which should be expressed for a complete model, is missing. In general, the torque is known as;

$$T_t = \frac{P_t}{\omega_t} \tag{2.27}$$

From the power equation of the turbine;

$$T_t = \frac{0.5C_p \rho \pi R^2 v^3}{\omega_t} = \frac{0.5C_p \rho \pi R^2 v^3}{\frac{\lambda v}{R}} = \frac{C_p}{\lambda} 0.5 \rho \pi R^3 v^2 = C_\Gamma(\lambda) 0.5 \rho \pi R^3 v^2 \tag{2.28}$$

In this equation C_Γ is known as torque coefficient which is a function of tip speed ratio for a constant blade angle [5]. As explained earlier, there is not an exact equation for the power coefficient. So that, many kinds of mathematical curve fitting techniques are used to reach such an equation from the measurements of the experiments. The kind of fitting equation is important for calculating the torque coefficient, because there is zero over zero indefiniteness for the zero tip speed ratio, and it is a big problem for the computers to calculate the torque coefficient correctly. Thus, a polynomial will be the best choice to overcome this problem. The general polynomial form of the power coefficient is given as flows;

$$C_p = a_0 + \sum_{k=1}^{n} a_k \lambda^k \tag{2.29}$$

Where a_i are the coefficients of the polynomial, and n is the degree of the polynomial. For zero tip speed ratio, C_p should be zero. So that, $a_0 = 0$. From this equation, the torque coefficient can be calculated like this.

$$C_\Gamma = \sum_{k=1}^{n} a_k \lambda^{k-1} \tag{2.30}$$

The wind velocity usually varies considerably, and has stochastic character. Therefore, in general, the wind should be modeled as a stochastic process, but for the analysis of WTGS operation in an electric power system, the wind variation can be modeled as a sum of harmonics with frequencies in the range of 0.1-10 Hz. Wind gusts are usually also included in the wind model [5].

$$v(t) = v_0\left(1+\sum_k A_k \sin(\omega_k t)\right)+v_g(t) \tag{2.31}$$

$$v_g(t) = \frac{2v_{g\max}}{1+e^{-4(\sin(\omega_g t)-1)}} \tag{2.32}$$

where v_0 is the mean value of the wind velocity, A_k is the amplitude of k^{th} harmonic, ω_k is the frequency (pulsation) of k^{th} harmonic, $v_g(t)$ is the speed of the wind gust, $v_{g\max}$ is the gust amplitude and ω_g is the gust frequency. The gust amplitude varies up to 10 m/s and the gust period can be in the range of 10-50 s.

2.3 Modeling of Permanent Magnet Synchronous Machine

2.3.1 Winding Inductances and Voltage equations

In a magnetically linear system the self-inductance of a winding is the ratio of the flux linked by a winding to the current flowing in the winding with all other winding currents zero. Mutual inductance is the ratio of flux linked by one winding due to current flowing in a second winding with all other winding currents zero including the winding for which the flux linkage are determined [7].

MMF is defined as the line integral of *H* (the magnetic intensity) which is also equal to multiplication of number of turns *(N)* and the current *(I)* of the winding.

$$Ni = MMF = \int H\, dl \tag{2.33}$$

In magnetic circuit, if it is assumed that the magnetic permeability ($\mu = \mu_r \mu_0$) of the core is infinite, in the magnetic circuit the only reluctance is caused by the air gap, because the relative magnetic permeability of the air is one ($\mu_{airgap} = \mu_0$). So, from this approach

$$B = \mu_0 H = \mu_0 \frac{MMF}{g} \tag{2.34}$$

where B is magnetic field density and g is the air gap length. The air gap field density, due to the current in the *as* winding can be obtained by setting the other currents zero. For the Figure 2.8, if it is assumed that the conductors are located to stator slots in such a way that the number of turns of the conductors is in sinusoidal form through the air gap, the instantaneous MMF through the air gap has also sinusoidal form. The distribution of the *as* winding may be written [7]

$$N_{as} = N_p \sin\phi_s \qquad 0 \le \phi_s \le \pi \tag{2.35}$$

$$N_{as} = -N_p \sin\phi_s \qquad \pi \le \phi_s \le 2\pi \tag{2.36}$$

where N_p is the maximum turn or conductor density expressed in turns per radian. If Ns represents the number of turns of the equivalent sinusoidally distributed winding then

$$N_s = \int_0^{\pi} N_p \sin\phi_s d\phi_s = 2N_p \tag{2.37}$$

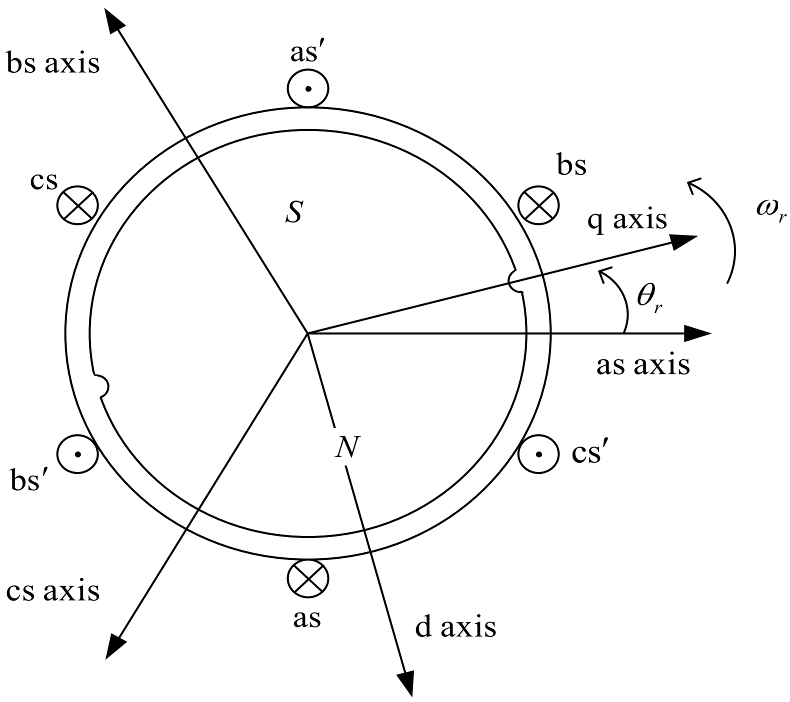

Figure 2.8: Basic structure of a two pole PMSG.

N_s is not the total number of turns of the winding which would rise to same fundamental component as the actual winding distribution. Because of the right hand rule, the angle between the current flow direction and magnetic field direction is 90^{o}. So that if the winding distribution is in like sinusoidal function, the MMF function will be like cosine function [7]. The MMF waveform of the equivalent *as* winding is

$$MMF_a = \frac{N_s}{2} i_a \cos\phi_s \quad \textbf{(2.38)}$$

In a similar way:

$$MMF_b = \frac{N_s}{2} i_b \cos\left(\phi_s - \frac{2\pi}{3}\right) \quad \textbf{(2.39)}$$

$$MMF_c = \frac{N_s}{2} i_c \cos\left(\phi_s + \frac{2\pi}{3}\right) \quad \textbf{(2.40)}$$

The total air-gap MMF produced by the stator currents can be expressed. This can be obtained by adding the individual MMFs [8].

$$MMF_s = \frac{N_s}{2}\left[i_a \cos\phi_s + i_b \cos\left(\phi_s - \frac{2\pi}{3}\right) + i_c \cos\left(\phi_s + \frac{2\pi}{3}\right)\right] \quad \textbf{(2.41)}$$

The magnetic flux density functions caused by each of the windings can be found. Thus the magnetic flux density with all other currents are zero except i_a is:

$$B = \mu_0 \frac{N_s}{2g} i_a \cos\phi_s \quad \textbf{(2.42)}$$

Similarly the flux density function with all other currents are zero except i_b is:

$$B = \mu_0 \frac{N_s}{2g} i_b \cos\left(\phi_s - \frac{2\pi}{3}\right) \quad \textbf{(2.43)}$$

And also with all currents other than i_c is zero.

$$B = \mu_0 \frac{N_s}{2g} i_c \cos\left(\phi_s + \frac{2\pi}{3}\right) \quad \textbf{(2.44)}$$

Flux linkages of a single turn of a stator winding which spans π radians and which is located at the angle ϕ_s can be considered [7]. In this case the flux is determined by performing a surface integral over the open surface of the single turn. In particular

$$\Phi(\phi_s) = \int_{\phi_s}^{\phi_s+\pi} B(\xi) rl d\xi \qquad \textbf{(2.45)}$$

where Φ is the flux linking a single turn oriented ϕ_s from the *as* axis, *l* is the axial length of the air gap of the machine, *r* is the radius to the mean of the air gap (essentially to the inside circumference of the stator), and ξ is a dummy variable of the integration. In order to obtain the flux linkages of an entire winding the flux linked by each turn must be summed. Since the windings are considered to be sinusoidally distributed and the magnetic system is assumed to be linear, this summation may be accomplished by integrating over all coil sides carrying current in the same direction. Hence, computation of the flux linkages of an entire winding involves a double integral [7]. As an example, in determining the total flux linkage of the *as* winding due to current flowing only in the *as* winding can be done like this.

$$\begin{aligned} \lambda_{as} &= L_{ls} i_a + \int N_{as}(\phi_s)\Phi(\phi_s) d\phi_s \\ &= L_{ls} i_a + \int N_{as}(\phi_s) \int_{\phi_s}^{\phi_s+\pi} B(\xi) rl d\xi \end{aligned} \qquad \textbf{(2.46)}$$

In Eq. 2.46 L_{ls} is the stator leakage inductance due primarily to leakage flux at the end turns. Generally this inductance accounts for 5 to 10 percent of the maximum self-inductance [7].

$$\begin{aligned} \lambda_{as} &= L_{ls} i_a - \int_{\pi}^{2\pi} \frac{N_s}{2} \sin\phi_s \int_{\phi_s}^{\phi_s+\pi} \mu_0 \frac{N_s}{2g} i_a \cos\phi_s rl \, d\xi \, d\phi_s \\ &= L_{ls} i_a + \left(\frac{N_s}{2}\right)^2 \frac{\pi\mu_0 rl}{g} i_a \end{aligned} \qquad \textbf{(2.47)}$$

The interval of integration is taken from π to 2π so as to comply with the convention that positive flux linkages are obtained in the direction of the positive *as* axis by circulation of the assumed positive current in the clockwise direction about the coil (right hand rule). The self inductance of the *as* winding is obtained by dividing λ_{as} by I_a.

$$L_{aa} = L_{ls} + \left(\frac{N_s}{2}\right)^2 \frac{\pi\mu_0 rl}{g} \tag{2.48}$$

The mutual inductance between the *as* and *bs* winding may determined by the first computing the flux linking the as winding due to current flowing only in the *bs* winding [7]. In this case it is assumed that the magnetic coupling which might occur at the end turns of the windings may be neglected. Thus

$$\begin{aligned}\lambda_{as} &= \int N_{as}(\phi_s) \int_{\phi_s}^{\phi_s+\pi} B(\xi) rl d\xi d\phi_s \\ &= -\int_{\pi}^{2\pi} \frac{N_s}{2}\sin\phi_s \int_{\phi_s}^{\phi_s+\pi} \mu_0 \frac{N_s}{2g} i_b \cos\left(\xi - \frac{2\pi}{3}\right) rl d\xi d\phi_s\end{aligned} \tag{2.49}$$

Therefore, the mutual inductance between the *as* and *bs* windings is determined by dividing λ_{as} by I_b. So this gives

$$L_{ab} = -\left(\frac{N_s}{2}\right)^2 \frac{\pi}{2g}\mu_0 rl \tag{2.50}$$

The other mutual and self inductances can be calculated in the some manner. In general inductances can be defined as

$$L_A = \left(\frac{N_s}{2}\right)^2 \frac{\pi\mu_0 rl}{g} \tag{2.51}$$

By using this definition the stator inductance elements can be expressed like this:

$$L_{aa} = L_{bb} = L_{cc} = L_{ls} + L_A \tag{2.52}$$

$$L_{ab} = L_{ba} = L_{ca} = L_{ac} = L_{bc} = L_{cb} = -\frac{1}{2}L_A \tag{2.53}$$

The matrix form of the stator flux linkage is given as:

$$\boldsymbol{\lambda_s} = \begin{bmatrix} \lambda_{as} \\ \lambda_{bs} \\ \lambda_{cs} \end{bmatrix} = \begin{bmatrix} L_{ls} + L_A & -\frac{1}{2}L_A & -\frac{1}{2}L_A \\ -\frac{1}{2}L_A & L_{ls} + L_A & -\frac{1}{2}L_A \\ -\frac{1}{2}L_A & -\frac{1}{2}L_A & L_{ls} + L_A \end{bmatrix} \begin{bmatrix} i_a \\ i_b \\ i_c \end{bmatrix} = \boldsymbol{L\,I} \qquad \textbf{(2.54)}$$

Where $\boldsymbol{L}$ is the inductance matrix and $\boldsymbol{I}$ is the winding current matrix.

2.3.2 The permanent magnet linkage

PMSG has permanent magnet sticks which are located on the surface of the rotor wheel. In equivalent system it can be assumed that the rotor is consist of a single magnet which can rotate around of its center. It is also assumed that the conductance of the magnet is poor that the flux which is produced by the stator currents do not induce a voltage on the magnet. So the mutual inductance between stator and the magnet is zero, or the magnet current is zero. This current will not appear as a state variable. Permanent magnets can be modeled as a constant flux linkage source with a constant value. The equivalent flux linkage circled by the phase windings depends on the angle between the stator and the rotor magnetic axis θ_r [7].

$$\boldsymbol{\lambda_r} = \begin{bmatrix} \lambda_{ra} \\ \lambda_{rb} \\ \lambda_{rc} \end{bmatrix} = \lambda_f \begin{bmatrix} \sin\theta_r \\ \sin\left(\theta_r - \frac{2\pi}{3}\right) \\ \sin\left(\theta_r + \frac{2\pi}{3}\right) \end{bmatrix} \qquad \textbf{(2.55)}$$

where λ_f is the maximum value of magnet flux linkage. So the total flux linkage in the machine is.

$$\boldsymbol{\lambda} = \boldsymbol{\lambda_s} + \boldsymbol{\lambda_r} = \begin{bmatrix} L_{ls} + L_A & -\frac{1}{2}L_A & -\frac{1}{2}L_A \\ -\frac{1}{2}L_A & L_{ls} + L_A & -\frac{1}{2}L_A \\ -\frac{1}{2}L_A & -\frac{1}{2}L_A & L_{ls} + L_A \end{bmatrix} \begin{bmatrix} i_a \\ i_b \\ i_c \end{bmatrix} + \lambda_f \begin{bmatrix} \sin\theta_r \\ \sin\left(\theta_r - \frac{2\pi}{3}\right) \\ \sin\left(\theta_r + \frac{2\pi}{3}\right) \end{bmatrix} \qquad \textbf{(2.56)}$$

The voltage equations for the PMSM

$$\boldsymbol{V} = \begin{bmatrix} v_a \\ v_b \\ v_c \end{bmatrix} = \boldsymbol{R}\,\boldsymbol{I} + \frac{d\boldsymbol{\lambda}}{dt} \tag{2.57}$$

$$\boldsymbol{R} = \begin{bmatrix} R_s & 0 & 0 \\ 0 & R_s & 0 \\ 0 & 0 & R_s \end{bmatrix} \tag{2.58}$$

2.3.3 The Torque Equation

For a linear magnetic system the torque induced in system is defined as the change of the energy in the magnetic coupling area according to position of the rotor. This means that [8]

$$T_e = \frac{\partial W_c}{\partial \theta_r} \tag{2.59}$$

$$W_c = \frac{1}{2}\boldsymbol{\lambda}\,\boldsymbol{I} \tag{2.60}$$

So that, the torque equation is given below.

$$\boldsymbol{T_e} = \frac{1}{2}\boldsymbol{I} \begin{bmatrix} \cos\theta_r \\ \cos\left(\theta_r - \frac{2\pi}{3}\right) \\ \cos\left(\theta_r + \frac{2\pi}{3}\right) \end{bmatrix} \lambda_f \tag{2.61}$$

Later this equation will equal to T_g, which is defined in the dynamic behavior of the turbine.

2.3.4 Reference-Frame Theory

It can be clearly seen that some of the machine coefficients of the differential equations (voltage equations) which describe the behavior of this machine are time-varying except when the rotor is stalled. Change of variables is used to reduce the complexity of these differential equations. There are several changes of variables which are used and it was originally thought that each change of variables was different and therefore they were treated separately. It was later learned that all changes of variables used to transform real variables are contained in one. This general transformation refers machine variables to a frame of reference which rotates at an arbitrary angular velocity. All known real transformations are obtained from this general transformation by simply assigning the speed of rotation of the reference frame [7].

A change of variables which formulates a transformation of the 3-phase variables of stationary circuit elements to the arbitrary reference frame may be expressed

$$f_{qd0s} = K_s f_{abcs} \tag{2.62}$$

where $\mathbf{K_s}$ is the transformation matrix between the frames, f_{abcs} is the variable matrix which are referred to *abc* frame and f_{qd0s} is transformed variable matrix which are referred to *dq* axes. The transformation matrix may have different forms. The most recently used one given below [7].

$$\boldsymbol{K}_s = \frac{2}{3}\begin{bmatrix} \cos\theta & \cos\left(\theta - \frac{2\pi}{3}\right) & \cos\left(\theta + \frac{2\pi}{3}\right) \\ \sin\theta & \sin\left(\theta - \frac{2\pi}{3}\right) & \sin\left(\theta + \frac{2\pi}{3}\right) \\ \frac{1}{2} & \frac{1}{2} & \frac{1}{2} \end{bmatrix} \tag{2.63}$$

where θ is the angle between q and a axes. If ω is the angular speed of frame set:

$$\theta = \int_0^t \omega(\xi)d\xi + \theta(0) \tag{2.60}$$

The inverse of the transformation matrix given below is:

$$\boldsymbol{K}^{-1} = \begin{bmatrix} \cos\theta & \sin\theta & 1 \\ \cos\left(\theta - \frac{2\pi}{3}\right) & \sin\left(\theta - \frac{2\pi}{3}\right) & 1 \\ \cos\left(\theta + \frac{2\pi}{3}\right) & \sin\left(\theta + \frac{2\pi}{3}\right) & 1 \end{bmatrix} \tag{2.65}$$

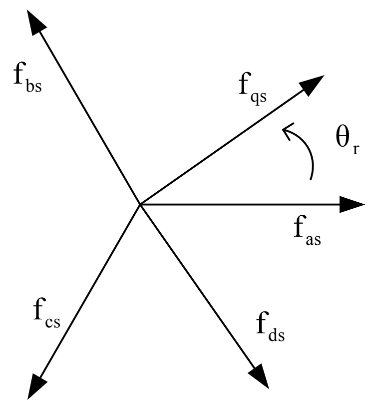

Figure 2.9: The abc and dq frames.

A transformation matrix has a constraint that the power in the *abc* frame should be equal to the power on the *dq* variables.

$$P_{abcs} = P_{qd0s} \qquad \textbf{(2.66)}$$

$$v_a i_a + v_b i_b + v_c i_c = \frac{3}{2}(v_q i_q + v_d i_d + 2v_0 i_0) \qquad \textbf{(2.67)}$$

and for balanced system which means that $f_a + f_b + f_c = 0$ the zero component of the *dq* axes is

$$f_0 = \frac{3}{4}(f_a + f_b + f_c) = 0 \qquad \textbf{(2.68)}$$

So that, the equation for the zero components, will drop. For the PMSM this means that the number of equation which describes the dynamic of the machine will decrease one. This transformation will be applied to voltage and torque equations which are derived below.

$$\boldsymbol{V} = \boldsymbol{RI} + \frac{d\boldsymbol{\lambda}}{dt} = \boldsymbol{RI} + \frac{d}{dt}(\boldsymbol{\lambda}_s + \boldsymbol{\lambda}_r) \qquad \textbf{(2.69)}$$

$$\boldsymbol{K}_s\boldsymbol{V} = \boldsymbol{K}_s\boldsymbol{R}\boldsymbol{K}_s^{-1}\boldsymbol{I}_{qd} + \boldsymbol{K}_s\frac{d}{dt}(\boldsymbol{K}_s^{-1}\lambda_{qd}) + \boldsymbol{K}_s\frac{d\boldsymbol{\lambda r}}{dt} \qquad \textbf{(2.70)}$$

$$\boldsymbol{V}_{dq} = \boldsymbol{K}_s\boldsymbol{R}\boldsymbol{K}_s^{-1}\boldsymbol{I}_{qd} + \boldsymbol{K}_s\frac{d\boldsymbol{K}_s^{-1}}{dt}\lambda_{qd} + \boldsymbol{K}_s\boldsymbol{K}_s^{-1}\frac{d\boldsymbol{\lambda}_{qd}}{dt} + \boldsymbol{K}_s\frac{d\boldsymbol{\lambda}_r}{dt} \qquad \textbf{(2.71)}$$

2.3.5 Resistive Elements

$$\boldsymbol{K}_s \boldsymbol{R} \boldsymbol{K}_s^{-1} = \boldsymbol{R} \qquad \textbf{(2.72)}$$

Thus, the resistance matrix associated with the arbitrary reference variables is equal to the resistance matrix associated with the actual variables if each phase of the actual circuit has the same resistance, but if the resistance are not balanced the transformed matrix will be include sinusoidal functions. To overcome this problem, a fixed reference frame can be selected [7].

2.3.6 Inductance Elements

Inductance elements are the elements which are related with stator flux linkage. First find the derivative of the inverse transformation matrix.

$$\frac{d\boldsymbol{K}_s^{-1}}{dt} = \omega \begin{bmatrix} -\sin\theta & \cos\theta & 0 \\ -\sin\left(\theta - \frac{2\pi}{3}\right) & \cos\left(\theta - \frac{2\pi}{3}\right) & 0 \\ -\sin\left(\theta + \frac{2\pi}{3}\right) & \cos\left(\theta + \frac{2\pi}{3}\right) & 0 \end{bmatrix} \qquad \textbf{(2.73)}$$

Multiplying it with the transformation matrix:

$$\boldsymbol{K}_s \frac{d\boldsymbol{K}_s^{-1}}{dt} = \omega \begin{bmatrix} 0 & 1 & 0 \\ -1 & 0 & 0 \\ 0 & 0 & 0 \end{bmatrix} \qquad \textbf{(2.74)}$$

Apply the results to inductance element part of the voltage equation.

$$\Rightarrow \boldsymbol{K}_s \frac{d\boldsymbol{K}_s^{-1}}{dt} \boldsymbol{\lambda}_{qd} + \boldsymbol{K}_s \boldsymbol{K}_s^{-1} \frac{d\boldsymbol{\lambda}_{qd}}{dt} = \omega \begin{bmatrix} \lambda_d \\ -\lambda_q \\ 0 \end{bmatrix} + \frac{d}{dt} \begin{bmatrix} \lambda_q \\ \lambda_d \\ \lambda_0 \end{bmatrix} \qquad \textbf{(2.75)}$$

The direct *(d)* and quadratic *(q)* flux linkages that are used in the above equation can be found by simply transferring the stator flux linkage to *dq* frame.

$$\lambda_s = \boldsymbol{L}\boldsymbol{I} \qquad \textbf{(2.76)}$$

$$\boldsymbol{\lambda_{dq}} = \boldsymbol{K_s L K_s}^{-1} \boldsymbol{I_{dq}} = \begin{bmatrix} L_{ls} + \frac{3}{2}L_A & 0 & 0 \\ 0 & L_{ls} + \frac{3}{2}L_A & 0 \\ 0 & 0 & L_{ls} \end{bmatrix} \begin{bmatrix} i_d \\ i_q \\ i_0 \end{bmatrix} \qquad \textbf{(2.77)}$$

The quadratic and direct inductances of the machine can be defined. The diagonal elements of the inductance matrix which is on *qd* frame are the inductance elements of the given axes. Because it is assumed that, there is no saliency neither on the rotor nor on the stator, the quadratic and direct inductance values equal. The definitions are given below [7]

$$\begin{aligned} &L_q = L_d = L_{ls} + 1.5L_A \\ &L_0 = L_{ls} \\ &\lambda_d = L_d i_d \\ &\lambda_q = L_q i_q \\ &\lambda_0 = L_0 i_0 = 0 \end{aligned} \qquad \textbf{(2.78)}$$

As seen earlier for a balanced system the zero components of the variables are zero. In our machine windings are wye connected. So that, the summation of winding currents will be zero and from the equation above the zero component of the flux linkage is zero. The final form is given below:

$$\Rightarrow \omega \begin{bmatrix} \lambda_d \\ -\lambda_q \\ 0 \end{bmatrix} + \frac{d}{dt} \begin{bmatrix} \lambda_q \\ \lambda_d \\ \lambda_0 \end{bmatrix} = \omega \begin{bmatrix} L_d i_d \\ -L_q i_q \\ 0 \end{bmatrix} + \begin{bmatrix} L_q \\ L_d \\ L_0 \end{bmatrix} \frac{d}{dt} \begin{bmatrix} i_q \\ i_d \\ 0 \end{bmatrix} \qquad \textbf{(2.79)}$$

Up to this point, an arbitrary reference frame set is used, which means that the angle θ is unaffected on the result of the resistive and stator inductive elements. In the transformation of magnetic element and the torque equation, we will see the importance of the selection of reference frame and later we will call this selection as park transformation [7].

2.3.7 Magnet Element

The magnetic element is given as

$$\boldsymbol{K}_s \frac{d\boldsymbol{\lambda}_r}{dt} \tag{2.80}$$

$$\frac{d\boldsymbol{\lambda}_r}{dt} = \lambda_f \omega_r \begin{bmatrix} \cos\theta_r \\ \cos\left(\theta_r - \frac{2\pi}{3}\right) \\ \cos\left(\theta_r + \frac{2\pi}{3}\right) \end{bmatrix} \tag{2.81}$$

Multiplying it with transformation matrix.

$$\boldsymbol{K}_s \frac{d\boldsymbol{\lambda}_r}{dt} = \frac{2}{3}\lambda_f \omega_r \begin{bmatrix} \cos\theta\cos\theta_r + \cos\left(\theta - \frac{2\pi}{3}\right)\cos\left(\theta_r - \frac{2\pi}{3}\right) + \cos\left(\theta + \frac{2\pi}{3}\right)\cos\left(\theta_r + \frac{2\pi}{3}\right) \\ \sin\theta\cos\theta_r + \sin\left(\theta - \frac{2\pi}{3}\right)\cos\left(\theta_r - \frac{2\pi}{3}\right) + \sin\left(\theta + \frac{2\pi}{3}\right)\cos\left(\theta_r + \frac{2\pi}{3}\right) \\ \frac{1}{2}\left(\cos\theta_r + \cos\left(\theta_r - \frac{2\pi}{3}\right) + \cos\left(\theta_r + \frac{2\pi}{3}\right)\right) \end{bmatrix} \tag{2.82}$$

The equation depends on the angle of the rotor and also the angle between the frames. If the frame angle is selected as equal to rotor magnetic angle θ_r and using the trigonometric identities that are given below, this dependence will be eliminated [8].

$$2\sin\alpha\cos\alpha = \sin 2\alpha \tag{2.83}$$

$$\cos^2\alpha + \cos^2\left(\alpha + \frac{2\pi}{3}\right) + \cos^2\left(\alpha - \frac{2\pi}{3}\right) = \frac{3}{2} \tag{2.84}$$

The final form is:

$$K_s \frac{d\lambda_r}{dt} = \lambda_f w_r \begin{bmatrix} 1 \\ 0 \\ 0 \end{bmatrix} \tag{2.85}$$

Combining the parts of the voltage equation reach the final form of for the voltage equation.

$$v_q = Ri_q + \omega_r L_d i_d + L_q \frac{di_q}{dt} + \lambda_f \omega_r$$

(2.86)

$$v_d = Ri_d - \omega_r L_q i_q + L_d \frac{di_d}{dt}$$

The voltage equations are obtained with transformation to *dq* frame simpler and number of the equations decreased by one. In general for a *2p* machine, the above equations can be modified [8].

$$v_q = Ri_q + p\omega_r L_d i_d + L_q \frac{di_q}{dt} + p\lambda_f \omega_r$$

(2.87)

$$v_d = Ri_d - p\omega_r L_q i_q + L_d \frac{di_d}{dt}$$

Where p is the number of pair of poles. Transferred torque equation is given below.

$$T_e = \frac{1}{2}\frac{\partial \lambda_r}{\partial t} K_s^{-1} I_{dq}^{T} \quad \textbf{(2.88)}$$

$$\Rightarrow T_e = 1.5 p \lambda_f i_q \quad \textbf{(2.89)}$$

2.3.8 Ideas to Find Out the Parameters of Voltage Equations

2.3.8.1 Determining the Permanent Magnet Flux

To determine the flux, the generator is connected to a variable speed motor. The generator windings are open circuited which means that no current will flow. From the voltage equations:

$$\lambda_f = \frac{v_q}{\omega} = \frac{2}{3\omega}\left(\cos(\theta_r) v_a + \cos(\theta_r - \frac{2\pi}{3}) v_b + \cos(\theta_r + \frac{2\pi}{3}) v_c \right) \quad \textbf{(2.90)}$$

For different rotor speeds, quadratic axes voltage is calculated and then flux of magnet is calculated from the above equation. For a good approximation the mean value of the calculated values is taken.

2.3.8.2 Determining the Resistance, Quadratic and Direct Axes Inductances

This time generator rotor locked which means that rotor speed will be zero. From the voltage equations, when rotor speed is zero the nonlinear elements in the equations will be eliminated. Linear voltage equations for zero speed are given below:

$$\frac{i_d}{v_d} = \frac{1}{L_d s + R} \tag{2.91}$$

$$\frac{i_q}{v_q} = \frac{1}{L_q s + R} \tag{2.92}$$

The values can be found by step response analysis, but in real machine there is hysteresis and skin effects which affect these values. So that system identification methods can be used to determine an average value. System identification is a discrete process, so the frequency domain equation should transform to z domain with a zero order hold.

$$\frac{i_d}{v_d} = \frac{1 - e^{-\frac{R}{Ld}T}}{R(z - e^{-\frac{R}{Ld}T})} \tag{2.89}$$

$$\frac{i_q}{v_q} = \frac{1 - e^{-\frac{R}{Lq}T}}{R(z - e^{-\frac{R}{Lq}T})} \tag{2.90}$$

where T is the sampling period. By applying PRBS or ARMA signals to voltage side of the system and taking measurements from the currents, the parameters can be calculated from linear regression [9].

2.4 Modeling of Uncontrolled Rectifier

2.4.1 Introduction

Uncontrolled three phase full wave rectifier is a bridge that contains six diodes (uncontrolled, self commutated switch) as shown the Figure 2.10 [10] where L_s is the source inductance, C_d is the dc side capacitance which filters DC component from the rectified wave. The value of the source inductance and source frequency is important because source inductance will cause a voltage drop on the DC side which is proportional to these variables.

There are many modeling types for converters which describe the input-output relations. For rectifiers the input variable is the effective value of the line to line phase voltage and the output variable is the mean value of dc link voltage[10].

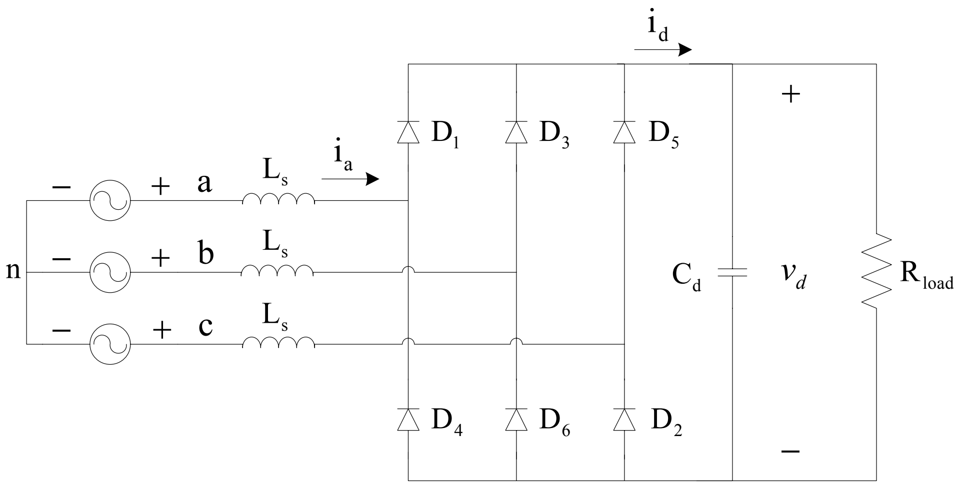

Figure 2.10: General circuit diagram of rectifier

2.4.2 Idealized Circuit with $L_s = 0$

For this approach the source side can be assumed to be voltage source and DC side a current source. The Figure 2.11 is given for this approach.

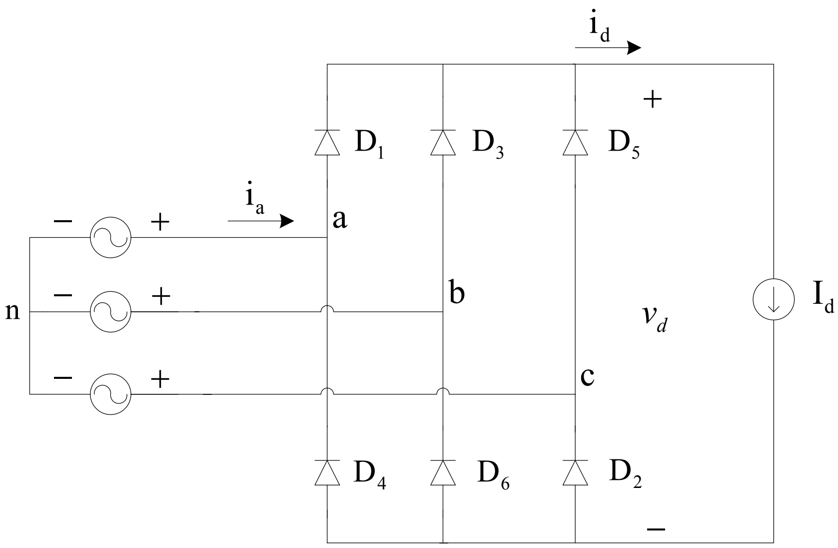

Figure 2.11: Idealized Circuit Diagram

With $L_s = 0$, the current I_d flows through one diode from the top group and one from the bottom group at nay instant. In the top group, the diode with its anode at the highest potential will conduct and the other two become reversed biased. In the bottom group, the diode with its cathode at the lowest potential will conduct and the other two become reverse biased [10].

The voltage waveforms in the circuit are shown in Figure 2.12 where v_{Pn} is the voltage at the point P (positive) with respect to the AC voltage neutral point n. Similarly, v_{Nn} is the voltage at the negative DC terminal N (negative). Since I_d flows continuously, at any time, v_{Pn} and v_{Nn} can be obtained in the terms of one of the AC input voltages v_{an}, v_{bn} and v_{cn}. Applying KVL in the circuit on a instantaneous basis, the dc side voltage is.

$$v_d = v_{Pn} - v_{Nn} \tag{2.95}$$

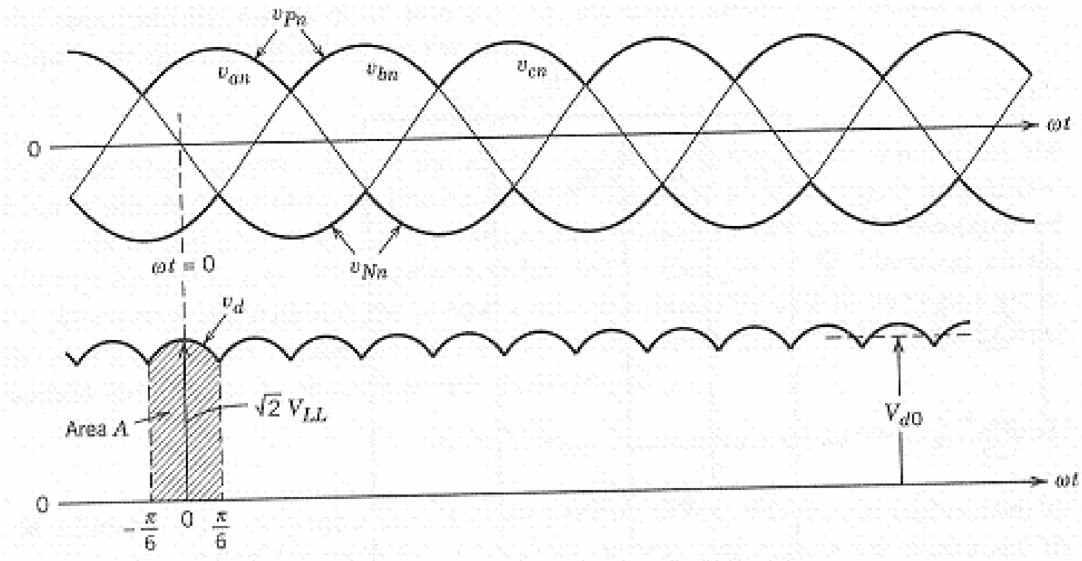

Figure 2.12: Rectifier Voltage Waveform [10].

The instantaneous waveform of v_d consists of six segments per cycle of the line frequency. Hence, this rectifier is often termed a six-pulse rectifier. Each segment belongs to one of the six line-to-line voltage combinations. Each diode conducts for 120^o. Considering the phase a current waveform

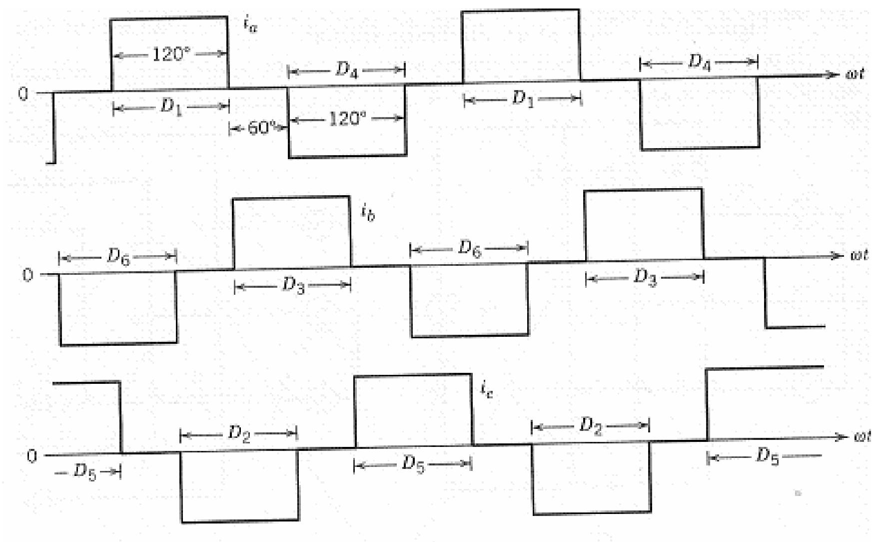

Figure 2.13: Phase Currents [10]

$$i_a = \begin{cases} I_d & \textit{when diode } 1 \textit{ is conducting} \\ -I_d & \textit{when diode } 4 \textit{ is conducting} \\ 0 & \textit{otherwise} \end{cases} \tag{2.96}$$

The commutation of current from one diode to the next is instantaneous, based on the assumption of *Ls =0*. The diodes are numbered in such a way that they conduct in a sequence 1,2,3, … Next, we will compute the average value of the output DC voltage and rms values of the line currents, where the subscript *o* is added due to assumption of *Ls =0*.

To obtain the average value of the output dc voltage, it is sufficient to consider only one of the six segments and obtain its average over a 60^o or $\pi/3$- rad interval. Arbitrarily, the time origin $t = 0$ is chosen when the line-to-line voltage v_{ab} is at its maximum [10]. Therefore,

$$v_d = v_{ab} = \sqrt{2}V_{LL}\cos\omega t \qquad -\frac{1}{6}\pi < \omega t < \frac{1}{6}\pi \tag{2.97}$$

where V_{LL} is the rms value of the line-to-line voltages. By integrating v_{ab}, the volt-second area A is given by

$$A = \int_{-\pi/6}^{\pi/6} \sqrt{2}V_{LL}\cos\omega t d(\omega t) = \sqrt{2}V_{LL} \tag{2.98}$$

and therefore dividing A by the $\pi/3$ interval yields

$$V_{d0} = \frac{1}{\pi/3} \int_{-\pi/6}^{\pi/6} \sqrt{2} V_{LL} \cos\omega t d(\omega t) = \frac{3}{\pi} \sqrt{2} V_{LL} = 1.35 V_{LL} \quad \textbf{(2.99)}$$

Using the definition of rms current in the phase current waveform, the rms value of the line current is in the idealized case is

$$I_s = \sqrt{\frac{2}{3}} I_d = 0.816 I_d \quad \textbf{(2.100)}$$

By means of Fourier analysis of it in this idealized case, the fundamental-frequency component has an rms value

$$I_{s1} = \frac{1}{\pi} \sqrt{6} I_d = 0.78 I_d \quad \textbf{(2.101)}$$

The harmonic component I_{sh} can be expressed in the terms of the fundamental-frequency component as

$$I_{sh} = \frac{I_{s1}}{h} \quad \textbf{(2.102)}$$

Where $h = 6k \pm 1$ the even and triple harmonics are zero. Since I_{s1} is in the phase with its utility phase voltage, the displacement power factor is

$$DPF = \cos(\phi) = 1.0 \quad \textbf{(2.103)}$$

where ϕ is the phase angle between current I_{s1} and phase voltage. Therefore the power factor is

$$pf = \frac{I_{s1}}{I_s} DPF = \frac{3}{\pi} = 0.955 \quad \textbf{(2.104)}$$

Total harmonic distortion can be written as:

$$THD = \frac{I_{dis}}{I_{s1}} = \frac{\sqrt{I_s{}^2 - I_{s1}{}^2}}{I_{s1}} = \frac{I_d \sqrt{0.816^2 - 0.78^2}}{0.78 I_d} = 30.731\% \quad \textbf{(2.105)}$$

The voltage waveform will be identical if the load on the dc side is represented by a resistance R_{load} instead of a current source I_d. The phase currents will also flow during identical intervals. The only difference will be that the current waveforms will not have a flat top [10].

2.4.3 Effect of L_s On current Commutation

We will include L_s on the AC side and represent the dc side by a current source $i_d = I_d$ as shown in Figure 2.14.

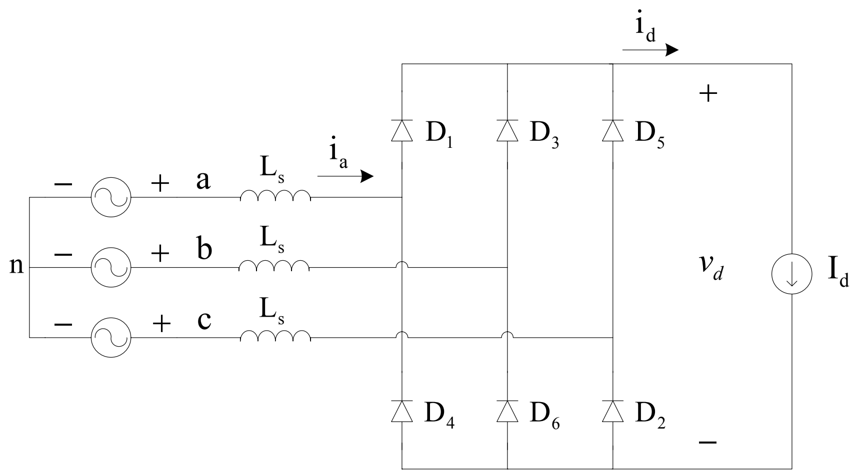

Figure 2.14: Rectifier Circuit Diagram with L_s

Now the current commutation will not be instantaneous. We will look at only one of the current commutations because all others are identical in a balanced circuit. Consider the commutation of current from the diode 5 to diode 1, beginning at t or $\omega t=0$ (the time origin is chosen arbitrarily). Prior to this, the current I_d is flowing through diodes 5 and 6. The commutation is shown in Figure 2.15.

The current commutation only involves phases a and c, and the commutation voltage responsible is $v_{comm} = v_{an} - v_{bn}$. The two mesh currents I_a and I_d are shown in Figure 2.15. The commutation current i_u flows due to a short-circuit path provided by the conducting diode 5. In terms of mesh current, the phase currents are

$$i_a = i_u \tag{2.106}$$

and

$$i_c = I_d - i_u \qquad \textbf{(2.107)}$$

i_u builds up from zero to I_d at the end of the commutation interval $\omega t_u = u$. In the circuit

$$v_{La} = L_s \frac{di_a}{dt} = L_s \frac{di_u}{dt} \qquad \textbf{(2.108)}$$

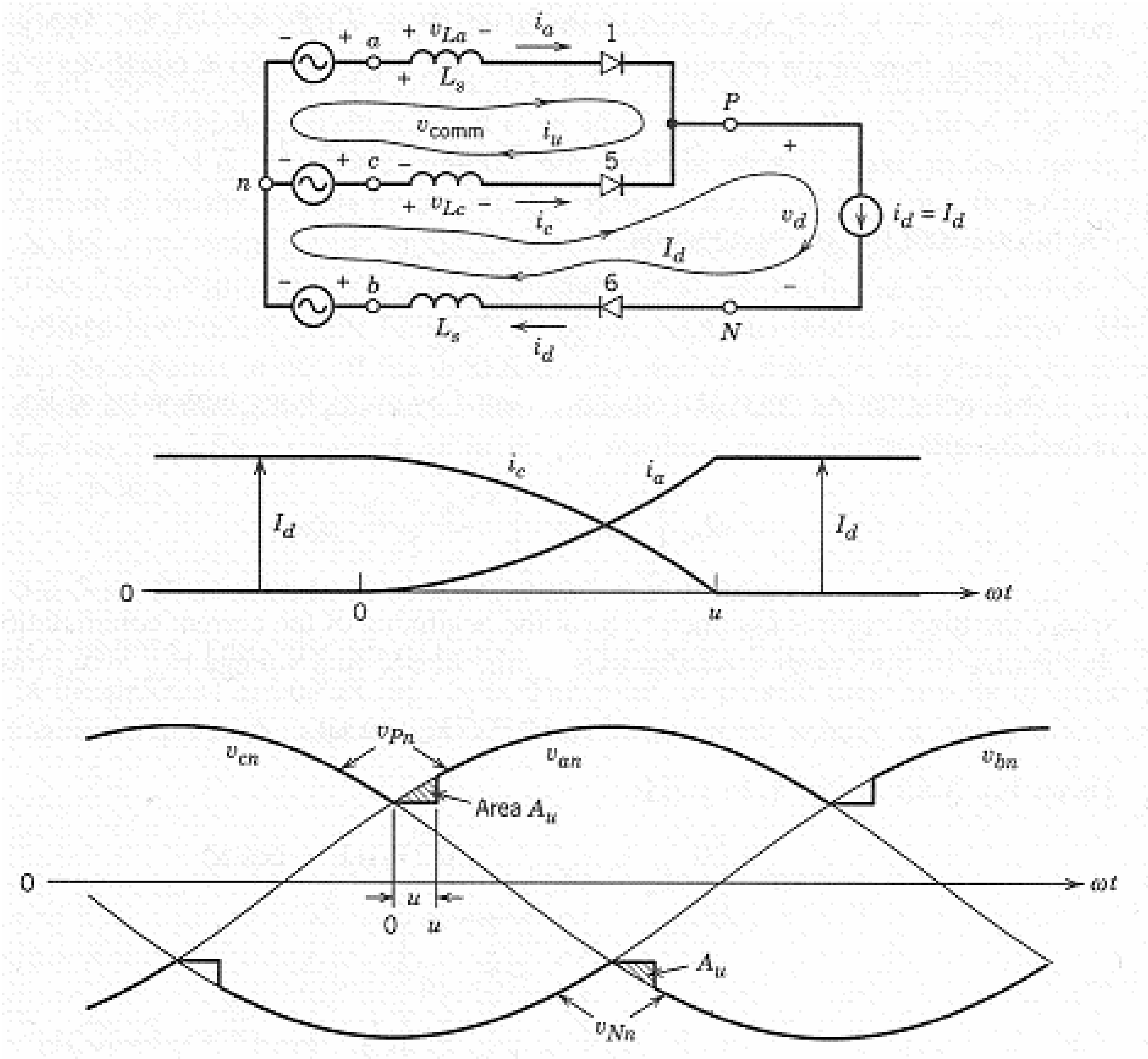

Figure 2.15: Current commutation [10]

and

$$v_{Lc} = L_s \frac{di_c}{dt} = -L_s \frac{di_u}{dt} \qquad \textbf{(2.109)}$$

Noting that $i_c = I_d - i_u$ and therefore $di_c / dt = d(I_d - i_u)/dt = -di_u / dt$. Applying KVL in the upper loop in the circuit and using the above equations yield

$$v_{comm} = v_{an} - v_{bn} = v_{La} - v_{Lc} = 2L_s \frac{di_u}{dt} \tag{2.110}$$

Therefore from the above equation,

$$L_s \frac{di_u}{dt} = \frac{v_{an} - v_{cn}}{2} \tag{2.111}$$

The commutation interval u can be obtained by multiplying both sides by ω and integrating:

$$\omega L_s \int_0^{I_d} d\, i_u = \int_0^{u} \frac{v_{an} - v_{cn}}{2}\, d(\omega t) \tag{2.112}$$

where the time origin is assumed to be at the beginning of the current commutation. With this choice of time origin, we can express the line to line voltage ($v_{an} - v_{cn}$) as

$$v_{an} - v_{cn} = \sqrt{2} V_{LL} \sin \omega t \tag{2.113}$$

$$\omega L_s \int_0^{I_d} di_u = \omega L_s I_d = \frac{\sqrt{2} V_{LL} (1 - \cos u)}{2} \tag{2.114}$$

or

$$\cos u = 1 - \frac{2 \omega L_s I_d}{\sqrt{2} V_{LL}} \tag{2.115}$$

If the current commutation was instantaneous due to zero L_s, then the voltage v_{pn} will be equal to v_{an} beginning with $\omega t=0$. However, with a finite L_s, during $0 < \omega t < \omega t_u$

$$v_{pn} = v_{an} - L_s \frac{di_a}{dt} = \frac{v_{an} + v_{cn}}{2} \tag{2.116}$$

where the voltage across L_s $(=L_s(di_u/dt))$ is the drop in the voltage v_{pn} during the commutation interval shown in Figure 2.15. The integral of this voltage drop is the area A_u which is

$$A_u = \omega L_s I_d \quad \textbf{(2.117)}$$

This area is lost at every 60° interval. Therefore, the average DC voltage output is reduced from its original value, and the voltage drop due to the commutation is

$$\Delta V_d = \frac{\omega L_s I_d}{\pi / 3} = \frac{3}{\pi} \omega L_s I_d \quad \textbf{(2.118)}$$

Therefore, the average DC voltage in the presence of a finite commutation interval is

$$V_d = V_{d0} - \Delta V_d = 1.35 V_{LL} - \frac{3}{\pi} \omega L_s I_d \quad \textbf{(2.119)}$$

Where V_{d0} is the average voltage with an instantaneous commutation with $L_s=0$. If we need to use the circuit model of the rectifier [11] for average valued model (voltage ripple is neglected)

$$R_d = \frac{3}{\pi} \omega L_s \quad \textbf{(2.120)}$$

$$V_{d0} = 1.35 V_{LL} \quad \textbf{(2.121)}$$

the circuit is given in Figure 2.16.

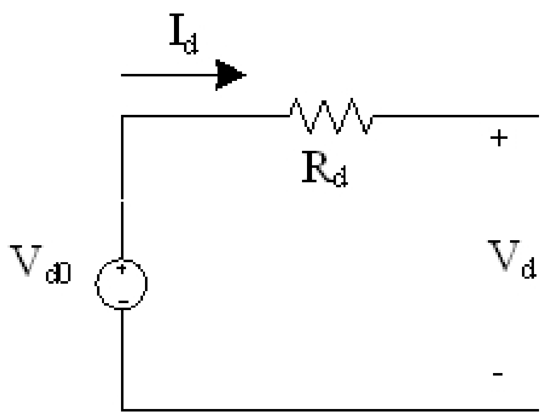

Figure 2.16: Averaged circuit model of uncontrolled rectifier

2.5 The Inverter Model

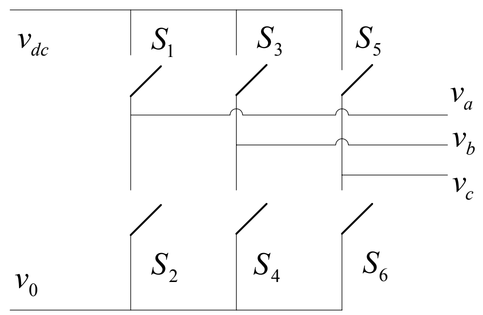

Figure 2.17: The Basic Structure of the 3 Phase Inverter

In general inverter is a kind of converter that converts the dc current into ac current. A three phase inverter in Figure 2.17 is consisted of six switches located on three arms for each phase. Thus each phase voltage is controlled by two switches. Inverter does not have recursive equation, so that its behavior can only be described by a series of logic equation. For this approach, S_i represents the logic inputs to each switch and their value determines i^{th} switches position. If S_i is logic '1', the switch is closed and if it is '0' the switch is open. This information leads to a model for inverter [11].

$$v_a = S_1 v_{dc} + S_2 v_0 \quad \textbf{(2.122)}$$

$$v_b = S_3 v_{dc} + S_4 v_0 \quad \textbf{(2.123)}$$

$$v_c = S_5 v_{dc} + S_6 v_0 \quad \textbf{(2.124)}$$

3. CONTROL OF THE SELECTED TOPOLOGY

3.1 The Task of the Control System

The most important task of the control system is to force the mechanic system to run at the optimum angular speed at which turbine will harvest the maximum power from the wind for different wind speeds. The second important task is to control the power factor of the power plant to cover the grid requirements.

The power equations for grid side are given below.

$$S = \sqrt{P^2 + Q^2} \qquad \textbf{(3.1)}$$

$$\begin{aligned} P &= S\cos\varphi \\ Q &= S\sin\varphi \end{aligned} \qquad \textbf{(3.2)}$$

$$S = \sqrt{3} I_L V_{LL} \qquad \textbf{(3.3)}$$

Where S is the apparent power, P is the active power, Q is the reactive power, φ is the phase angle and $\cos\varphi$ is the power factor. Active power: The mean of the instantaneous power over an integral number of periods giving the mean rate of energy transfer from source to load in watts (W). Reactive power: The maximum rate of energy interchange between source and load in reactive volt-amperes (VAR).

The output voltage or in other words grid voltage is constant. So from the equations 3.1, 3.2, 3.3 changing the line current will change the apparent power and changing phase angle will change the active and reactive power supplied to the grid. This means that a current controller is needed which will control the amplitude or the effective value and phase shift of the current and IGBT drivers which will produce the gating signals for the switches in the inverter. Hysteresis current controller is chosen which contains both the controller and driver.

A MPPT algorithm will be proposed which will produce current reference for the current controller. This algorithm will watch out the angular speed, its change and will calculate new current reference for the next cycle. This is a global optimization problem that algorithm will always track for the optimum point and find global maximum point for the power.

3.2 Hysteresis Current Controller

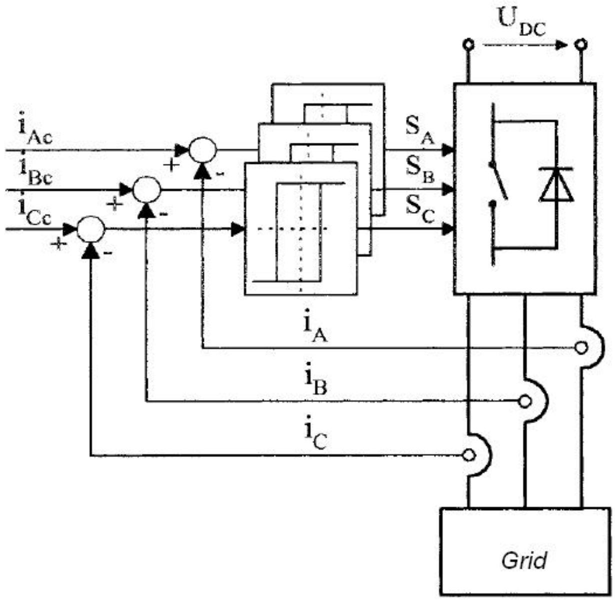

Figure 3.1: Hysteresis Control Circuit Diagram [12]

Hysteresis control schemes are based on a nonlinear feedback loop with two level hysteresis comparators. The switching signals S_A, S_B, S_C are produced directly when the error exceeds an assigned tolerance band *h* [12].

3.2.1 Variable switching frequency controllers:

Among the main advantages of hysteresis current controller are simplicity, outstanding robustness, lack of tracking errors, independence of load parameter changes, and extremely good dynamics limited only by switching speed and load time constant. However, this class of schemes, also known as free running hysteresis controllers has the following disadvantages [12].

1) The converter switching frequency depends largely on the load parameters and varies with the ac voltage.

2) The operation is somewhat rough, due to the inherent randomness caused by the limit cycle; therefore, protection of the converter is difficult.

It is characteristic of the hysteresis current controller that the instantaneous current is kept exact in a tolerance band, except for systems where the instantaneous error can reach double the value of the hysteresis band

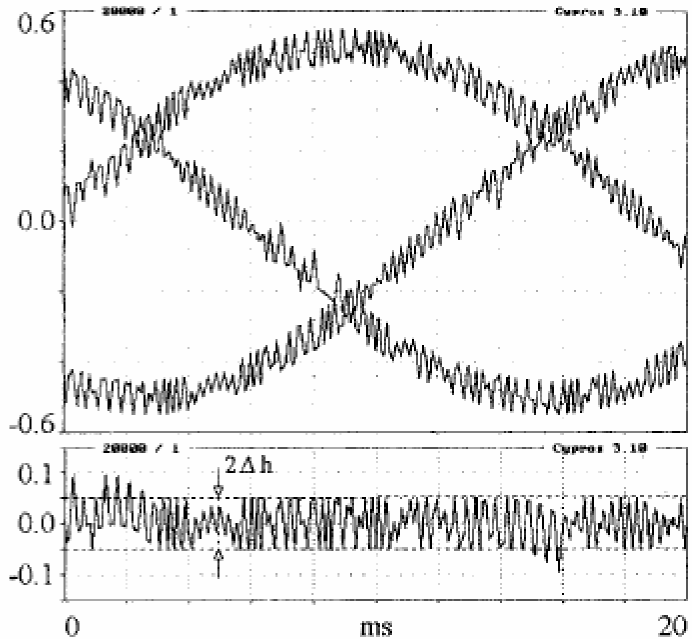

Figure 3.2: Current waveform and Hysteresis Band [12].

This is due to the interaction in the system with three independent controllers. The comparator state change in one phase influences the voltage applied to the load in two other phases (coupling). However, if all three current errors are considered as space vectors, the interaction effect can be compensated, and many variants of controllers known as space-vector based can be created. Moreover, if three-level comparators with a lookup table are used, a considerable decrease in the inverter switching frequency can be achieved. This is possible with appropriate selection of zero-voltage vectors [12].

In the synchronous rotating *d–q* coordinates, the error field is rectangular, and the controller offers the opportunity of independent harmonic selection by choosing different hysteresis values for the *d* and *q* components. This can be used for torque-ripple minimization in vector-controlled AC motor drives (the hysteresis band for the torque current component is set narrower than that for the flux current component)

Recent methods enable limit cycle suppression by introducing a suitable offset signal to either current references or the hysteresis band.

3.2.2 Constant switching frequency controllers:

A number of proposals have been put forward to overcome variable switching frequency. The tolerance band amplitude can be varied, according to the ac-side voltage, or by means of a PLL control

An approach which eliminates the interference, and its consequences, is that of decoupling error signals by subtracting an interference signal derived from the mean inverter voltage.

Similar results are obtained in the case of "discontinuous switching" operation, where decoupling is more easily obtained without estimating load impedance. Once decoupled, regular operation is obtained, and phase commutations may (but need not) be easily synchronized to a clock.

Although the constant switching frequency scheme is more complex and the main advantage of the basic hysteresis control— namely, the simplicity—is lost, these solutions guarantee very fast response together with limited tracking error. Thus, constant frequency hysteresis controls are well suited for high performance high-speed applications [12].

In the selected topology, for the sake of simplicity variable switching frequency concept is selected. In front of the controller reference currents are produced by simply multiplying the reference produced by the MPPT with the modulation signals (120^0 phase shifted sinusoidal functions). In reality a PLL is needed to match the waveform of the current with line voltage. It can be easily notice of that the phase shift between the line voltage waveform and the modulation signals will effect on the power factor of the system with no change in apparent power.

3.3 MPPT

3.3.1 The Wind Turbine Stable Working Point

As explained earlier the MPPT will directly act on the apparent power which is drawn from the power plant. As a result of this situation the angular speed of the plant will change. But for a given power reference (calculated by MPPT), the curve of the turbine gives two working points of which the reference line intersects with the curve.

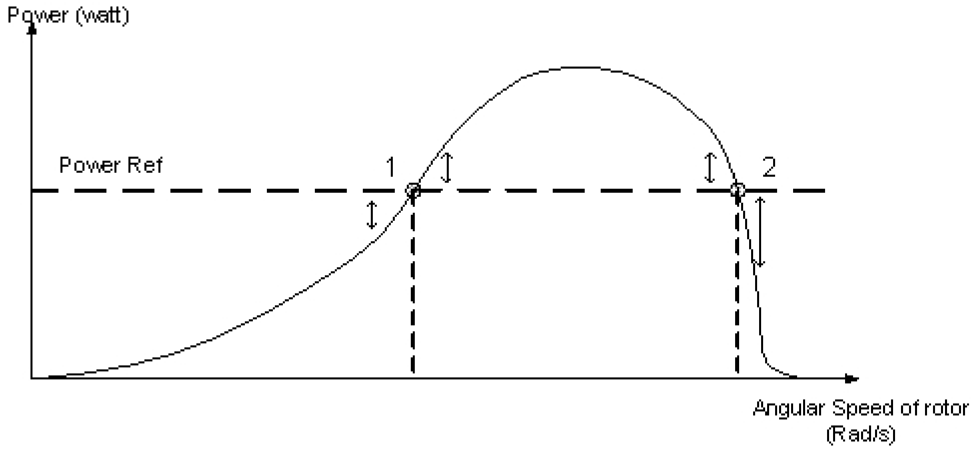

Figure 3.3: The intersection of power reference with the turbine curve

System has only one stable speed. Let us examine the point 1 and 2 in the Figure 3.3 above. First the system is assumed to be working at the point 1. If system slows a little, power reference will be larger than the turbine produces, so that system will stall. If system speeds up a little, power reference will be smaller than that of the turbines, so that system will speed up. As a result point 1 is not a stabile working point.

This time system is assumed to be in point 2. If system slows a little, power reference will be smaller than the turbine gives, so that system will speed up. If system speeds up a little, power reference will be larger that the turbines, so that system will slow down. In each case the speed will go to point 2. As a result this point is a stable working point. So only the right hand side of the curve will be dealed.

The Figure 3.3 shows another situation about the control. At the start up of the system MPPT should set the power ref zero or shutdown the energy transfer and keep it until system passes to right hand side of the system.

3.3.2 Some Control Scenarios

3.3.2.1 If wind speeds up:

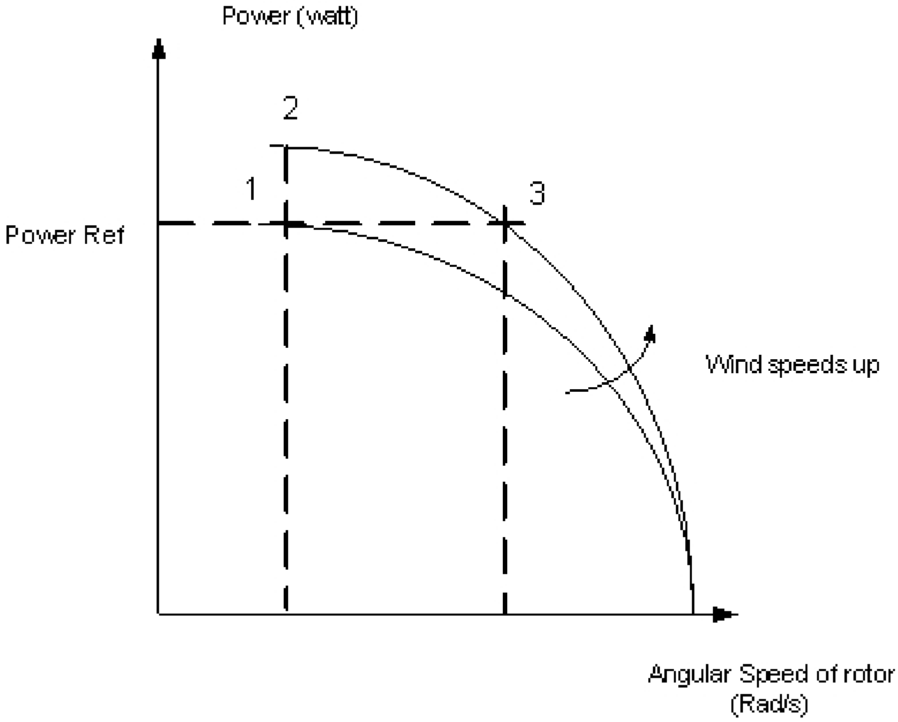

Figure 3.4: The change of working point in the case of speed up of the wind

From the Figure 3.4 above, if the wind speed increases while system was working at the optimum point (1), system will instantaneously jump to point (2). At the point (2) turbine power is bigger than power ref. The generator will speed up to point (3) and will stay stable but point (3) is not the optimum point. So the MPPT should continue searching the optimum point from point (3).

3.3.2.2 If Wind Slows Down:

In Figure 3.5 system is assumed to be running at the optimum point (1). When speed reduces, the curve of the turbine will narrow down. The working will jump to point (2). At this point the power from the turbine is lower than the reference power value. Because of that, system will slow down and stall. MPPT should watch out this behavior and should reset all the process and start from the beginning. Because, the mechanical time coefficients are larger than electrical ones, the DC bus voltage will reduce much rapidly. So watching out the dc bar voltage will help to control this behavior. MPPT only works at each sampling time. So that MPPT needs some help to detect the sudden drop in DC voltage link.

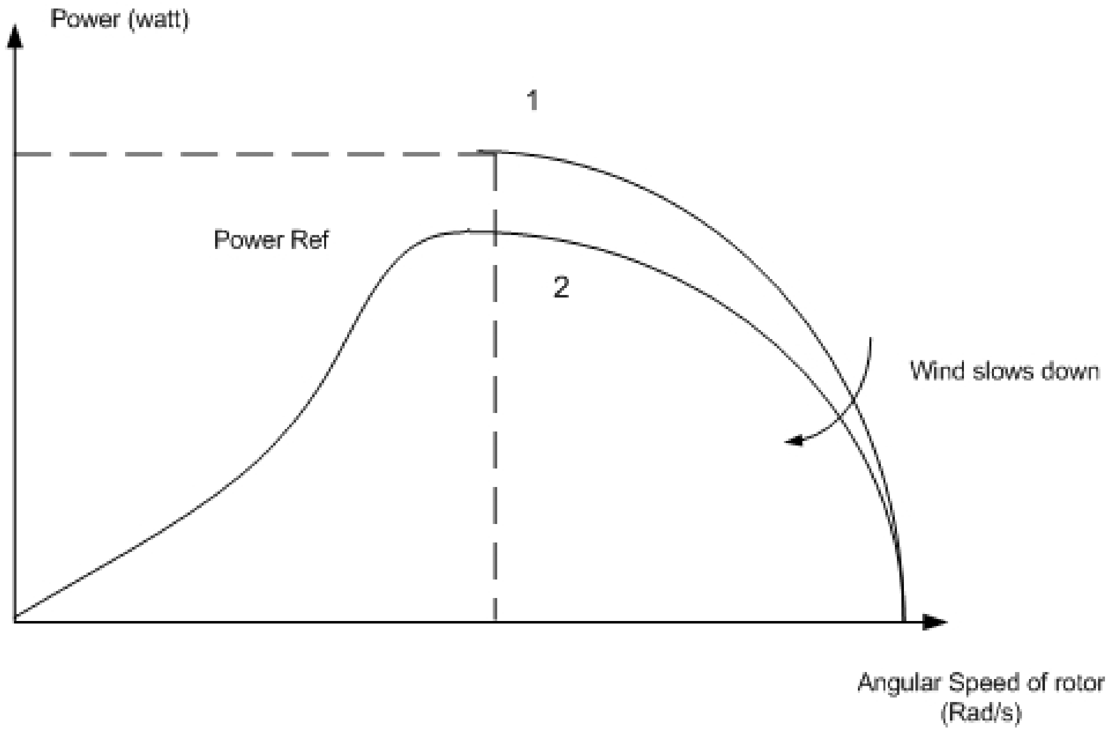

Figure 3.5: The change of working point in the case of slow down of the wind

3.3.3 The Flow Diagram of the MPPT

Some scenarios can be tested from the flow chart given below in Figure 3.6. Under constant wind speed, the algorithm starts. It first waits for the system to reach the stable point. Then it sets initial value and applies it to the system. The rotor speed will decrease according to this initial value. Then MPPT will calculate the new step size. This calculated step size is compared with a limit value. If the step size is larger than that value, it calculates the new reference to the system. If it is smaller, this means that system is near enough to optimum point thus MPPT stops tracking.

As the wind speed increases, the rotor speed will also increase. Algorithm again calculates the step size (delta). Because it uses the absolute value, it passes the step size control and starts again tracking the optimum point.

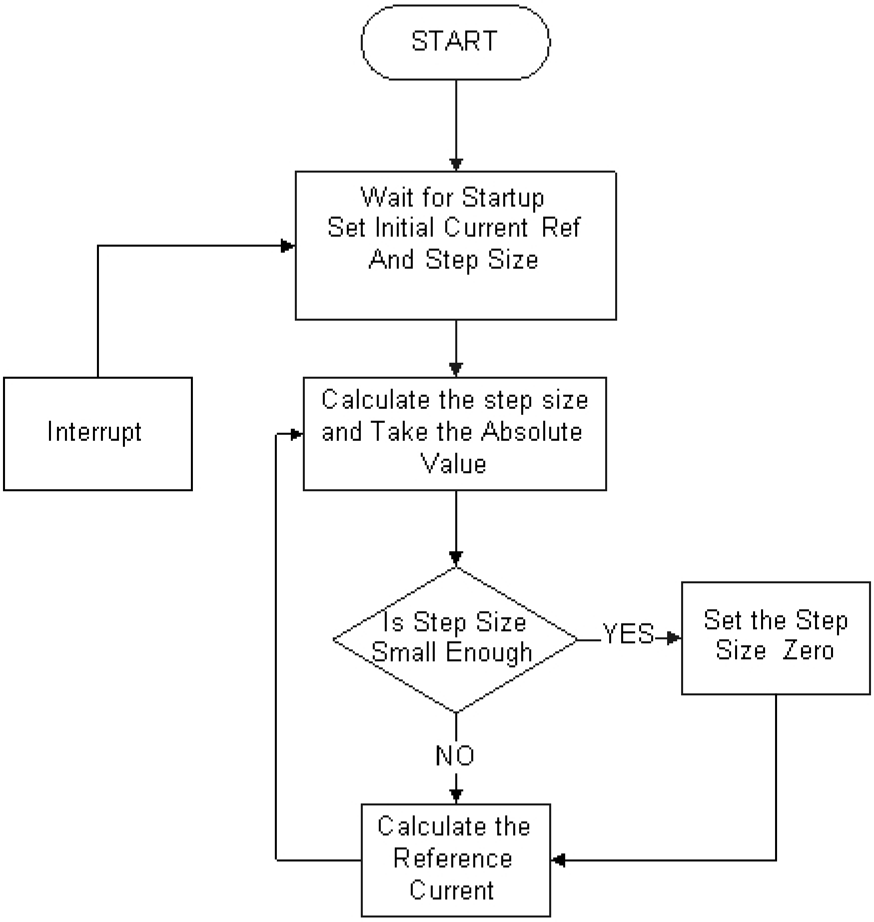

Figure 3.6: The flow chart of MPPT

Another scenario is the decrease of the wind speed. When the wind speed decrease, the dc voltage will drop rapidly. An external interrupt producer (sudden change detector) sends an interrupt signal to the MPPT. MPPT stops tracking and reset itself which means that starting from the beginning.

3.3.4 Calculation of the new current references

3.3.4.1 Steepest Decent Algorithm as a Line Search Method

The problem we are interested in solving is:

$$P : \text{minimize } f(x)$$

$$\text{s.t.} \quad x \in R^n$$

where $f(x)$ is differentiable. If $x = \bar{x}$ is a given point, $f(x)$ can be approximated by its linear expansion

$$f(\bar{x} + d) \approx f(\bar{x}) + \nabla f(\bar{x})^T d \qquad \textbf{(3.4)}$$

if d is "small", i.e., if $\|d\|$ is small. Now notice that if the approximation in the above expression is good, then we want to choose d so that the inner product $\nabla f(\bar{x})^T d$ is as small as possible. Let us normalize d so that $\|d\|=1$. Then among all directions d with norm, $\|d\|=1$ the direction

$$\tilde{d} = \frac{-\nabla f(\bar{x})}{\|\nabla f(\bar{x})\|} \qquad \textbf{(3.5)}$$

makes the smallest inner product with the gradient $\nabla f(\bar{x})$. This fact follows from the following inequalities:

$$\nabla f(\bar{x})^T d \geq -\|\nabla f(\bar{x})\|\|d\| = \nabla f(\bar{x})^T \left(\frac{-\nabla f(\bar{x})}{\|\nabla f(\bar{x})\|} \right) = -\nabla f(\bar{x})^T \tilde{d} \qquad \textbf{(3.6)}$$

For this reason the un-normalized direction:

$$\tilde{d} = -\nabla f(\bar{x}) \qquad \textbf{(3.7)}$$

is called the direction of steepest descent at the point $\bar{x}$

Note that $\tilde{d} = -\nabla f(\bar{x})$ is a descent direction as long as $\nabla f(\bar{x}) \neq 0$. To see this, simply observe that

$$d^T \nabla f(\bar{x}) = -(\nabla f(\bar{x}))^T \nabla f(\bar{x}) < 0 \qquad \textbf{(3.8)}$$

so long as $\nabla f(\bar{x}) \neq 0$.

A natural consequence of this is the following algorithm, called the steepest descent algorithm.

Steepest Descent Algorithm:

Step 0. Given x^0,set $k := 0$

Step 1. $d^k := -\nabla f(x^k)$. If $d^k = 0$, then stop.

Step 2. Solve $\min_\alpha f(x^k + \alpha d^k)$ for the step size α^k, perhaps chosen by an exact or inexact line search.

Step 3. Set $x^{k+1} \leftarrow x^k + \alpha^k d^k, k \leftarrow k+1$. Go to Step 1.

Note from Step 2 and the fact that $d^k = -\nabla f(x^k)$ is a descent direction, it follows that $f(x^{k+1}) < f(x^k)$.

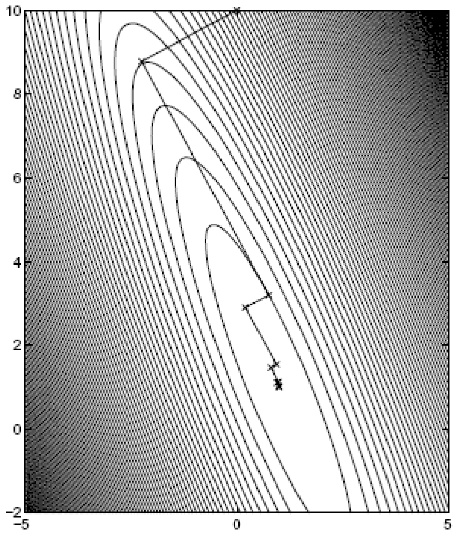

Figure 3.7: An example of steepest algorithm minimum search [13]

The Figure 3.7 shows the behavior of the steepest decent algorithm. Each circle is the output of the equation *f(x)* .The output value decrease as the algorithm searches for the minimum value [13].

Convergence Theorem: Suppose that $f(.): R^n \to R$ is continuously differentiable on the set $S = \{x \in R^n \mid f(x) \le f(x^0)\}$, and that S is a closed and bounded set. Then every point $\bar{x}$ that is a cluster point of the sequence $\{x^k\}$ satisfies $\nabla f(\bar{x}) = 0$ [13].

3.3.4.2 Steepest Decent Algorithm in MPPT

As explained earlier, a recursive equation for the turbine is variable, but we know that the curve is continuous. So that it is differentiable over the variable. Because, it is impossible to calculate the derivative of the turbine curve, we should find it out from the definition of the derivative. The curve has only one input variable which is the current reference and the out put variable is the angular speed of rotor. So that the derivative of the curve is:

$$\nabla f = \frac{\omega(t) - \omega(t-1)}{I_{ref}(t) - I_{ref}(t-1)} \tag{3.9}$$

where t is the index element. Now, we can find out the iteration form for current reference.

$$I_{ref}(t+1) = I_{ref}(t) + \alpha\nabla f \tag{3.10}$$

It is impossible to calculate α for each step. So a constant value is selected. Selection of this constant value is important because, it will determine the speed of convergence. If it is large, algorithm will be fast, but if it is bigger than a certain value (this certain value can only be found by experiments) it will pass the optimum point and it will lost its stability. Most safety one is to select this value small to keep the system stable.

Another approach is to use the absolute value of the ∇f instead of using it directly. Because when wind speeds up the sign of ∇f will reverse, but it is still required that current reference should increase. If the absolute value is taken, MPPT will not need to watch the speed increase to change the sign of the ∇f .

$$I_{ref}(t+1) = I_{ref}(t) + \left|\alpha\nabla f\right| \tag{3.11}$$

4. Simulation Results and Comments

This section deals with the simulation results of the proposed control system. As explained earlier this control system is designed for selected topology. To observe the behavior of the controllers, first of all a model of topology is built up in Matlab 7.0.1 Simulink program. This model is given in Figure 4.1.

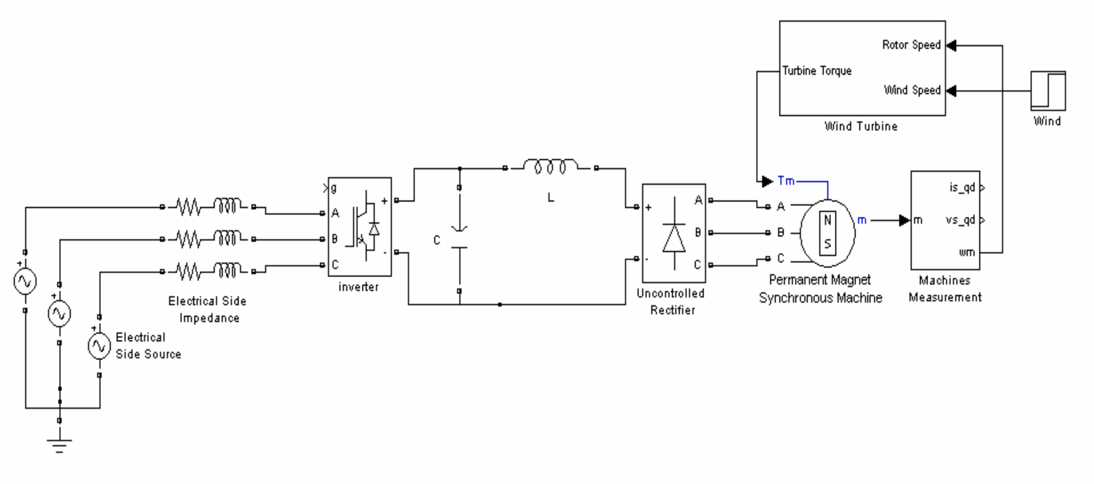

Figure 4.1: Matlab Model of the Topology

The turbine model from the matlab toolbox is reconstructed by curve fitting technique and it is given in a polynomial form. For this process matlab curve fitting toolbox is used. Following equations are obtained.

$$C_p = -0.000002189\lambda^6 + 0.0001165\lambda^5 - 0.002111\lambda^4 + 0.01449\lambda^3 - 0.02588\lambda^2 + 0.0158\lambda \quad \textbf{(4.1)}$$

$$C_\Gamma = -0.000002189\lambda^5 + 0.0001165\lambda^4 - 0.002111\lambda^3 + 0.01449\lambda^2 - 0.02588\lambda + 0.0158 \quad \textbf{(4.2)}$$

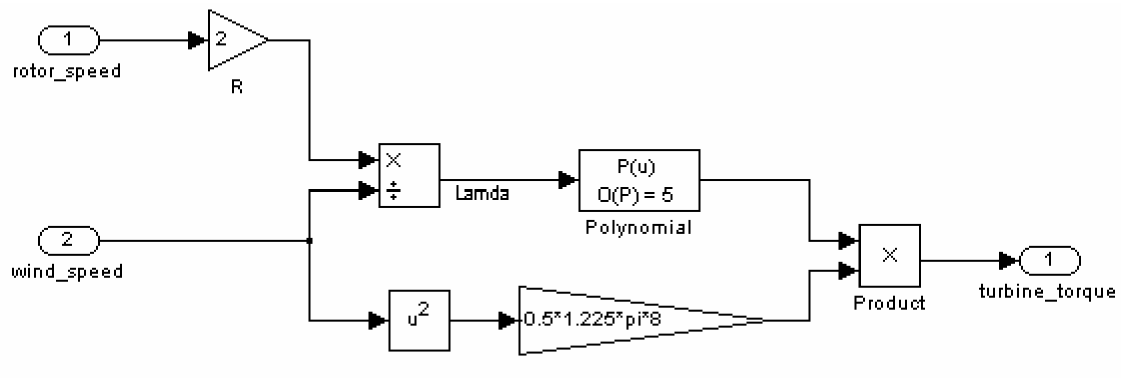

Figure 4.2: Turbine Model in Matlab

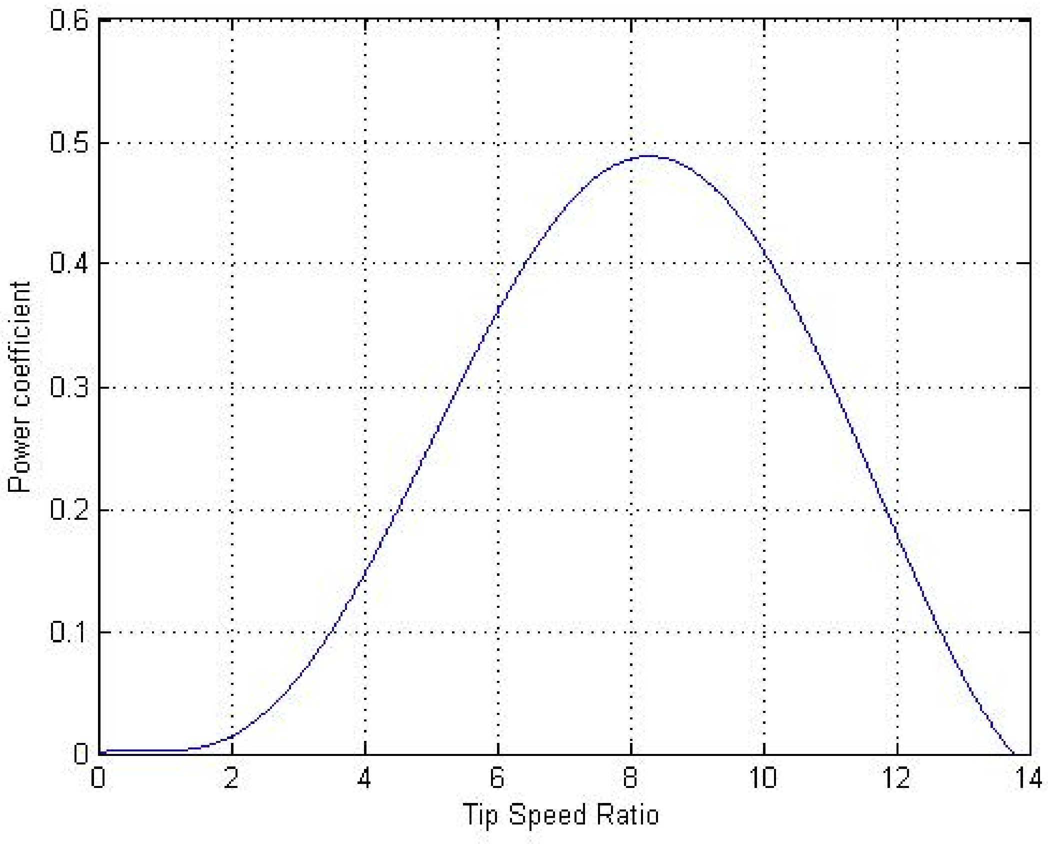

Figure 4.3: Graph of power coefficient

For the permanent magnet synchronous generator, the parameters are

$$R = 0.085\Omega \quad \textbf{(4.3)}$$

$$L_q = L_d = 0.095mH \quad \textbf{(4.4)}$$

$$\lambda_f = 0.192Wb \quad \textbf{(4.5)}$$

For the mechanical side

$$J_g = 0.008 Kgm^2 \quad \textbf{(4.6)}$$

$$B_g = 0.0012 Nms \quad \textbf{(4.7)}$$

These mechanical parameters are selected to keep the mechanical time small and also to speedup the simulation, because the sampling time of MPPT depends to mechanical time constant. In real application the inertia is much bigger than this value. The rated power of the generator is 11 kW and number of poles are 16. For the DC filter

$$C = 1mF \quad \textbf{(4.8)}$$

$$L = 1mH \quad \textbf{(4.9)}$$

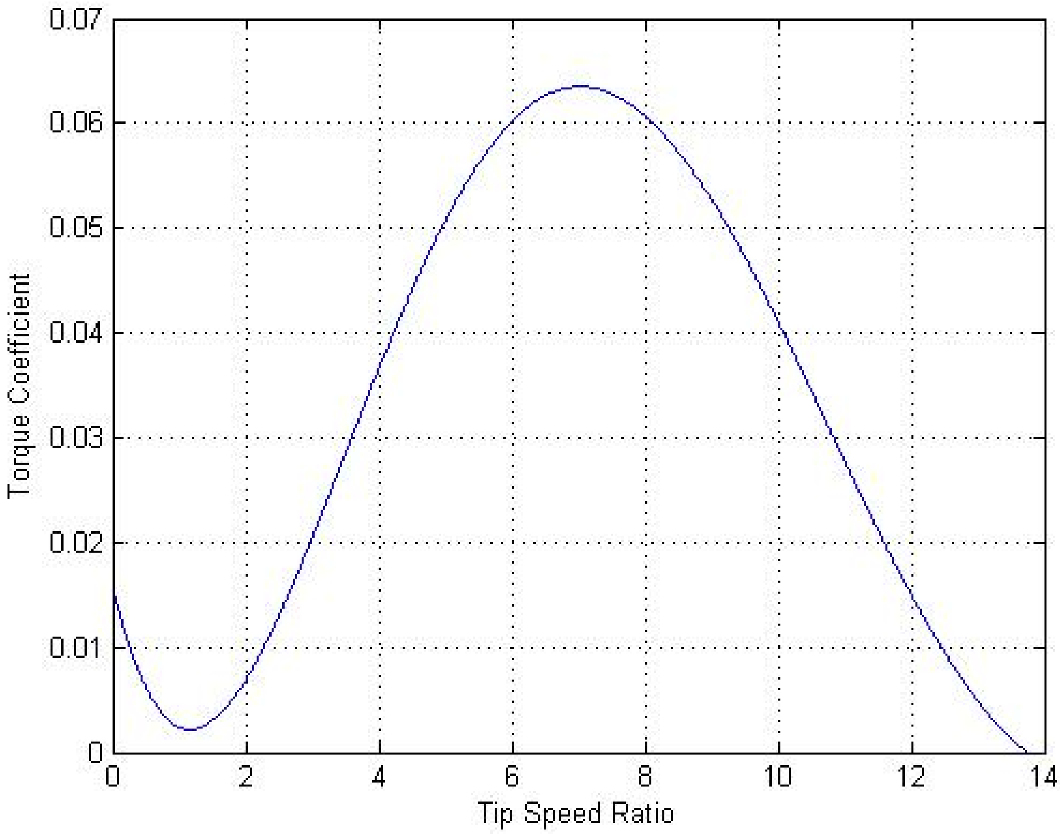

Figure 4.4: Graph of torque coefficient

The model of the system with control system is given in Figure 4.5. Control system is composed of three main parts. First one is the MPPT. MPPT takes the measurements of current and speed, and then it calculates the delta value (the step size) for the next step. It also takes information from other blocks, for initialization and interrupt. The second main part is sudden change detectors. These blocks watch the derivative of the dc link voltage. If the derivative value is smaller than a given value, one of them sends an interrupt to MPPT to inform it about the situation and the other sudden change detector block takes the control of reference current value for small time. This time depends on the sampling time of the MPPT, because MPPT can not change the output value until the next step time. At the next step time after the interrupt signal MPPT makes calculations to fix the problem. The third part is the current control and reference generator part. Signal generator which produces reference current wave forms, takes the reference current and generates three phase sinusoidal waves. These waveforms are the reference inputs for the current controller. Current controller measures the current value and calculates the error with the reference, then it produces gate signals for the inverter switches.

To observe the behavior of the control system properly, two simulations are carried out. Each simulation deals with different scenarios. First one is increase of wind speed when the system is operating at a stable point and second one is decrease of the wind speed when the system is at a stable point.

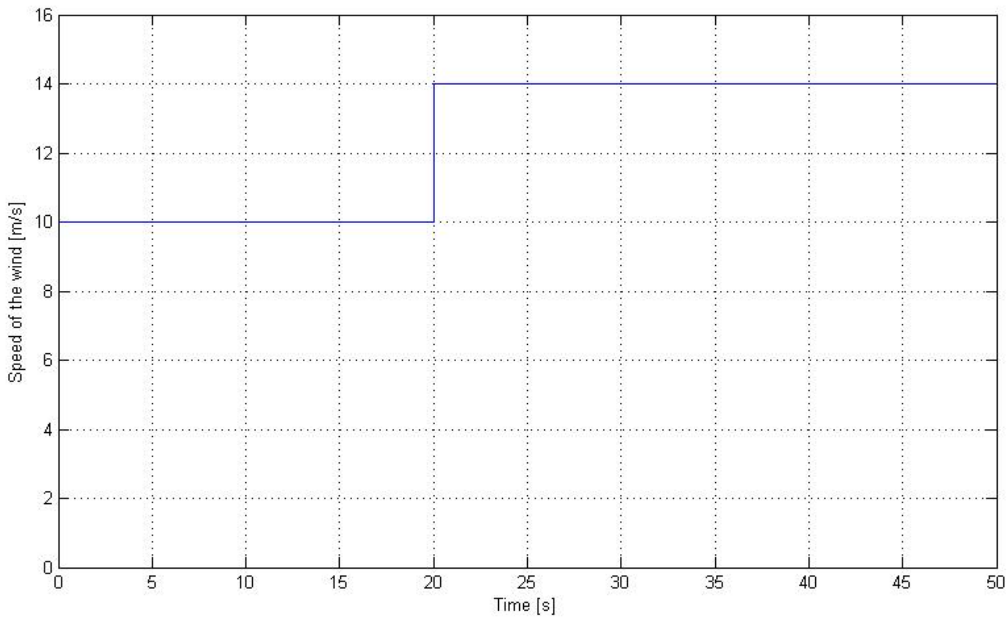

Figure 4.6: Wind Speed Change over time

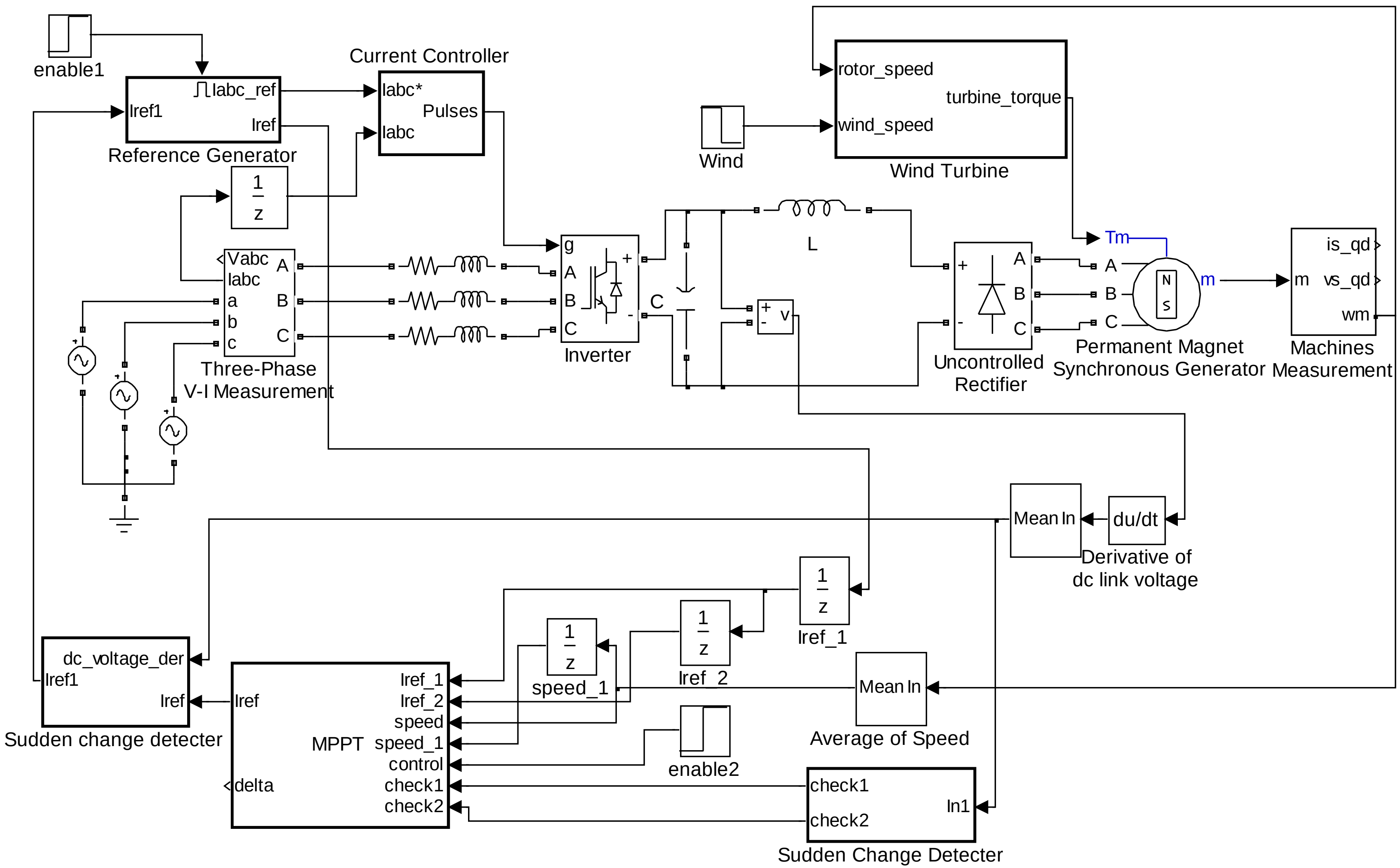

Figure 4.5: Matlab Model of the System With the Controller

4.1 First Scenario

In this scenario, the following step function in figure is applied to turbine model. The simulation is started by 10 m/s wind speed and after 20 s. the wind speed increased to 14 m/s.

For this wind speed the power curves of the turbine are given below in Figures 4.7 and 4.8.

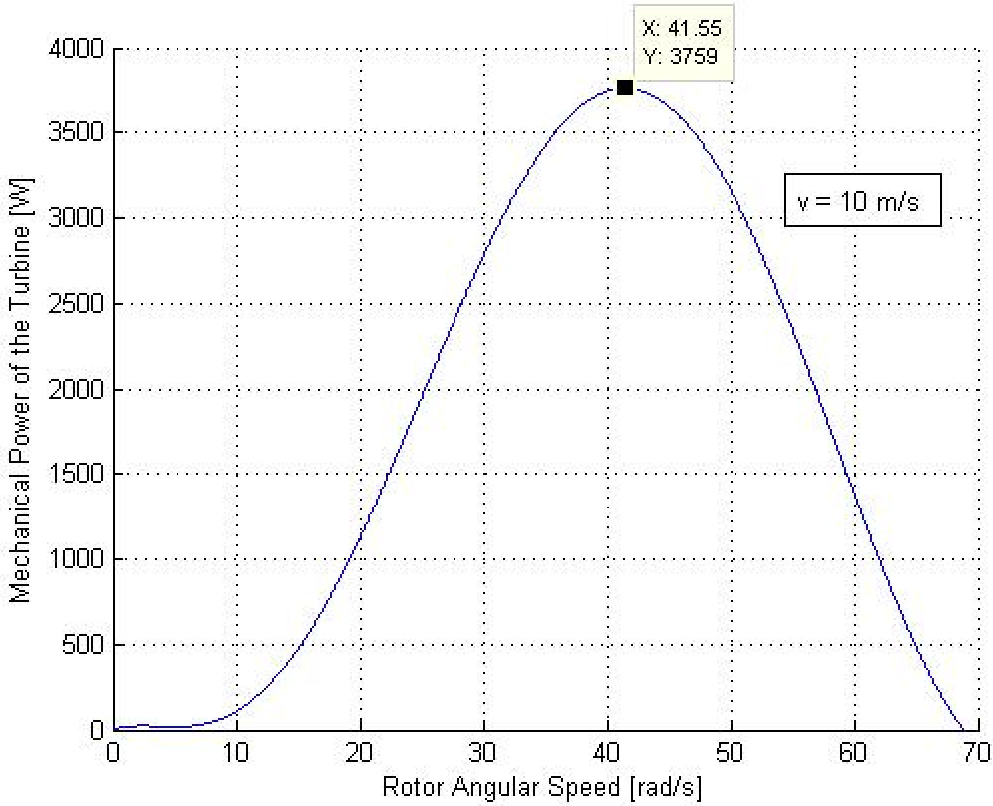

Figure 4.7: Mechanical power curve of the turbine for 10 m/s wind speed

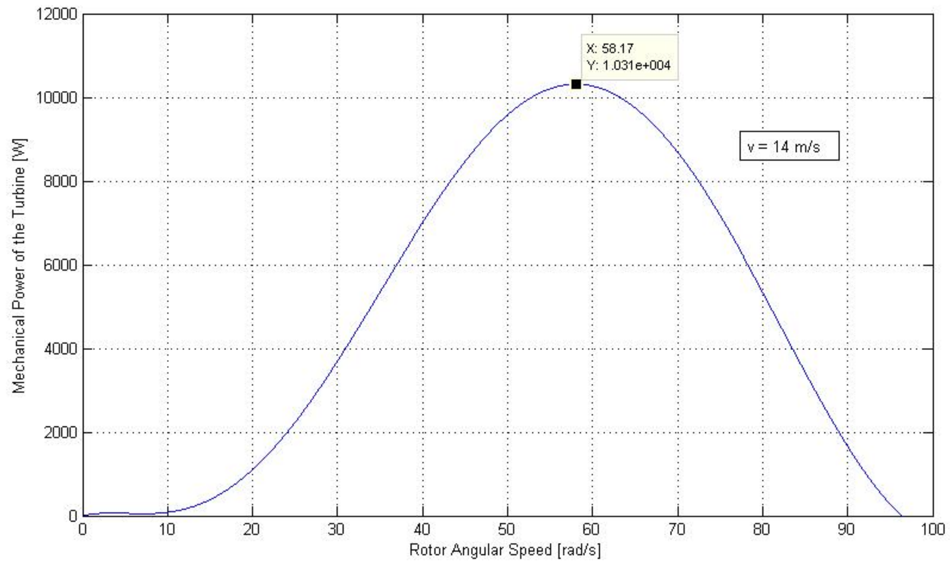

Figure 4.8: Mechanical power curve of the turbine for 14 m/s wind speed

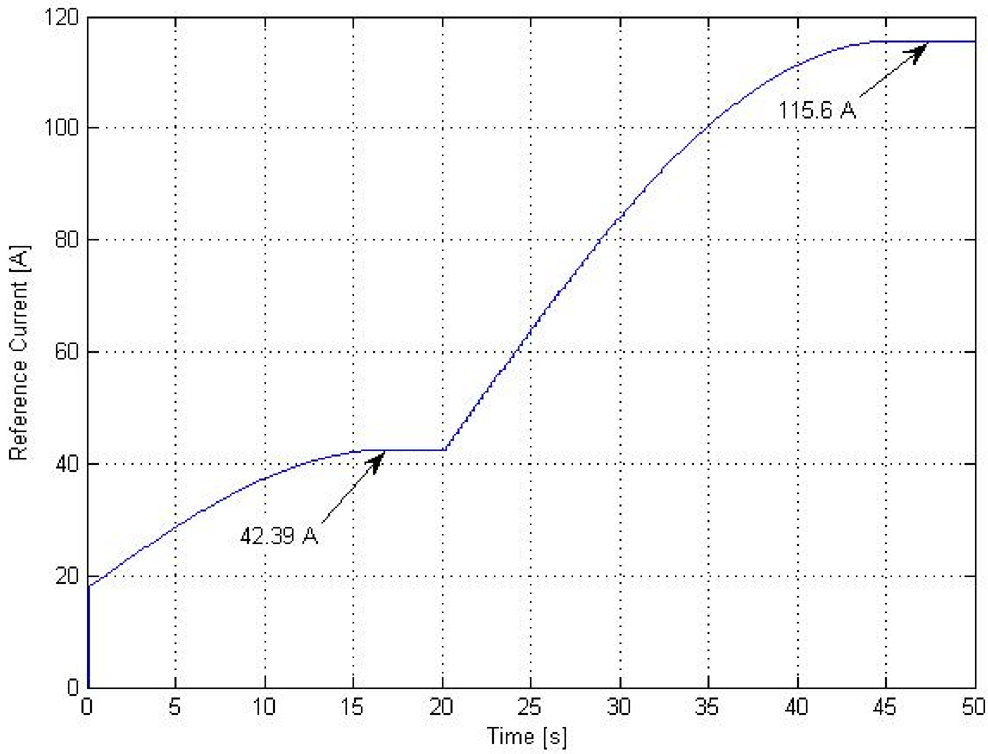

Figure 4.9: Reference current over time

Figure 4.9 is the reference current values of the system which are generated by MPPT. From this figure it can be seen that after 15 s system caught the optimum point. After wind speed increase, control system detected that and continued to search the optimum working point then found it at nearly 43 s.

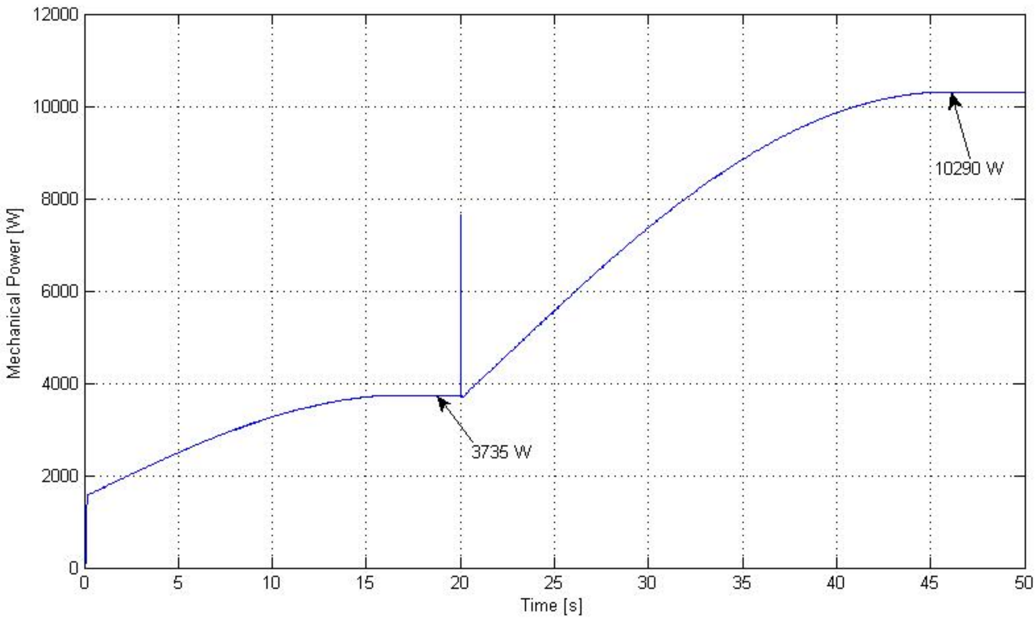

Figure 4.10: Mechanical Power of the Generator over time.

The Figure 4.10 above shows that the control system tracks the optimum point with nearly 40 watts error. This error is caused by the safety gap. If the calculated absolute value of the delta (step size) of the system is between 0.0015 and 0, MPPT stops searching, keeps the reference constant, until wind speed changes. The absolute value of the delta is used in steepest decent algorithm, so that if the delta value gets greater than 0 when wind speed increases system does not effected and continuous to search the optimum point.

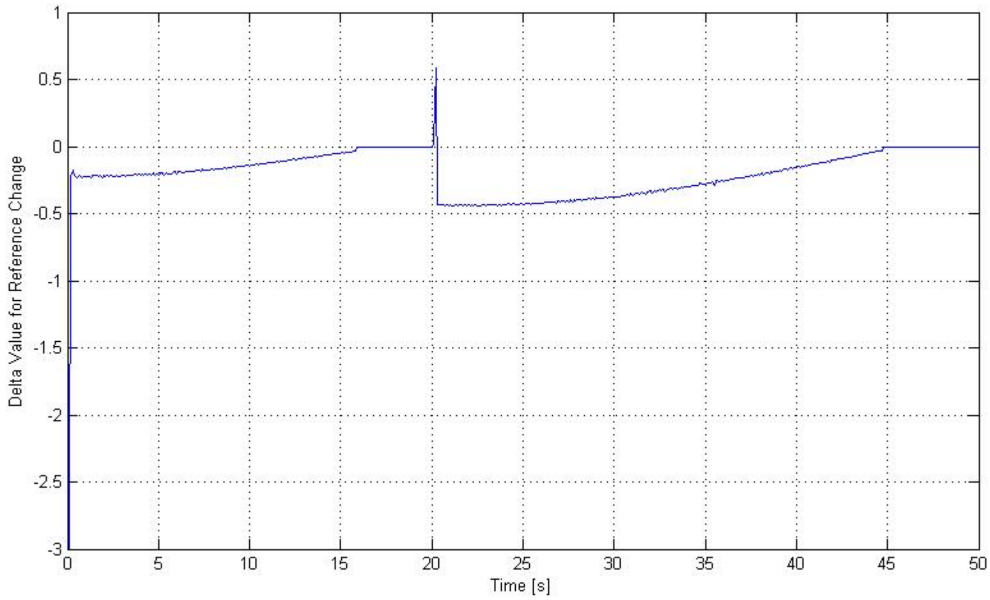

Figure 4.11: Step size values calculated by the MPPT

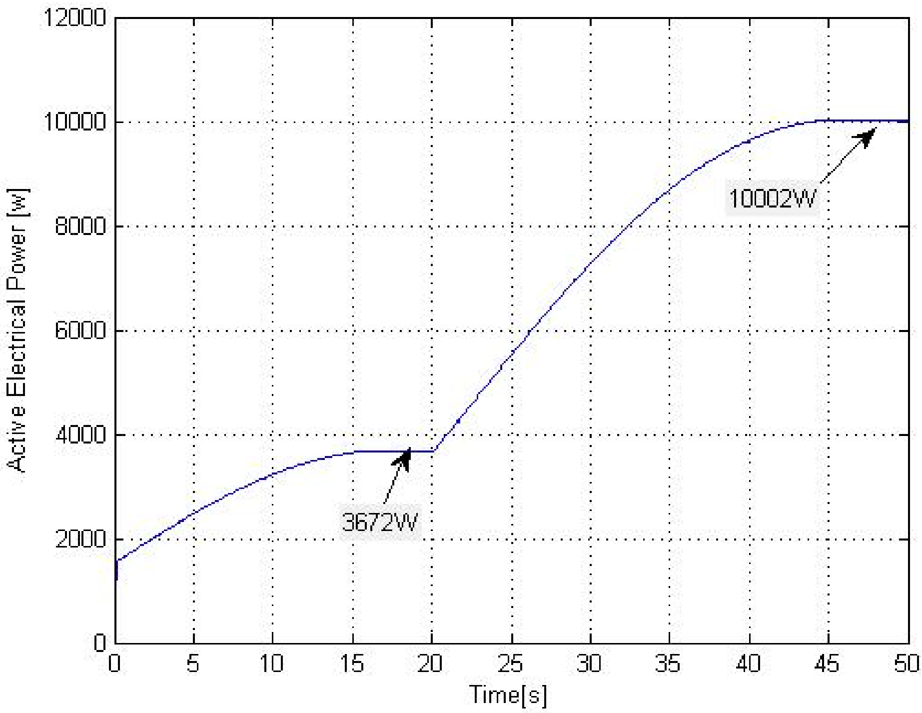

Figure 4.12: Active power supplied to utility

Active power in Figure 4.12 behaves similarly with the mechanical power. The difference between electrical and mechanical power is the losses in the system. Reactive power of the system is zero, because the current and voltage are in phase.The other results are given Figures 4.13 and 4.14.

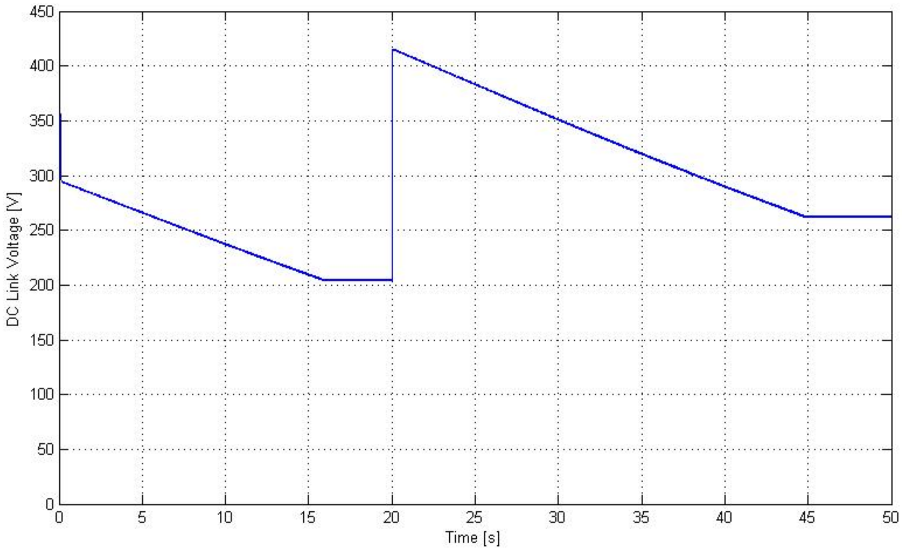

Figure 4.13: DC link voltage

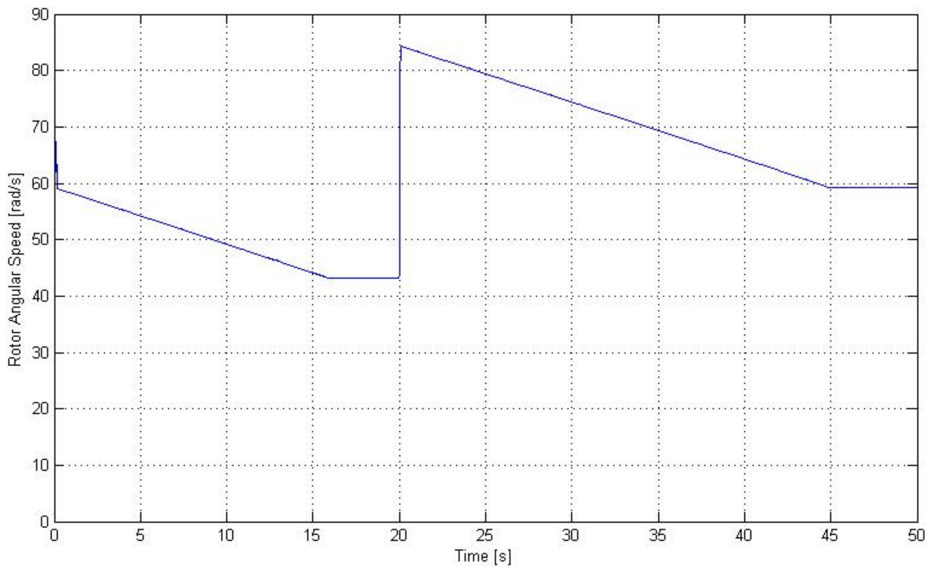

Figure 4.14: Rotor speed over time

4.2 Second Scenario

In this scenario, the simulation is started by 10 m/s wind speed and after 20 s. the wind speed increased to 14 m/s Figure 4.15.

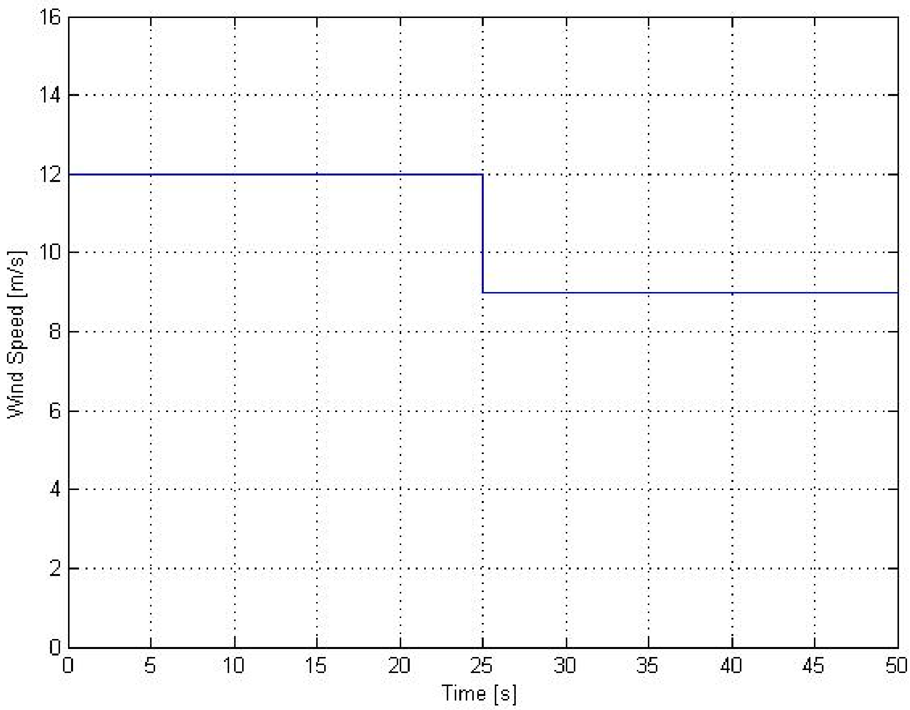

Figure 4.15: Wind speed change over time

The behavior of the system is nearly same with the first scenario except the sudden voltage drop when wind speed decreased. When wind speed decreased, because the system can not meet the power harvested by the grid, the dc link voltage drops rapidly. When the derivative of the Dc voltage falls under a certain value at 25th second, control system detected it and reset system. After that, system continuous searching the optimum point.

Again from the figures it is obvious that system tracks the optimum point with only a small error.

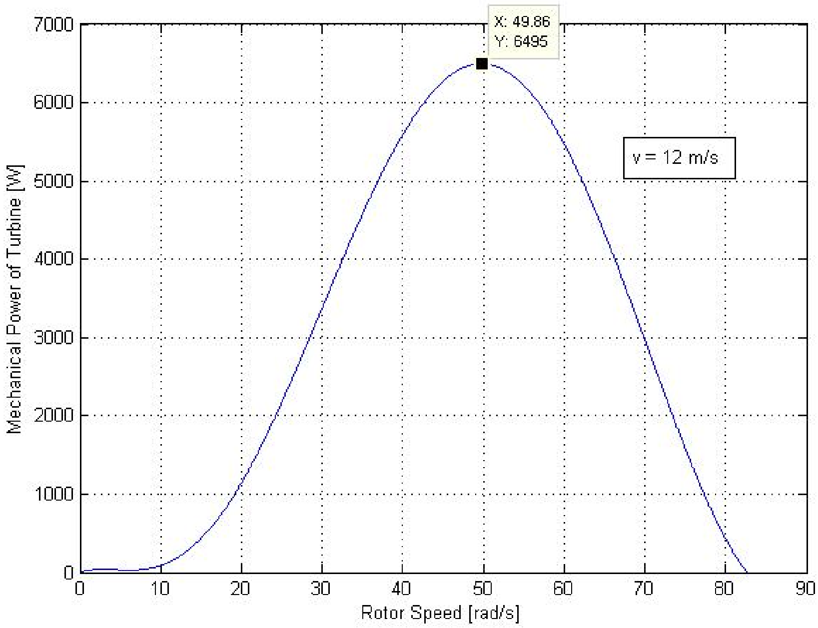

Figure 4.16: Mechanical power curve for 12m/s wind speed

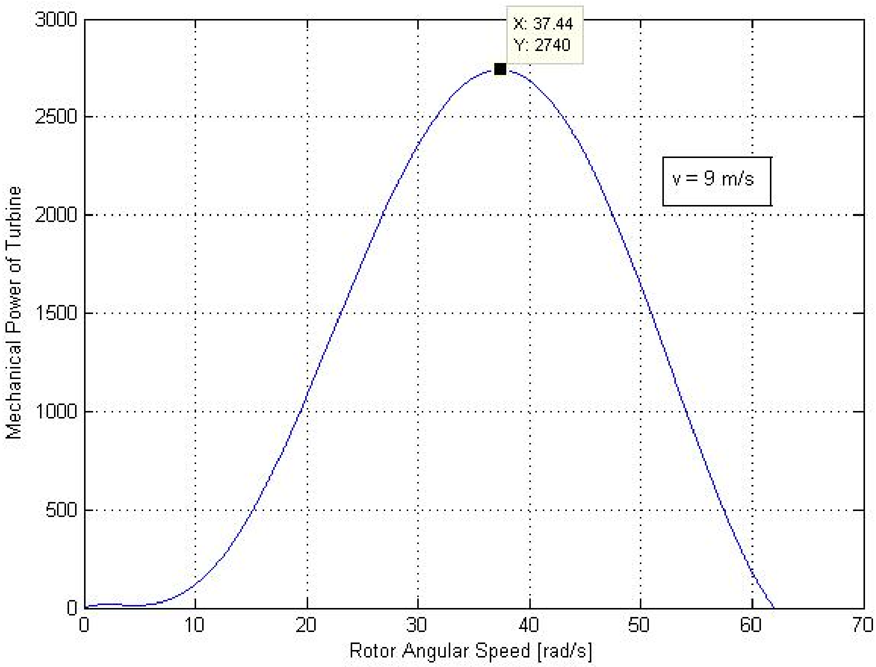

Figure 4.17: Mechanical power curve for 9 m/s wind speed

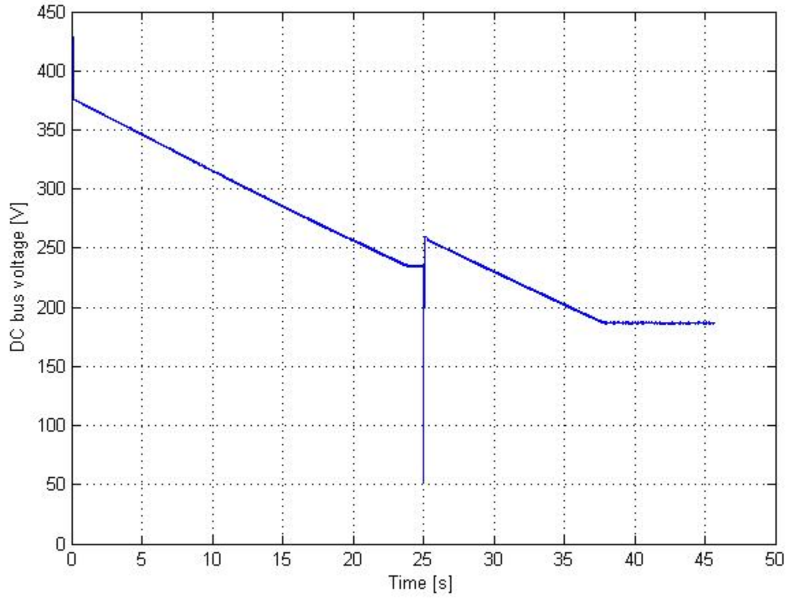

Figure 4.18: DC link voltage over time

The sudden voltage drop can be observed from the Figure 4.18

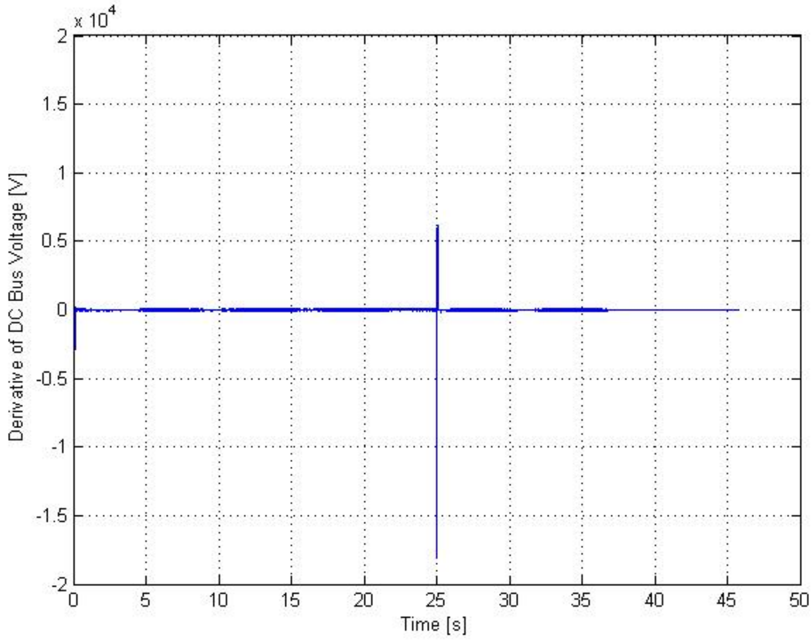

Figure 4.19: Derivative of DC link voltage

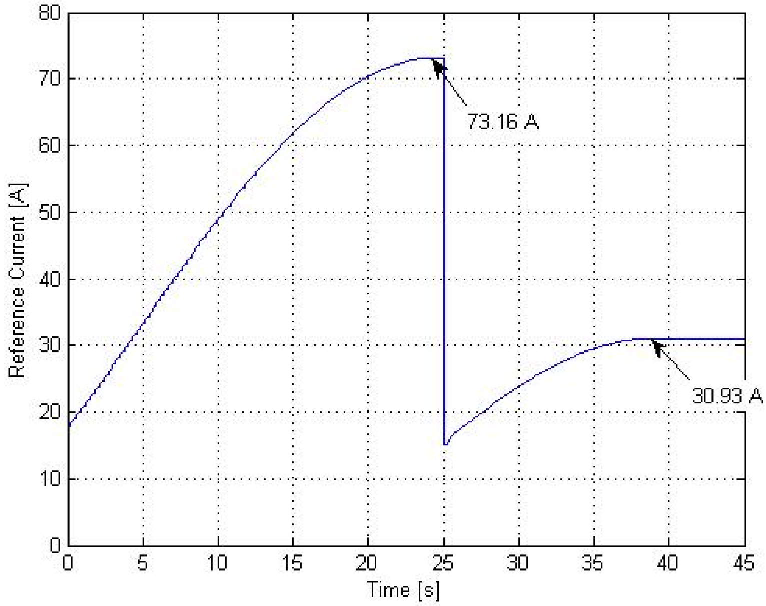

Figure 4.20: Reference current calculated by MPPT

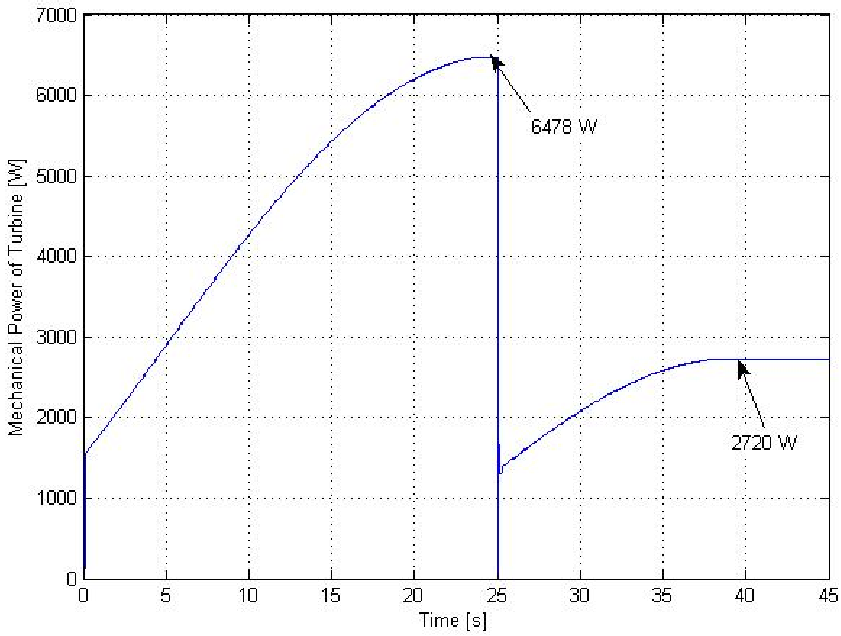

Figure 4.21: Mechanical power of the turbine

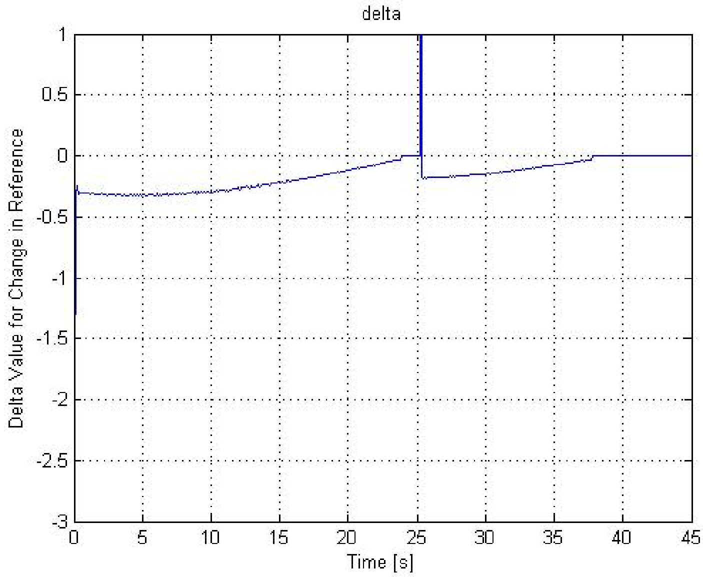

Figure 4.22: Step size values over time

From the Figure 4.22 and 4.23, it can be observed that as the step size approaches to zero the active power approaches to its maximum value.

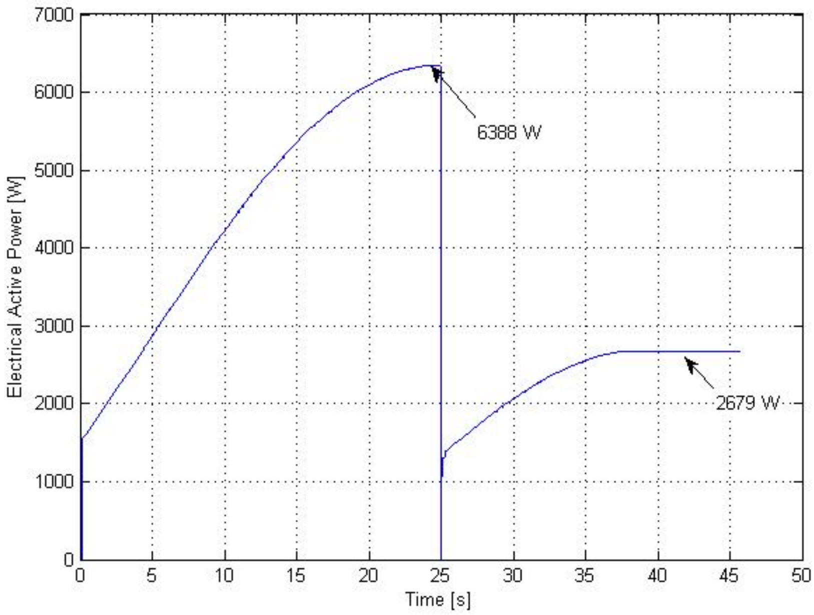

Figure 4.23: Active Power of Electrical Side

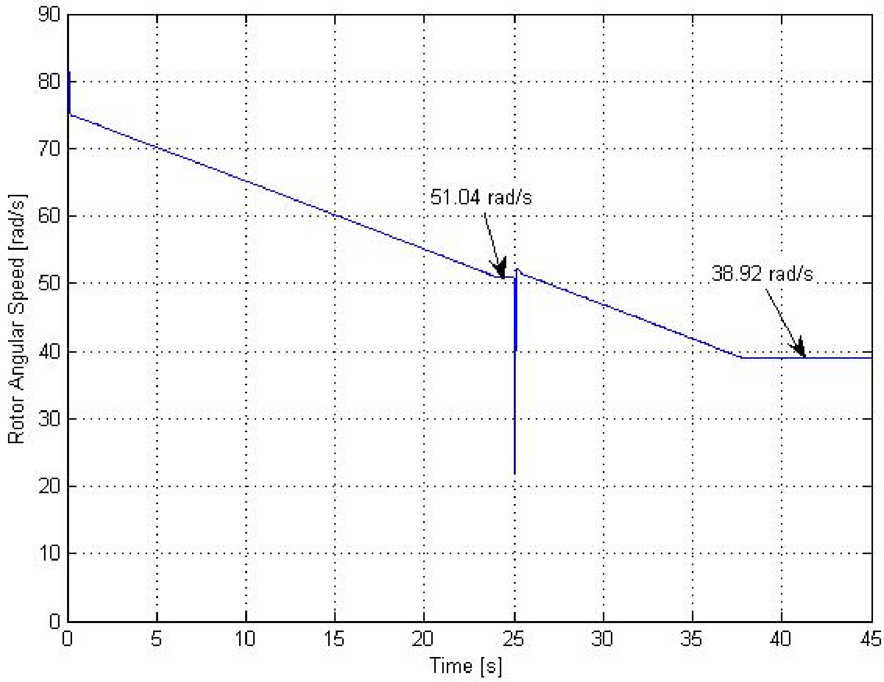

Figure 4.24: The Rotor Speed of the Generator

4.3 General Simulation Results

In this section, some general simulations results are given. Firstly in Figure 4.25, it can be seen that current and phase voltage are in the same phase, so that the reactive power is zero. Other figures are about the compare of FFT analysis of different switching schemes of inverter. Variable switching means a messy FFT result. This means the current includes so many harmonics, but the THD value is smaller. Small hysteresis band means, small THD. Because the shape of the current is more likely to be a pure sine.

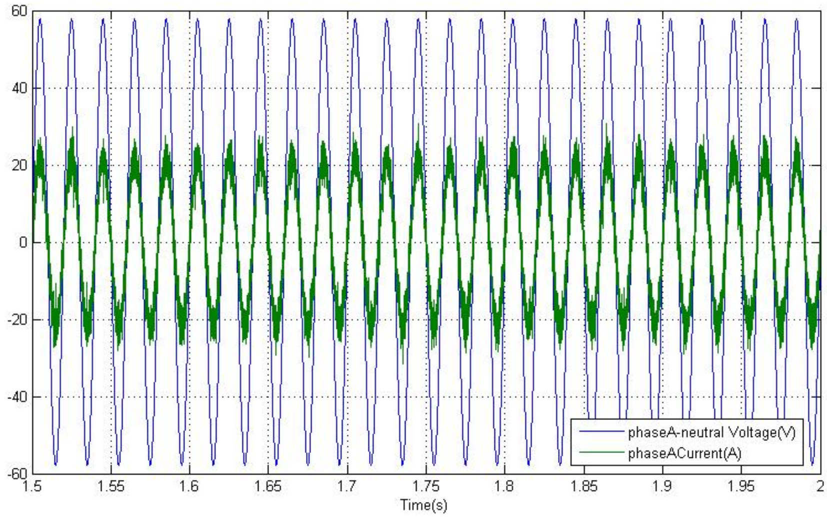

Figure 4.25: An Example Phase Voltage and Current

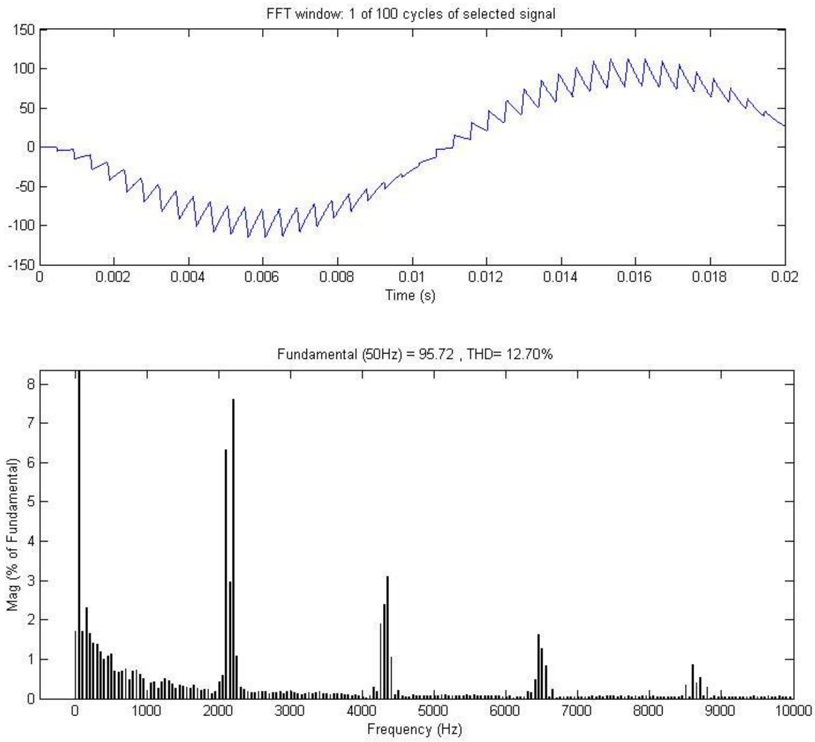

Figure 4.26: FFT Analysis of Phase Current with Constant Switching Frequency

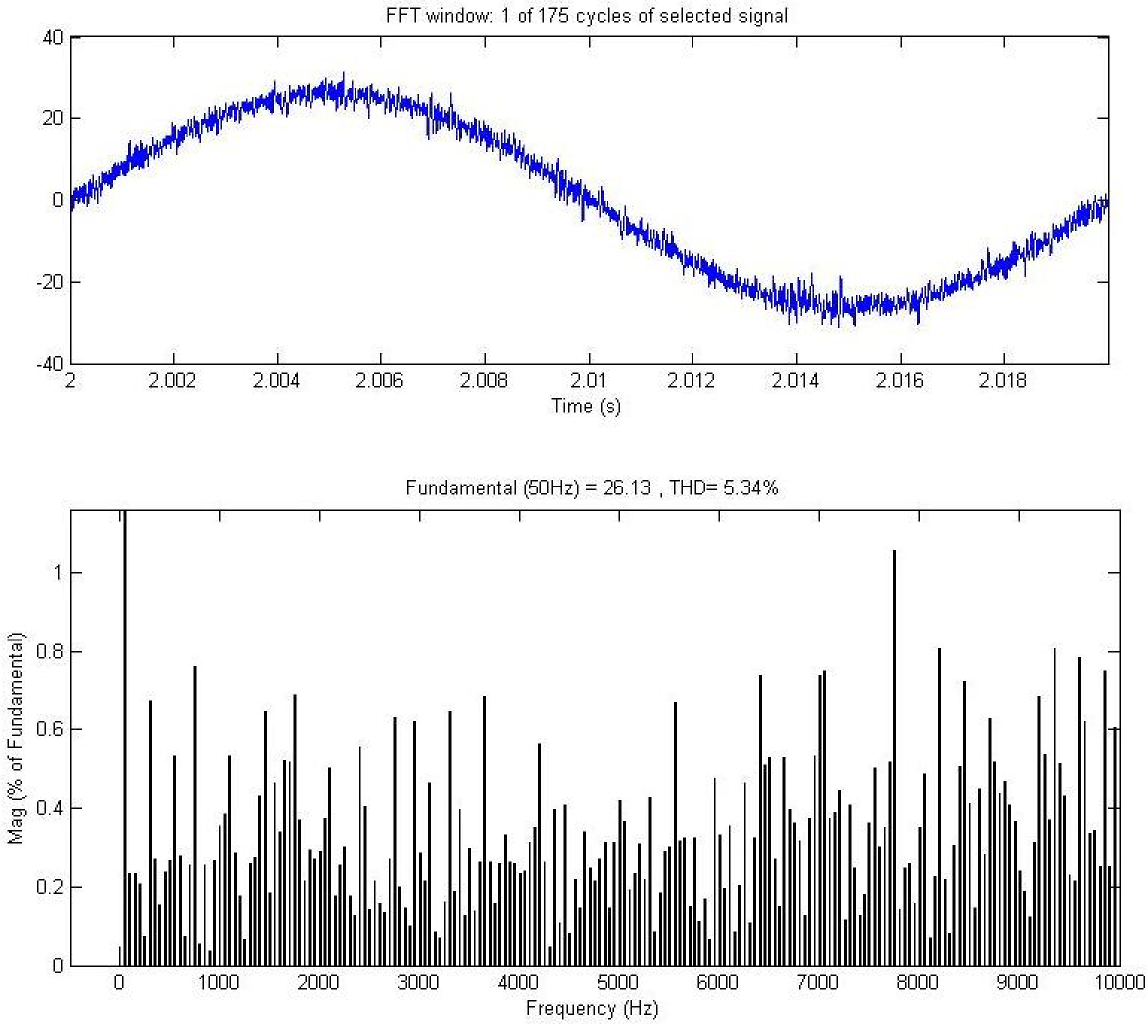

Figure 4.27: FFT Analysis of Phase Current with Variable Switching Frequency

Although it seems that hysteresis controller is best choice for controlling the phase current, it is hard to realize it. Variable frequency switching applies more stress on the switches and for high frequencies the efficiency of the inverter drops dramatically.

5. CONCLUSION

Each component of the system is modeled successfully. In PMSM modeling the saliency on the rotor and stator is neglected so that a model of a special type SM model is employed. For uncontrolled rectifier an average value modeling is done. In this model the input is selected as the rms value and output selected as mean value. A equivalent circuit of the model is also given. For turbine model, firstly wind is modeled as an energy source then from this model all turbine static model is calculated. A basic dynamic model of the turbine also introduced.

A control system is designed for this model. The first tasks of the control system is to keep the system stable under of all conditions and second task is the force the system to work at the optimum point. This systems optimum working point is the point where plant harvests the maximum power from the wind at that time. Thus a MPPT algorithm which is based on the steepest decent algorithm is proposed. To keep system stable detection blocks are added to help MPPT. To control the inverter, a robust, parameter independent current controller is selected. This controller is hysteresis controller which bases on variable switching scheme.

To test control system whether it is meeting requirements or not, the model of the whole system is constructed with a simulation program Matlab Simulink. Different scenarios are tried out and the behavior of the control system is observed. From this observations it seen that control system tracks the optimum point with a small error and keeps the system stable whenever wind speed changes. Compared with the other topologies, the advantage of it that the rectifier side does not require any control and only inverter includes controlled switches. This reduces the complexity of the control. Control system directly tracks the optimum point by observing the current from utility side of the plant, thus MPPT does not only tracks the optimum point, but also tracks the most efficient working point of the plant.

For future works, power factor control can be added which will watch the active and reactive powers and will change the phase shift of the modulation signal of the current reference, but should be careful because the change in power factor for constant active power will effect on the DC bus voltage. Instead of changing the power reference and observing the speed, directly changing the speed and observing the power will make the system more stable and MPPT will work more efficiently. To do this job, a full controlled rectifier is needed. For this approach MPPT can control the rectifier and also the speed of the generator, another control block (PID maybe) can control the inverter to keep the DC bus voltage in reliable value.

REFERENCE

[1]National Wind Technology Center, Wind Resource Information, http://www.nrel.gov/wind/animation.html#animation 09.08.2006

[2] Marques J., Pinheiro H., Gründling H.A., Pinherio J, R., Hey H, L., 2003, A survey on variable-speed wind turbine system, conferrals, Cientifico Greater Forum of Brazilian Electronics of Power, COBEP'03, Cortaleza, 732-738.

[3] Danish Wind Industry Association, http://www.windpower.org/, 09.08.2006

[4] Yeşil E., 2006, KOM 504 Bulanık modelleme ve control Class notes, *Bulanık Modelleme*, ITU

[5] Lubosny Z., 2003, Wind Turbine Operation in Electric Power Systems, Springer Press

[6] The MathWorks, 2004, MATLAB 7.0.1 and Simulink for Technical Computing, Simpower Toolbox Help Files, *Wind Turbines*.

[7] Krause P. C., Wasynczuk O., Sundhoff S. D., 1995, Analysis of Electric Machinery, IEEE Press, Piscataway, NJ

[8] Sarioglu K. M., 1975 Dynamics of Electrical Machines, Classnotes for EE 497 MKS, University of Illinois, Urbana, IL.

[9]Söderström T., Stoica P., 1989, System Identification, Prentice Hall.

[10] Mohan N., Undeland T. M., Robbins W. P., 1995, Power Electronics, Converters, Applications and Design, John Wiley & Sons inc., NewYork

[11] Agrawal J. P., 2001, Power Electronic Systems: Theory and Design, Prentice Hall, Upper Saddle River, N.J.

[12] Kazmierkowski M. P., Malesani L., 1998, Current control techniques for three-phase voltage-source PWM converters: A Survey, *IEEE transactions on industrial electronics* Vol. 45, No 5, 691 – 703.

[13] Freund R. M., 2004, Nonlinear Programming Class Notes, *the Steepest Descent Algorithm for Unconstrained Optimization and a Bisection Line-search Method*, Massachusetts Institute of Technology.

[14] Tan K., Islam S., 2001, Mechanical Sensorless Robust Control of Wind Turbine Driven Permanent Magnet Synchronous Generator For Maximum Power Operation, *International Journal of Renewable Energy Engineering*.

[15] Raju A. B., Chatterjee K., Fernandes B. G., 2003, A simple maximum power point tracker for grid connected variable speed wind energy conversion system with reduced switch count power converter, *IEE Conference Proceeding*, Volume 2, No 15-19, 748 – 753.

[16] Schiemenz I., Stiebler M., 2001, Control of a permanent magnet Synchronous Generator Used in a Variable Speed Wind Energy System, IEE Conference Proceeding, *Electric Machines and Drives Conference*, *IEMDC 2001*, 872 – 877

[17] Yamamura N., Ishida M., Hori T., 1999, A Simple Wind Power Generating System with Permanent Magnet Type Synchronous Generator, *Power Electronics and Drive Systems, PEDS '99*, Volume 2, No: 27-29 ,849 – 854.

RESUME

He was born in New York in 23 April 1982. He graduated the primary and Anatolian high school in Istanbul. In 2004 he graduated from the electrical engineering program and in 2005 he graduated from the electronics and communication engineering program from ITU. He is now R&T assistant in Electrical Engineering department in Control and Automation Systems division.